2015

Proxy-PET Building Blocks as a Design Element for Library Synthesis

Lainey Jo Mallin
Wright State University

Proxy-PET Building Blocks as a Design Element for Library Synthesis

A thesis submitted in partial fulfillment
of the requirements for the degree of
Master of Science

By
LAINEY JO MALLIN
B.S., Wilmington College, 2013

2015
Wright State University

WRIGHT STATE UNIVERSITY
SCHOOL OF GRADUATE STUDIES

July 22, 2015

I HEREBY RECOMMEND THAT THE THESIS PREPARED UNDER MY SUPERVISION BY Lainey Jo Mallin ENTITLED Proxy-PET building blocks as a Design Element for Library Synthesis BE ACCEPTED IN PARTIAL FULFILLMENT OF THE REQUIREMENTS FOR THE DEGREE OF Master of Science.

Committee on Final Examination

Daniel Ketcha, Ph. D.

Daniel Ketcha, Ph. D.
Thesis Director

David Grossie, Ph. D., Chair
Department of Chemistry
College of Science and Mathematics

William Feld, Ph. D.

Kenneth Turnbull, Ph. D.

Robert E.W. Fyffe, Ph. D.
Vice President for Research and
Dean of the Graduate School

Abstract

Mallin, Lainey Jo.M.S., Department of Chemistry, Wright State University, 2015.
Proxy-PET building blocks as a Design Element for Library Synthesis

In exploring radioligands for positron emission tomography (PET) imaging, it is not unusual to synthesize a library of compounds around some targeting scaffold, screen for optimal binding to a relevant diagnostic cellular target, remove some portion of optimized molecule so as to append the requisite reporter group, and then re-evaluate. To this end, the use of "click labeling" in radiochemistry is proving an increasingly attractive means of conjugating a ^{18}F-reporter group, wherein the targeting scaffold bearing a terminal alkyne is allowed to react with a 2-[^{18}F]-fluoroethylazide to forge a linkage as a 1,2,3-triazole substituent. Since the triazole linked prosthetic group is a necessary portion of the eventual PET imaging agent, it was envisioned that building blocks possessing a "cold" version of the triazole linked fluoroethyl group might be incorporated early in the synthetic plan as a crucial library design element. The analog so designed and exhibiting optimal binding would, in a radioactive form, represent the eventual PET imaging agent. To that end, we have prepared such building blocks from the copper(I) catalyzed click reaction between sodium azide, 2-fluoroethyl tosylate (or benzyl bromide) and propargylic alcohol. Conversion of the alcohol building block to the corresponding aldehyde could be effected using MnO_2, which was appended to a scaffold of interest using an aldol condensation. Conversion to the bromomethyl derivative was achieved with PBr_3 in the case of the benzyl surrogate but not the fluoroethyl derivative. The

usefulness of such building blocks has been demonstrated in the case of synthesizing and evaluating small libraries around the oxindole and isatin privileged scaffolds. Subsequent manipulations led to the ultimate target structure, being a benzylidene oxindole bearing a *N*-triazole linked moiety. For instance, whereas the bromomethyl triazole can be utilized for *N*-alkylations of the aforementioned scaffolds towards targets of importance in Alzheimer's disease (such as tau proteins, caspase-3, cdk5, and AChE), the aldehyde can be employed in aldol reactions. The introduction of such proxy-PET moieties at an early stage of the library synthesis has an added benefit of avoiding the presence of copper species in the last step before biological testing.

Table of Contents

List of Figures

Acknowledgements

First and foremost I would like to thank Dr. Ketcha for the advice, encouragement, and guidance he bestowed to me over the last 2 years in chemistry and in life. I will be forever grateful. I would also like to thank my parents, Scott and Mardi Mallin, for always being there for me and pushing me to be my best self. I couldn't wish for better parents. Thanks to Reid, for being there for me always. Finally, I would like to extend thanks to everyone who has helped me along this journey.

INTRODUCTION

The year was 1906 and Auguste D. was losing her mind. Dr. Alois Alzheimer observed this 51 year old woman who was suffering from progressive memory loss as well as other neurological disturbances such as unwarranted jealousy towards her husband and delusions that someone was trying to kill her. Upon Auguste's death, Dr. Alzheimer studied her brain by using silver staining. He identified two types of senile plaques, namely neuritic plaques (amyloid-β proteins) and neurofibrillary tangles (tau-proteins).[1] Dr. Alzheimer presented his findings and clinical characteristics of the disease at a conference in 1906.[2]

Alzheimer's disease (AD) is a type of dementia that slowly destroys brain function and leads to cognitive decline as well as behavioral and psychiatric disorders. Dementia is an umbrella term which describes any disease that irreversibly damages nerve cells in the brain resulting in a decline in mental ability severe enough to interfere with performing the activities associated with daily life.[3] Main pathological features of the disease include the co-occurrence of plaques and tangles, loss of connections between neurons, and finally neuronal death and brain shrinkage.[4]

Over 100 years has passed since Dr. Alzheimer disclosed his discovery of a new type of neurodegenerative disease later to be named after its discoverer.[1,2,5] Little did Dr. Alzheimer know or could have suspected that the disease he described would become an

epidemic in the 21st century. Between 1906, when Alzheimer's disease was first documented, and 2006, one hundred years later, human life expectancy in the United States increased from 48.5 years to 78.5 years.[6,7] Considering the fact that the principle risk factor for Alzheimer's disease is age,[8] the prevalence of this disease has risen dramatically and will continue to do so as life expectancy continues to increase. At present, there are no cures, treatments, or drugs that can so much as slow the progression of Alzheimer's disease, nor are there means of diagnosing malady.

Amyloid-beta (Aβ) plaques and neurofibrillary tangles (NFTs) are the hallmarks of the AD, however with no approved imaging agent to visualize a diagnostic protein in vivo, it is very difficult to accurately determine pre-mortem if a patient has AD especially since the symptoms characteristics of AD are similar to those present in other dementias associated with aging.[9,10] While there are imaging agents used in AD research, such agents target proteins in the brain which do not necessarily correlate well with the cognitive decline observed.

Symptoms of Alzheimer's disease include memory impairment, decline in language skills and decision making, behavioral changes, loss of ability to recognize family, and ultimately loss of self.[11] Such a list of pathological symptoms does come near to describing the devastation and anguish experienced by the patient and their family. Ronch said it best when he stated: "but worse, the loss of self happens before the very eyes of the person whose self is vanishing. The basis of unique personal identity established over the life span eventually deteriorates."[12]

Based on Dr. Alzheimer's findings and another 80+ years of research on the post-mortem brains of people who exhibited symptoms similar to those of Auguste D., two main hypotheses have been developed concerning the cause of the disease. The first, the so-called "amyloid cascade hypothesis" was developed in 1992 by Hardy and Higgins,[13] who implicated the Aβ plaques as being the causative agent in AD pathology.[13] The plaques are the result of the sequential cleavage of the amyloid precursor protein (APP) by β-secretase and ɣ-secretase enzymes which result in the generation of amyloid protein fragments of 36 to 43 amino acids in length. Of these monomeric species produced, the $A\beta_{42}$ fragment is the most toxic and most prone to aggregation while $A\beta_{40}$ is the most prevalent.[14,15] As illustrated by **Figure 1**; the enzyme β-secretase cleaves the protein in the extracellular area and then ɣ-secretase cleaves the protein via intra-membrane proteolysis resulting in formation of the fragments.[15] Another secretase, α-secretase is also involved in the cleavage of APP, however if α-secretase cleaves the protein then no toxic fragments will be formed.[15] In any event, the monomers (especially $A\beta_{42}$) then aggregate to form the Aβ plaques thought to initiate the cascade of events leading to AD.[16] At the time, and until very recently, it was thought that since these plaques were likely the cause of AD, therapeutic strategies aimed at preventing the formation of and/or facilitating the clearance of these plaques would at least slow down if not cure the disease.

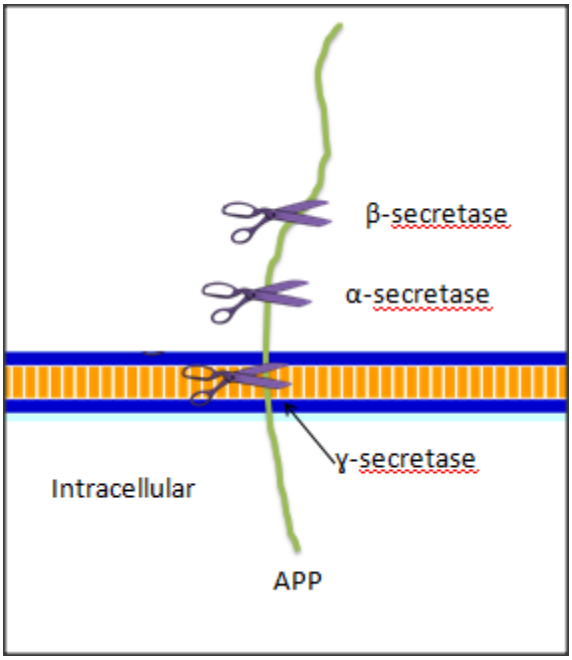

Figure 1: APP cleavage by secretases

Now, after several drugs capable of clearing Aβ plaques have been developed and studied, we are beginning to suspect that ridding the brain of these plaques may have little or no effect on the progression of the disease.[17,18] Three out of five drugs that have been developed (none of which have been approved by FDA) to reduce or clear Aβ plaques are shown. Flurizan[19] (**1**)and Semagacestat[20] (**2**) reduce Aβ burden via γ-secretase modulation (Flurizan)[21] or complete inhibition (Semagacestat). Phenserine[22] (**3**) works to modulate Aβ generation by non-competitively inhibiting acetylcholinesterase.

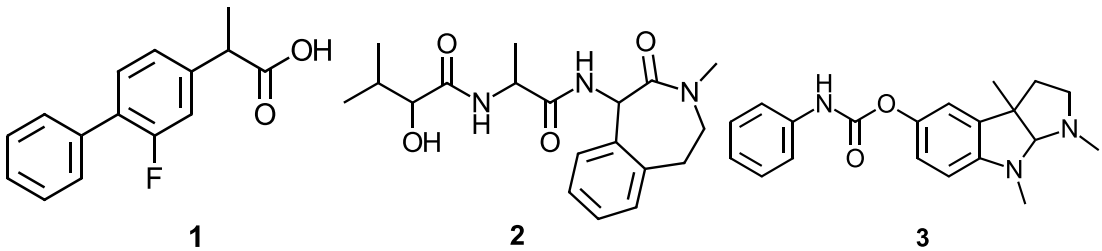

1 **2** **3**

Two other drugs not shown, Bapineuzumab[23] and Solanezumab,[24] are antibodies that work by binding to the plaques in the brain and activating phagocytosis. When these drugs were tested on mice, results were very promising showing that plaques were cleared and symptoms of the disease disappeared causing the mice to seem as though they were not diseased anymore.[25-27] Unfortunately, all of these drugs described had no effect on the progression of AD in humans and in some cases caused negative side effects to the patients.[22, 28-31] Also, research has shown that the amount of Aβ plaque in the brain has no correlation with the degree of cognitive impairment; additionally, plaques can be present in the brain without that person displaying any symptoms of AD.[17,32,33] Hardy did state in 1994 that "the amyloid cascade hypothesis is just a skeletal outline/framework not meant to imply that genetics, APP metabolism, and beta-amyloid neurotoxicity are the only important topics of research in AD or that amyloid deposition is the only cause of dementia".[34] He stated that the hypothesis only implied that the disease process would become more biochemically complex with the onset of the cascade.[34] Perhaps his statements were meant to warn researchers to not to put all their eggs in one basket and to continue exploring the complexity of AD; however there is no question that most of the research and funding for AD over the past 20 years has been aimed at targets implemented with this hypothesis.

Another hypothesis gaining momentum is known as the tau hypothesis. Since 2004, more attention has been given to this hypothesis which was coined by Trojanowski in 2005,[35-38] and suggests that AD pathology starts with hyperphosphorylation of the tau protein, which in turn, leads to NFT's and finally the other pathological characteristics of the disease.[39-41] Along with amyloid plaques, NFT's were first noticed and described by

Dr. Alzheimer in 1906, however the protein involved in forming these tangles was not identified as hyperphosphorylated tau until 1986.[42] In contrast to amyloid plaques, the amount of neurofibrillary lesions found in the brain does correlate better with the severity or progression of the disease.[43] Research showing that tau pathology appears in certain areas of the brain decades before Aβ plaques, as well as before signs of dementia surface; supports the tau hypothesis.[44,55] Increased levels of NFT's in the brain[46,47] and in cerebrospinal fluid[48] are positively correlated to reduced scores on cognitive tests[17,46] whereas appearance of Aβ plaques (as mentioned before) do not necessarily mean a person will ever develop AD.[49]

In 2011, the Alzheimer's Association, the National Institute on Aging, and the U.S. National Institute of Health jointly issued new criteria and guidelines to diagnose AD. Diagnosis is now based on three clinical stages; preclinical AD, mild cognitive impairment, and dementia caused by AD. Preclinical AD doesn't have any detectable symptoms but there is thought to be changes in biomarker levels, however there is no definite biomarker tracer as of yet so this stage cannot yet be clinically identified pre-mortem. The second stage of AD is mild cognitive impairment which causes symptoms in the patient such as some memory loss, however, these symptoms are ones that do not affect the everyday life of the patient. Dementia caused by AD, the third stage, is where symptoms do interfere with everyday life and those affected become unable to care for themselves. When AD is diagnosed, there are only a couple of options for the patient: they can choose to take no action against the disease or they can take palliative medications which may have little or no effect on the disease progression.[4]

As of 2015, there are five medications that have been approved by the FDA as palliative treatments for the symptoms caused by AD. These drugs vary in effectiveness and have shown only marginal benefits when found effective.[50] Four of the drugs are acetylcholinesterase (AChE) inhibitors and one is an *N*-methyl-D-aspartate (NMDA) receptor antagonist.[51] AChE inhibitors work by slowing down the process that breaks down acetylcholine (Ach), a key neurotransmitter.[52] NMDA receptor antagonists work by regulating the activity of glutamate, an important neurotransmitter that regulates the calcium uptake necessary for proper brain functioning.[53] However, too much of a good thing can be bad. Excess glutamate can be released from damaged neuronal cells leading to overexposure to calcium and expedited cell damage. These drugs can help AD patients manage their symptoms, however they are not disease specific and do not always work.[51]

Other drug options that are being explored are ɣ-secretase inhibitors, β-secretase inhibitors, and α-secretase inhibitors. ɣ-Secretases are involved with a number of critical processes within the human body and because of that, this protein must be modulated and not completely inhibited; a challenge which has significantly limited progress in this area.[54] One idea would be to block the ATP binding site on ɣ-secretase that modulates APP processing.[55,56]Netzer et al.[56] and Fraering et al.[55] describe how modulating the ATP binding site can reduce Aβ burden. Nonsteroidal anti-inflammatory drugs (NSAID's) which allosterically modulate ɣ-secretase so as to produce more of the less toxic 40 amino acid fragments versus 42 fragments might also be an option.[57,58] A better option would be a drug that interferes with β-secretase because it is not involved in any other physiological processes. Human APP transgenic mice that have β-secretase genetically shut off did not have memory defects that they would have normally exhibited.[59] With β-

secretase shut off it cannot cleave APP thus no toxic monomers will be formed which means that no plaques will form. Alternatively, α-secretase processes the APP at a point that prevents the more toxic fragments from being produced, which means up-regulation of this secretase might be a target for intervention.[60] Immune mechanisms to clear plaques in the brain associated with AD could help also, however as mentioned earlier, five drugs that do this have already failed, so it does not seem like a very promising avenue.[18] Small molecules that can disrupt aggregation might be a viable option as well.[61] One such small molecule is Alzhemed (**4**), (shown in neutral form) also known as 3-amino-1-propanesulfonic acid or 3-aminopropylsulfonic acid. In vitro studies showed preferential binding to soluble Aβ thus inhibiting Aβ aggregation. Additionally, treatment of mice with Alzhemed resulted in reduction of Aβ in the brain.[62] Unfortunately, in August of 2007 the FDA deemed the stage 3 clinical trials inconclusive.[63]

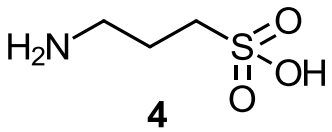

4

Non-pharmaceutical treatments such as physical and reminiscence therapy have also been studied. These therapies do not alter the progression of the disease and in the few studies on effectiveness of these types of treatments; they did not seem to help the patient all that much.[64] The spice curcumin (**5**) is often used in Indian food to flavor and give color. It has been proposed that curcumin may be a risk reducer for developing AD since it is thought to have neuronal protective properties.[65] Caffeine (**6**) is another natural remedy that is thought to guard against AD as well as have restorative effects once

symptoms appear. There have been a couple of studies that involve mice predisposed to develop AD and when given the equivalent of 5 cups of coffee a day (for a human) they take longer to exhibit AD symptoms. Additionally, when the mice are already exhibiting symptoms of the disease they show improved brain function after they are given caffeine.[66,67]

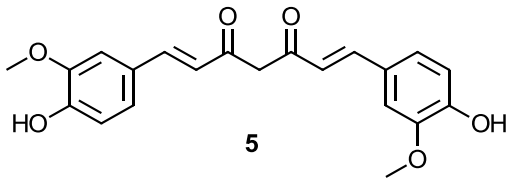

5

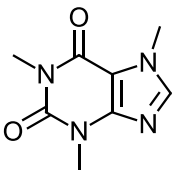

6

As alluded to earlier, an imaging agent for Alzheimer's is desperately needed. Currently, AD can only be diagnosed post-mortem which is not much help except to give an official cause of death in some cases when an autopsy of an elderly individual is conducted. A conclusive imaging agent could not only distinguish between the various dementias associated with aging to provide for better diagnosis, but it could also help monitor the progression of patients undergoing treatments as they are developed.[68] Out of the five Aβ positron emission tomography (PET) imaging agents (*vide infra*) that have had human trials, three have been approved by the FDA. All of the imaging agents developed to date have been based on the structures of highly fluorescent dyes: Congo Red (**7**), Chrysamine G (**8**), and Thioflavin T (**9**) that are used to detect Aβ plaques and NFTs in the brain post-mortem.[70] Amyvid (**10**) (a.k.a. Florbentapir) was the first to be approved by the FDA in 2012, followed by Vizamyl (**12**) (a.k.a. Flutemetamol) in 2013, and finally, Neuraceq (**11**) (a.k.a. Florbetaben) in 2014.[69]Amyvid and Neuraceq have structural similarities to Congo Red and Chrysamine G while Vizamyl is similar to

Thioflavin T. Each of these agents has been shown to be effective for the non-invasive imagingof amyloid plaques in the pre-mortem brain. Despite this progress, in 2012 the Human Amyloid Imaging Conference suggested that appearance of amyloid plaques in a person's brain is not good news but not a sentence for developing Alzheimer's either.[68]

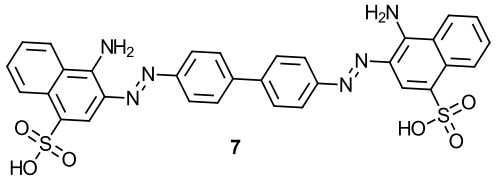

7

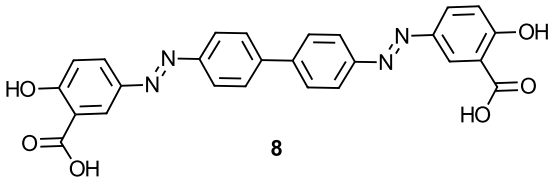

8

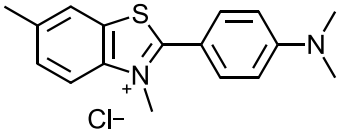

9

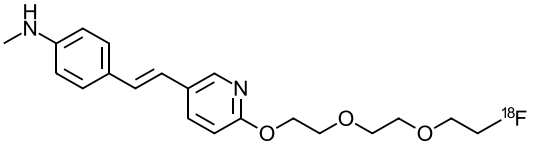

10

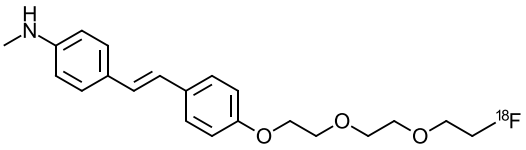

11

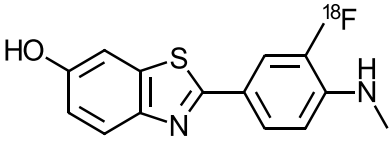

12

Seven molecules, belonging to three classes of compounds, have recently been developed as possible tau PET imaging agents. Of this group, [^{18}F]THK523 (**13**), [^{18}F]THK5105 (**14**), and [^{18}F]THK5117 (**15**) are quinoline derivatives, [^{18}F]T807 (**16**) and [^{18}F]T808 (**17**) are pyrimidine derivatives, and [^{11}C]PBB3 (**18**) and [^{18}F]FDDNP (**19**) are benzothiazole derivatives.[71] [^{18}F]FDDNP (**19**) was the first tau imaging agent tested

in vivo and while it was shown to target tau it also targeted Aβ which is undesirable.[72] Additionally, [^{18}F]THK-523 (**13**) failed to visualize NFTs clearly[73] and [^{11}C]PBB3 (**18**) is tagged with a radioactive carbon which is not favored when it comes to developing a PET-imaging agent.[74] In-vivo human studies of [^{11}C]PBB3,[74] [^{18}F]T807,[75] (**16**) and [^{18}F]THK5105[76] (**14**) showed promising results, however, an imaging agent for tau has yet to be approved by the FDA.

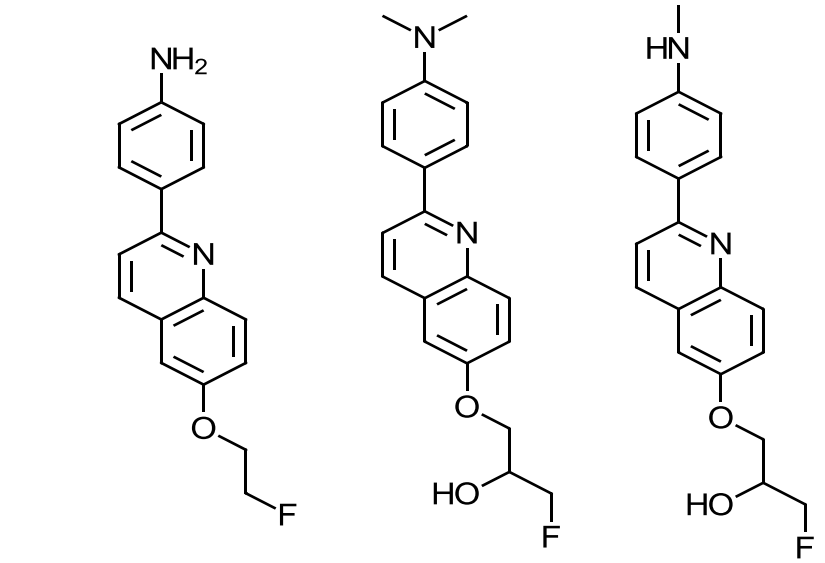

13 **14** **15**

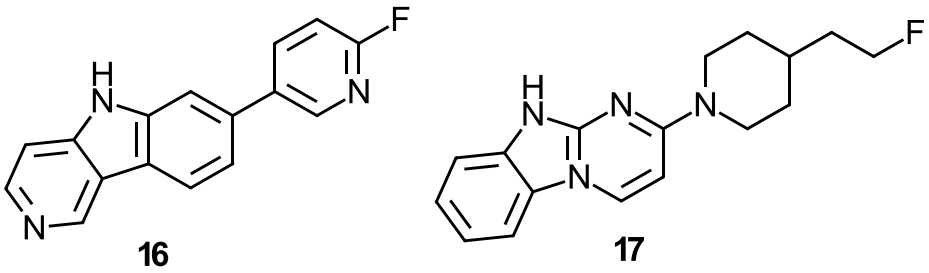

16 **17**

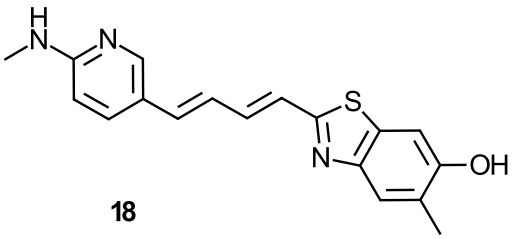

18

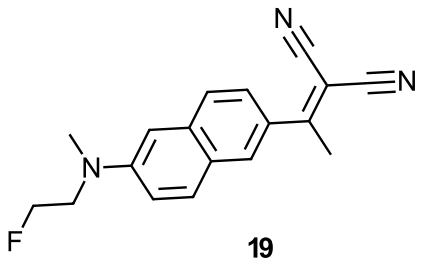

19

If AD continues to progress at its current rate and we do not develop a disease altering medication, it will be devastating for not only the 13.8 million people projected to have the disease by 2050 but also their families and the economy.[3] A consensus about what needs to be done about this epidemic needs to be reached. Broadly speaking, either multiple drugs with different modes of action, or a single drug that has multiple functions, will be required for individualized regimens which means we, as a nation, have a long way to go considering what is currently available.

While the amyloid cascade and tau hypotheses offer insight to the pathology and possible causes of AD, they do not individually explain the full complexity of AD. In order to move forward with drug discovery efforts for this multi-factorial disease[77] there is growing consensus that the paradigm of the "one-compound-various targets"[78,79] must be employed. Though the etiology of AD is not completely known, experts do know of several components that contribute to the disease, including Aβ deposits, tau protein aggregation, oxidative stress, and a decrease in ACh levels. Other "players" involved in AD development include, but are not on any terms limited to, Ca^{2+} imbalance, excess of Cu^{2+}/Zn in the brain, impairment of mitochondrial function and apoptotic neuronal death.[80]

Development of drugs such as Bapineuzumab, Phenserine, Flurizan, Semagacestat, and Solanezumab which help clear Aβ plaques out of the brain (outlined earlier) and tacrine, donepezil, rivastigmine, and galantamine which inhibit AChE to increase Ach,[79] have not been able to even alter or slow progression of the disease. For a review of all drugs (failed and approved by FDA) developed for AD prior to 2010 refer to the article by Sabbagh.[81]Noteworthy is the fact that the development of these drugs over the past decades has been based on the "one target one compound" paradigm which has been very successful in the past for some diseases. However, with a disease as complex as AD this paradigm has not been, and will not likely be successful.[80] This disease seems to be very efficient at finding a window to proceed through when a door is closed in its path. The complexity of this disease, as well as a century old history of failed single target drugs, warrants the progression into developing a drug that can target more than one proposed cause of disease at a time. Most efforts along these lines have been based upon coupling drugs which inhibit acetycholinestease along with targeting some other component of the disease. Memoquin (**20**) is an example of a multitarget lead drug that has been tested and shown to be effective at targeting multiple factors believed to lead to Alzheimer's disease, including AChE inhibition, altering expression and deposition of Aβ and altering hyperphosphorylation and deposition of tau.[82,83] Recently, a dual inhibition lead compound was disclosed as being capable of inhibiting Dyrk1A (a major tau kinase) and formation of Aβ plaques.[84,85] Although such multitarget drugs are at an early stage of development, it is clear that this approach is becoming more widespread. For a general review covering the paradigm of one-compound-various targets (a.k.a.

polypharmacology) read the article by Rastelli[86] or for a review that specifically relates to AD read the article by León.[80]

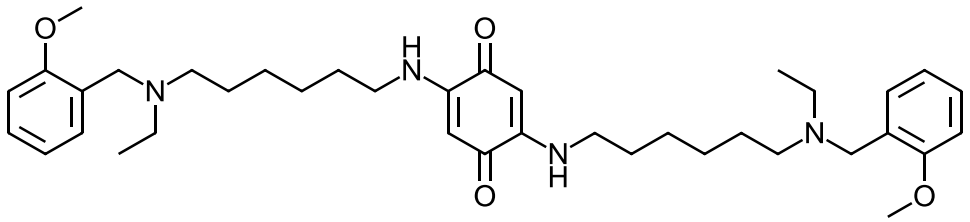

20

The Ketcha research group at WSU is exploring the idea of polypharmacology by designing molecules to inhibit caspase-3 and acetylcholinesterase or caspase-3 and cyclin-dependent kinase 5 (cdk5). These biological targets have the ability to affect gamma secretase activating protein (GSAP) and the Golgi apparatus which have been shown to be involved in the development of Alzheimer's disease. Greengard showed in 2007 that arylidene oxindoles, specifically IC261 [(E)-3-(2,4,6-trimethoxybenzylidene)indolin-2-one] (**21**), could reduce endogenous Aβ production by possibly inhibiting casein kinase 1 (CK1).[87] However, *N*-alkylation, which is known to nullify activity against kinases, of a similar molecule, BSc3927 (**22**), still showed Aβ-inhibitory activity therefore showing that CK1 was likely not involved.[88]

GSAP was discovered to be capable of affecting Aβ production without affecting other important biologic pathways such as the Notch signaling pathway which is important for neuronal cell communication. GSAP interacts with amyloid precursor protein c-terminal fragment (APP-CTF). This interaction directs gamma secretase to "cut" APP which in turn results in formation of the toxic Aβ-42 fragment. Since,

inhibiting GSAP does not directly inhibit gamma secretase which has other biologic function; it is considered a good target for possible Alzheimer's disease treatment.[89] Almost 15 years ago was the first time caspase-3 was shown to have a link to the development of Alzheimer's disease by causing neuronal cell death via apoptosis;[90] however in 2014 Practico linked caspase-3 to GSAP.[91] He discovered that GSAP must be activated by caspase-3 in turn showing that caspase-3 may be a good enzyme target to lower Aβ plaque formation.[91]

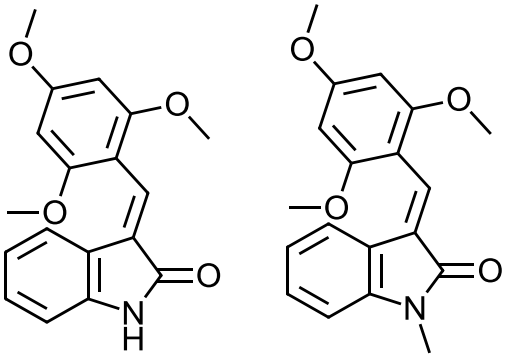

21 **22**

Cyclin dependent kinase (cdk5) is also a target of interest because of the implications that it is linked to the phosphorylation of tau protein and GRASP65 which is involved in the stacking of the Golgi apparatus.[92] Cdk5 has also been implicated in causing neuronal apoptosis.[93] In 1992, it was determined that cdk5 was involved in the hyperphosphorylation of tau[94] but only recently was it also linked to fragmentation of the Golgi apparatus.[92] Furthermore, it is thought Golgi fragmentation can lead to the development of AD.[92,95] With a disease as complex as Alzheimer's disease nothing can be ruled out as a possible cause. At WSU interest is focused on using moieties capable of

lowering Aβ plaque production by inhibiting caspase-3 and/or cdk5 utilizing compounds designed around the privileged heterocyclic scaffolds of oxindole and isatin.

Privileged scaffolds are useful starting points for drug discovery efforts because by definition they are capable of binding as ligands to multiple unrelated receptors. Oxindole (**24**) and isatin (**23**) are considered *privileged* scaffolds[96] because of their broad range of biological activities and the multiple sites for diversification that they offer. In relation to Alzheimer's disease it is important to note that an oxindole derivative, **25**, has been shown to have binding affinity for tau protein.[97] Other oxindole derivatives have been shown to be protein kinase inhibitors[98] which have been implicated as being involved with AD pathology.[93] Additionally, compounds containing the isatin privileged scaffold have been used to inhibit caspase-3, also known as cysteine aspartyl-specific proteases,[91,99-101] which has also been woven into the web of pathology leading to AD.

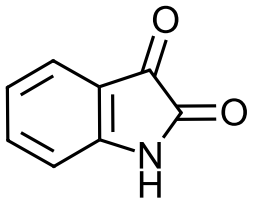

23

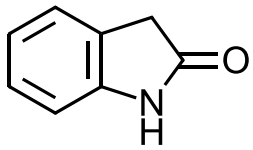

24

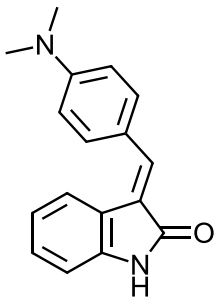

25

Based on the usefulness and success of isatin (**23**) and oxindole (**24**) in pharmaceuticals, linking a radioactive tag to such scaffolds could lead to the next imaging agent or even a drug for Alzheimer's disease. Since the nitrogen atom of these heterocycles represents a convenient linkage point through N-alkylation, one might envisage appending the fluorine tag via a simple fluoroethyl linker (e.g., **26**)[102,103] or via a polyethylene glycol spacer as in **27**.[104,105] Since modulating the lipophilicity of PET imaging is often a critical factor in terms of cell entry and/or wash out from the brain, the fluoroethyl group might possibly make the targeting molecule too lipophilic.[102] Rapid wash out from non-specific binding sites is necessary to obtain good resolution in the PET image.[106] Introducing the polyethylene glycol moiety between the molecule and the fluorine tag decreases lipophilicity, however the size of such a linker might preclude binding to certain targets.[102,104,105] A third option that is becoming rather popular is using fluorethyl azide to introduce the tag to a molecule charged with a propargylic moiety by "click" chemistry leading to a triazole based linking moiety such as **28**.[103, 107-111]

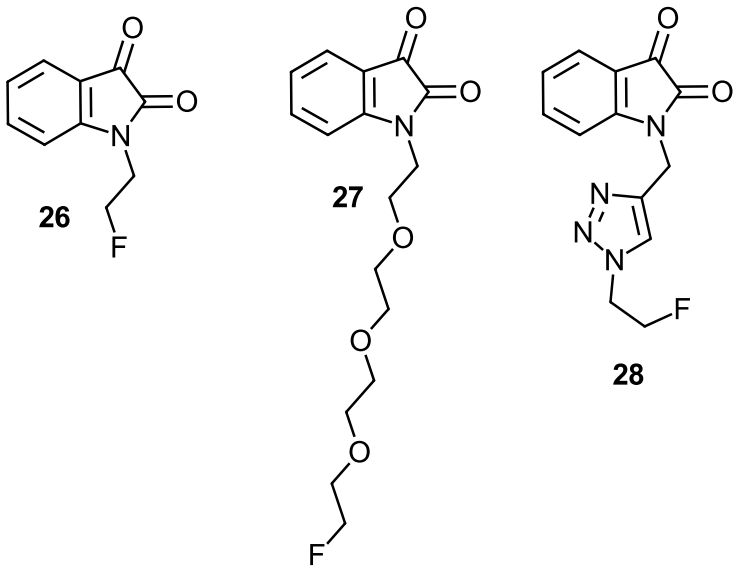

Positron Emission Tomography

Positron emission tomography (PET) is an imaging technique that utilizes compounds labeled with a positron emitting radioisotope in order to image and measure biochemical processes in vivo.[112-114] Rapid development of PET has occurred since the 1970's with advances in detector systems, improved computing capabilities, and advances in radiochemistry.[115] Imaging agents that have been developed to date are often labeled with ^{11}C or ^{18}F. Half-life of the radioisotope is an important characteristic to consider. At a mere 20.4 min the half-life of a ^{11}C labeled compound requires that a facility wishing to employ it to have an on-site cyclotron for production. The half-life of ^{18}F, at 109.7min, is more than 5x longer allowing imaging agents bearing this reporter to be shipped to distant facilities after production. This quality alone makes ^{18}F label more desirable in most cases.[113]

The development of safe and selective fluorinating agents has allowed for fluorine to be incorporated into more organic molecules and thus the use of fluorine in

pharmaceuticals has increased.[116] Even with the increase in incorporating fluorine into more molecules, introducing radioactive fluorine into a molecule for use with PET imaging still comes with challenges.[116,117]

Radioactive fluorine is produced in two forms: the electrophilic form and the nucleophilic form. The nuclear reaction $^{20}Ne(d, \alpha)\ ^{18}F$ produces $[^{18}F]F_2$ after the addition of fluorine-19 carrier gas to remove the very reactive electrophilic form from the target. The addition of the carrier gas decreases specific activity and maximum radiochemical yield because for each reaction there is only a 50% chance that the radioactive electrophilic flourine will react. This reaction is used only when specific activity is not a concern. The $^{18}O(p, n)^{18}F$ reaction is used much more often because it employs an enriched water target with can be regenerated when the nucleophilic form, $[^{18}F]F^-$, is trapped on an exchange resin (commonly K_{222}). This reaction provides the nucleophilic form of fluorine-18, which has high specific activity, in high yields.[113,114,117]

Standard strategy for identifying new potential pharmaceutics involves screening a library of compounds for binding to target (biomarker) and finding optimal candidates. Then, if a fluorine group was not already present in the precursor molecule, part of the molecule would be removed so as to append a fluorine containing prosthetic group. This standard strategy is inconvenient because the molecule would have to have biological and physical properties re-evaluated.[118] This is where the novel idea of Proxy-PET building blocks will be very helpful.

The idea of Proxy-PET is focused on creating entire libraries of compounds that are readily available for screening, as well as being potential imaging agents, by using

only a few building blocks with cold fluorine incorporated. The building blocks could be attached to various compounds to create a new library of potential PET imaging agents before screening the library of compounds for binding to target biomarker. If a molecule has the desired properties, the ^{18}F can replace the "cold" fluorine and no additional testing would be required because the physical and biological properties will not affected.

Results and Discussion

The goal of this project was, first and foremost, to develop "cold" versions of potential diagnostic PET imaging agents for use in Alzheimer's disease in which the requisite fluoro "tag" (*vide infra*) would be appended to the targeting agent via a triazole prosthetic group. In the event that the triazole linker impeded binding to the anticipated target (tau), these molecules would be studied for alternate purposes such as imaging caspases or other targets relevant to AD.

In order to image a biological target with a PET scan, a targeting agent with a radioactive reporter tag such as ^{18}F or ^{11}C must first be administered to the patient (usually intravenously), the imaging agent should then bind to some target of diagnostic relevance and the photons emitted upon positron annihilation be detected. The ^{18}F isotope has become the radiolabel most commonly used with PET imaging because of its biologic and physical properties as discussed previously. One might imagine two scenarios by which a radioactive ^{18}F-tag might be incorporated into an imaging agent. In the first situation, an ^{18}F-atom might be substituted in place of a fluorine atom already present in a targeting agent with a demonstrated affinity for the target of interest. Alternatively, an ^{18}F-atom might be appended to the targeting agent by means of some prosthetic or linking group which ideally would not impede affinity for the target. However, since less than 30% of molecules of therapeutic interest contain fluorine in their structure; appending fluorine to a structure is the most commonly employed

stratagem, although this sometimes changes the physical and biological properties of the composite molecule possibly rendering it inactive.[117]

As many groups recently have also done as a means of appending the fluorine tag, we chose to explore the use click of chemistry, specifically, the **Cu**(I)-catalyzed **a**zide-**a**lkyne 1,3-dipolar Huisgen **c**ycloaddition (CuAAC).[118]This copper mediated reaction was first demonstrated by Sharpless and Meldal[119,120] to regioselectively produce 1,4-disubstituted-1,2,3-triazolesand has become increasingly popular as a means of rapidly introducing radiolabeled tags for use with PET. Azides and alkynes are essentially inert to most biological conditions and will only react with each other;[119,121] a feature termed *orthogonality*. Additionally they are small in size and can easily be introduced into organic compounds.[121,109]

In developing an imaging radiotracer by the "click labeling" process, a library of compounds is normally synthesized around a certain targeting scaffold and screened for optimal binding to a relevant diagnostic cellular target. Upon identification of an optimal binding substrate, an alkynyl substituent is introduced at some position deemed non-critical for binding, whereupon the triazole linked ^{18}F-reporter can be introduced by a click process with [^{18}F]fluoroethyl azide ([^{18}F]FEA) (*vide infra*) and the radiolabeled composite molecule then reassessed for affinity to the target.[118]

In order to avoid the possibility that introduction of a radiolabeled prosthetic group interferes with binding to the ultimate biological target in the normal discovery paradigm, the so-called *Proxy-PET* concept was developed at WSU and detailed herein. This new discovery mode for PET imaging agents takes the prospective view that since

the commonly employed fluoroethyl triazole appendage must be present in any eventual imaging agent based upon this prosthetic group, building blocks incorporating "*cold"* versions of this requisite feature might be prepared and utilized early on in the discovery process. With such a cold reporter group present in the initial binding assays it can be readily appreciated that an optimal targeting agent, once discovered, represents the *de facto* PET imaging agent when prepared with an ^{18}F-reporter.

It is important to consider why the 1,2,3-triazole group would make a good prosthetic group to append the fluorine tag into a molecule. The 1,2,3-triazole moiety possesses a moderate dipole character as well as hydrogen bond acceptor capabilities due to the ring nitrogen atoms, and is stable under *in vivo* conditions. Additionally, triazoles are resistant to cleavage hydrolytically or otherwise and are almost impossible to oxidize or reduce.[122]Employing the triazole ring as a linker is expected to be advantageous with regard to the pharmacological properties of a molecule because of biologically favorable modifications[110] such as altered lipophilicity and polarity[123] as well as providing a surrogate for the amide bond.[124]

Marik and Sutcliffe were the first to employ the CuAAC reaction to label a protein with ^{18}F-fluorine by coupling 3-azido-propionic acid (**29**) to the *N*-terminus of a protein**30** and then 'clicking' it with a terminal fluoroalkyne **32** to form the triazole as seen on the protein labeled **33**. This illustrated that the CuAAC reaction was a very fast and efficient method to radiolabel peptides/proteins with ^{18}F for targeted imaging using PET.[107] Furthermore, Hausner used the method developed by Marik and Sutcliffe to label a protein and illustrated how the introduction of the triazole ring does, in fact, have a significant impact on the in vivo behavior of a radiotracer by altering the above

mentioned characteristics.[125] The triazole linked ^{18}F-reporter **33** was compared to two analogues capped with typical acyl linkers (e.g. **34** and **35**)which were introduced to the protein **30** at the *N*-terminus via condensation reactions. The fluorinated tag **36** was introduced via a click reaction as described previously. The 3-labeled proteins were injected into mice and *in vivo* characteristics such as concentration in certain organs and metabolism were studied. This was the first time that a radiotracer that had been introduced via CuACC was studied in vivo and it was concluded that the "clicked" radiotracer can be considered comparable to other radiotracers; however there were noticeable differences in pharmacokinetics between each radiotracer underlining the importance of investigation of each linking group.[125]

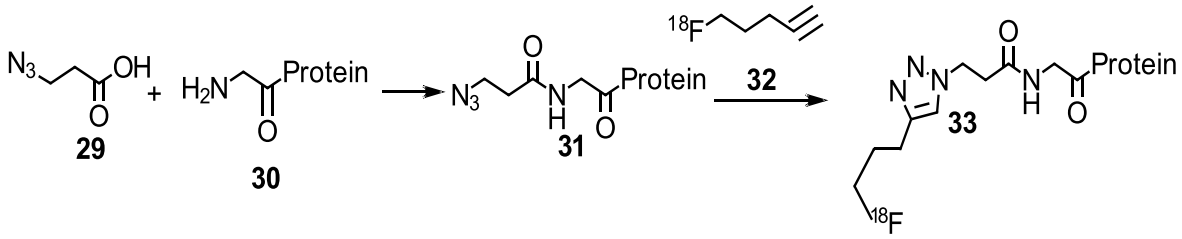

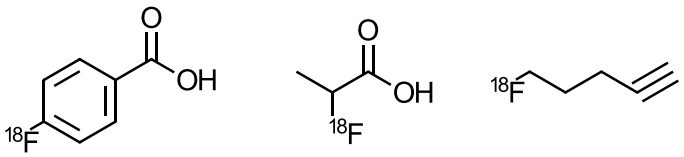

34 **35** **36**

An alternative method to introducing ^{18}F via the CuAAC reaction would be to attach the ^{18}F to the azide moiety as in the case of [^{18}F]fluoroethylazide ([^{18}F]FEA) (**37**), and then clicking with an alkyne that had been pre-installed in a protein (e.g. **38**). In 2007, Glaser and Aarsted first synthesized [^{18}F]FEA by nucleophilic fluorination of 2-azidoethyl-4-toluenesulfonate (**40**) with anhydrous no-carrier-added Kryptofix 2.2.2

$K^+[^{18}F]F^-$.This was done in acetonitrile (ACN) and after 15min the [^{18}F]FEA was isolated via flow-and-trap process.[103] Other groups have developed alternative syntheses of [^{18}F]FEA over the years, but all involved some sort of distillation procedure to purify the product such as flow-and-trap or vacuum trap-to-trap. In 2015, Zhou et al. developed a method to synthesize and isolate [^{18}F]FEA without distillation. A series of solid phase extraction cartridges were used to purify the radioisotopically labeled FEA (that had been synthesized in the same method as previously described) to increase radiochemical yields and provide a possible platform to perform the click reaction.[126]

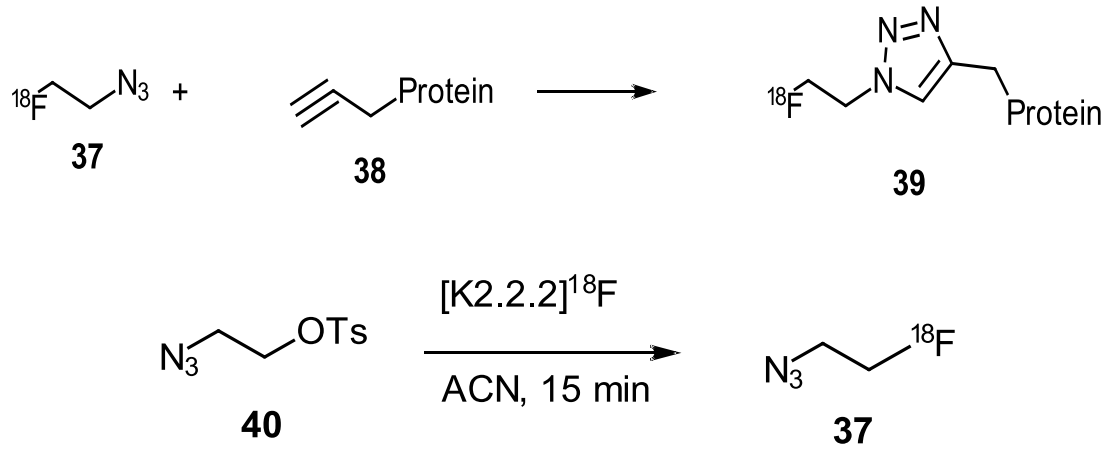

The examples cited so far involved reporter groups that were introduced onto a peptide but there is interest in labeling small drug like molecules. In 2009, Nguyen et al. developed the first small molecule that was labeled with ^{18}F via the CuAAC reaction. The molecule that Nguyen developed was prepared from an isatin 5-sulfonamide derivative **41** that had been *N*-alkylated with propargyl bromide and then clicked with [^{18}F]FEA (**37**) in the presence of $CuSO_4$ and sodium ascorbate to yield **42**. This molecule was found to be an effective caspase-3 specific radiotracer to image tumor apoptosis.[127] This

discovery was especially important for many reasons. One, it showed that a small molecule could be labeled with the triazole linker.[108] Moreover, the small molecule entailed a scaffold which was one of the backbones to which we envisioned attaching our building blocks.

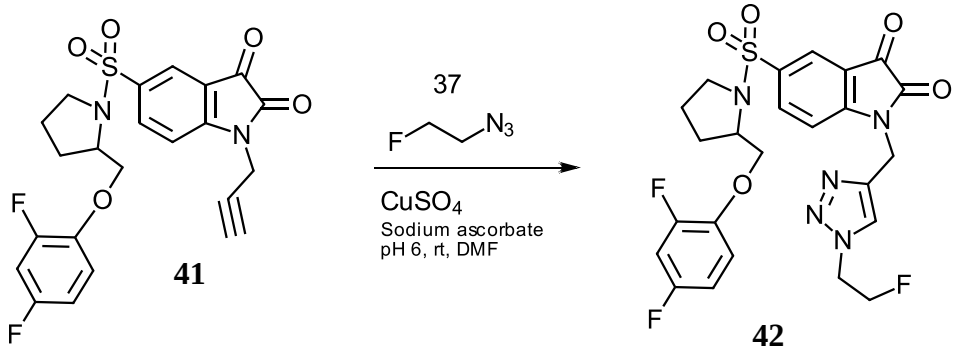

41 **42**

As stated at the outset, we envisioned synthesizing cold "building blocks" using click chemistry. The term building block was used because these molecules would incorporate a non-radioactive FEA moiety into a molecule (via the CuAAC reaction) that would also contain a linking functionality that would be used to append the "block" onto other molecules. The development of these building blocks as well as how and why they were introduced to other molecules will be detailed within this section.

Before a fluorine containing building block could be produced, it was necessary to develop an efficient synthesis of 2-fluoroethyl tosylate (**45**). Once in hand, it was anticipated that it could later be reacted with NaN_3 and a propargyl moiety in a one pot synthesis to produce the desired triazole containing building blocks.

To this end, 2-fluoroethanol (**43**) was treated with *p*-toluenesulfonyl chloride (**44**) in the presence of triethylamine in EtOAc to produce 2-fluoroethyl tosylate(**45**).

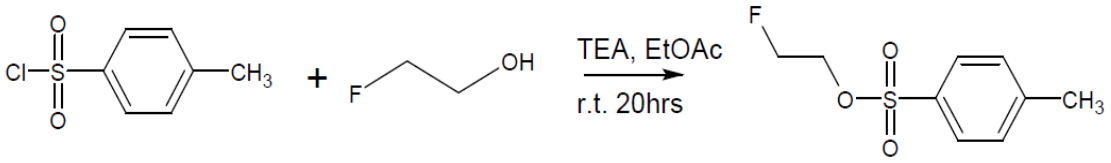

44 **43** **45**

This method was modified from a preparation described by Shealy in a U.S. patent.[128]The original method called for tosyl chloride (**44**) to be added to EtOAc chilled in an ice bath and then 2-fluoroethanol (**43**) and triethylamine (premixed) were to be added dropwise over 30min, the reaction stirred in an ice bath for 3h and then put in the refrigerator overnight. The next day the triethylamine hydrochloride that had formed would be filtered off and the filtrate diluted with hexane to induce precipitation of the product. The modified method consisted of adding all the reagents except for the 2-fluoroethanol (**43**), which was then added dropwise over 15 min, after which time the reaction was stirred at rt for an additional 20 h. The product was then purified via column chromatography using hexanes:ether (1:1). Due to reoccurring low yields, three initial samples of this product were combined for characterization and the ^{1}H and ^{13}C NMR as well as GCMS spectra of this composite mixture were obtained.

In the ^{1}H NMR spectrum of **45** (Figure 2), the multiplet at 7.84-7.80 ppm, labeled **c** represents the two H's on the aromatic ring closest to the SO_2, whereas the multiplet **d** at 7.39-7.36 ppm corresponds to the two H's on the aromatic ring nearest the methyl group. Both of these peaks are expected to be doublets and one can see they resemble doublets with a few extra tiny peaks at the base of each peak. The four multiplets labeled **a** and **b** between 4.68 and 4.31 ppm correspond to the four H's on the ethyl moiety. There are four multiplets instead of two because of the splitting caused by the fluorine atom.

The two multiplets labeled **a** represent the two hydrogens on the carbon adjacent to the fluorine, while the multiplets labeled **b** are the hydrogens on the carbon adjacent to the oxygen. These peaks are expected to be doublets of triplets due to splitting by the fluorine (doublet) and by neighboring methylene hydrogens (triplet). It can be seen in the spectrum that the pattern is consistent with doublets of triplets (with a few additional peaks represented within each triplet). Finally, the singlet, **e**, at 2.47 ppm integrates to 3H and represents the H's of the methyl group.[129]

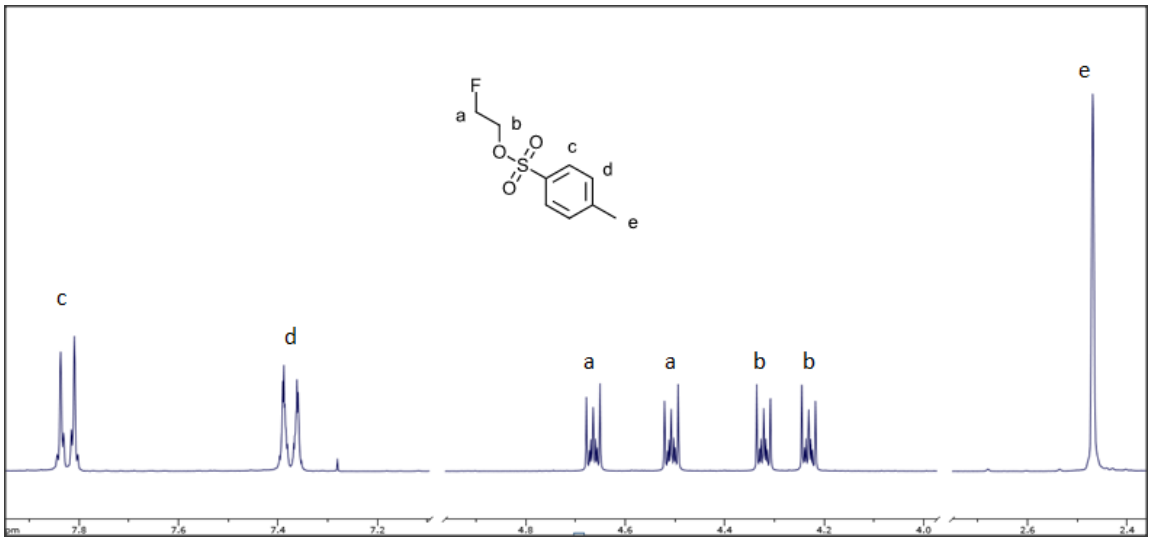

Figure 2- ^{1}H NMR Spectrum of 2-fluoroethyl tosylate (**45**)

The ^{13}C NMR of **45**, Figure 3, shows nine peaks when there are only seven unique carbons. This is because of splitting caused by the ½ spin interaction of the two carbons closest to the fluorine. The set of peaks labeled **a** and **b** are actually doublets and represent the two CH_2 carbons ($J_{C\text{-}F}$=173.5 Hz and $J_{C\text{-}F}$=21.23 Hz respectively). The peak at 145.1 ppm labeled **c** represents the quaternary carbon with the same label; it is furthest downfield because of its proximity to the sulfonyl group. The peak labeled **f**,

represents the quaternary carbon adjacent to the methyl group. The peak at 129.9 ppm labeled **d** represents two carbons on the aromatic ring closer to the sulfonyl group and the peak at 127.9 ppm labeled **e** represents the other two carbons on the ring ortho to the methyl moiety. Finally, the peak at 21.6 ppm, **g**, represents the methyl carbon. The peaks represented match literature values closely.[129]

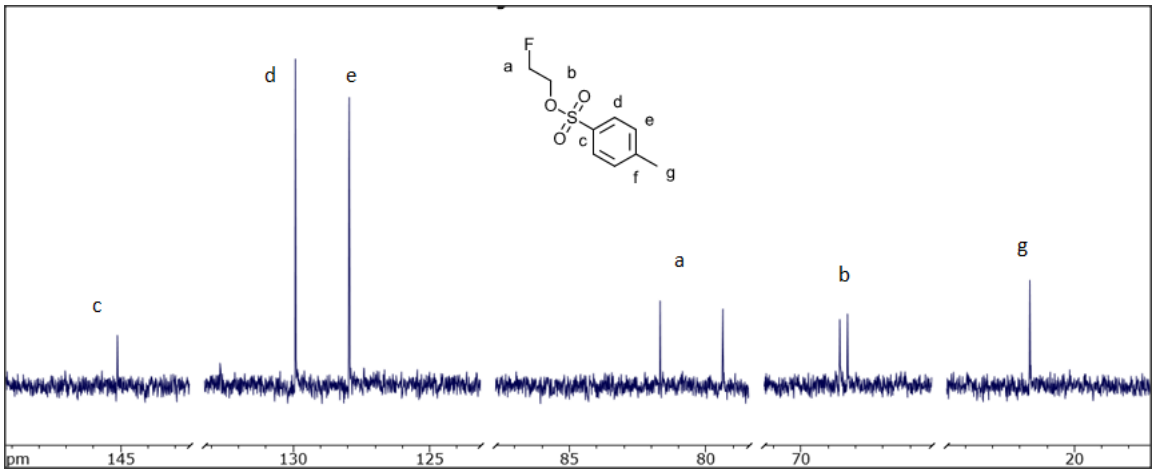

Figure 3- ^{13}C NMR spectrum of 2-fluoroethyl tosylate (**45**)

As mentioned earlier, our group could initially only obtain this product in low yield and thus it was deemed necessary to purchase 2-fluoroethyltosylate (**45**) (ChonTech). Although this molecule was relatively expensive to purchase, the 2-fluoroethanol (**43**) starting material was also costly and one would need a 50% yield every time to make buying the starting material more cost effective than buying the product. Most of the molecules made using 2-fluoroethyl tosylate (**45**) in this thesis were made using the purchased variety versus the synthesized variety. However, since we initially tried to make 2-fluoroethyl tosylate in 2013, an intern in our lab (John van Vliet) found an alternative method which provides the 2-fluoroethyl tosylate in 70% yield.[130]

To gain experience with performing click reactions, before using the expensive 2-fluoroethyltosylate, a known compound **49** was synthesized to test reaction parameters. The compound was produced by reacting benzyl bromide (**46**) with sodium azide (**47**) and propargyl alcohol (**48**) in the presence of copper sulfate and sodium ascorbate in, at first, $^{t}BuOH/H_2O$ as a solvent based on reactions reported by Fokin and Sharpless.[119] While these authors used copper sulfate and sodium ascorbate in catalytic amounts of 1 mol % and 5 mol %, respectively, we chose to increase the proportions of these species to 5 mol % and 10 mol % as described by Rivero.[131] Although this reaction was successful, yields at first were not particularly desirable, ranging from 3% to 33.3%. In looking for ways to improve upon this process, we noted that several groups had success synthesizing 1,2,3-triazoles in the most environmentally friendly solvent, H_2O.[132-134] Of the groups that used H_2O, Kacprzak[134] utilized the $CuSO_4*H_2O$ and sodium ascorbate catalyst system as described previously, however the other groups employing water used different catalysts such as Cu/C and Cu(II) acetate.[132,133] Unfortunately, in the present work, when the reaction was attempted using water as the only solvent, the reaction was unsuccessful. A group in 2007 had performed this same reaction in $EtOH/H_2O$ (1:1) in the presence of triethylamine (TEA)[135] and obtained almost 100% yield. Attempting this reaction under those conditions led to production of **49** in greater than 90% yield.

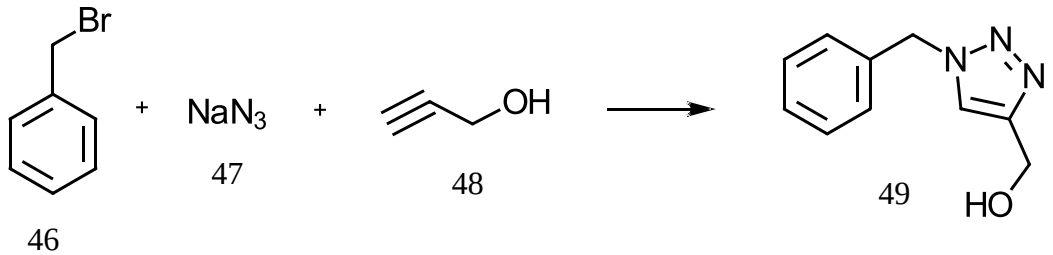

46 47 48 49

The structure of **49** was confirmed via ^{1}H and ^{13}C NMR; further evidence was corroboration with literature melting point and published NMR data.[131]Comparison of experimental data to data of a fully characterized product confirmed 1-benzyl-4-(hydroxymethyl)-1*H*-1,2,3-triazole (**49**) had been produced.

In the ^{1}H NMR spectrum of **49** ($CDCl_3$) the peak labeled **e**, at 7.47 ppm, is a singlet representing the proton on the triazole ring. The multiplet at 7.40-7.31 ppm represents three (**a**, **b**, **b**,) of the protons on the benzene ring while the multiplet at 7.28-7.21 ppm represents the remaining two protons (**c, c**) on the benzene ring. The benzylic methylene CH_2 (**d**) located between the benzene ring and the triazole ring is represented by the singlet at 5.48 ppm, while the other singlet at 4.7 ppm represents the other CH_2, labeled **f**, adjacent to the alcohol functional group. The protons at **d** were located further down field because of their proximity to the triazole nitrogens. Finally, the hydroxyl proton labeled **g** is represented by the broad peak at 4.0 ppm.

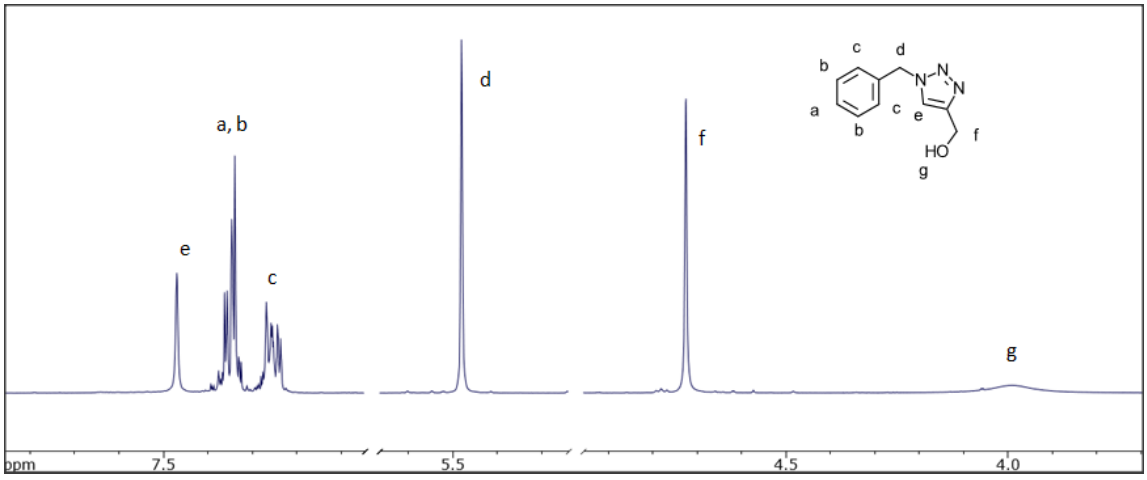

Figure 4- ^{1}H NMR ($CDCl_3$) spectrum of 1-benzyl-4-(hydroxymethyl)-1*H*-1,2,3-triazole(**49**)

Following is another ^{1}H NMR spectrum of compound **49**. This spectrum was collected on compound **2** in DMSO-d_6 rather than $CDCl_3$. There are some noticeable changes when solvents are changed. Most notably the downfield shift of the hydrogen, labeled **g**, of the OH group shows the effect of the DMSO-d_6 on this molecule. This shift is due to the OH group interacting with DMSO-d_6 which is a strong hydrogen bond acceptor.

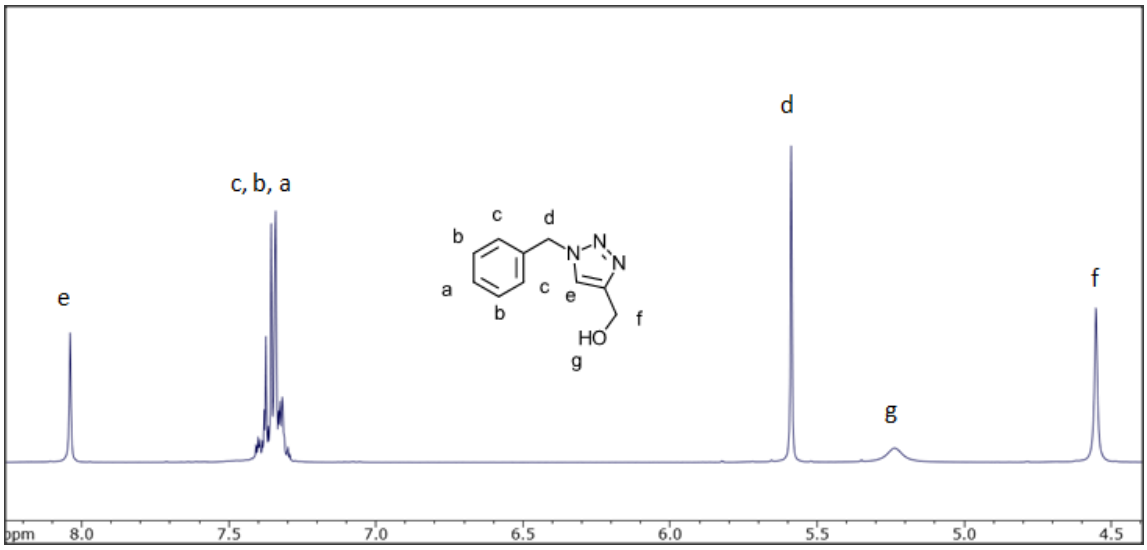

Figure 5- ^{1}H NMR (DMSO-d_6) spectrum of 1-benzyl-4-(hydroxymethyl)-1*H*-1,2,3-triazole(**49**)

The ^{13}C NMR of compound **49,** Figure 6in $CDCl_3$, shows the eight peaks expected. This is because one of the quaternary carbon peaks is not showing up. The quaternary carbon, labeled **g** is predicted to appear at 148.2 ppm,[131] and can be observed in this spectrum at 148.9 ppm. The peak at 136.6 ppm represents the quaternary carbon labeled **d**. Peaks at 129.2, 128.5, and 128.4 ppm represent **c**, **a**, and **b**, five of the carbons on the benzene ring. The peak at 123.3 ppm, labeled **f**, represents the C-H on the triazole

ring**.** The placement of the C-H labeled **f** was determined via a DEPT90 ^{13}C NMR. The carbon of the CH_2 between the rings is labeled **e** and appears at 54.2 ppm, whereas the carbon of the CH_2 adjacent to the OH moiety, labeled **h**, is represented by the peak at 56.1 ppm.

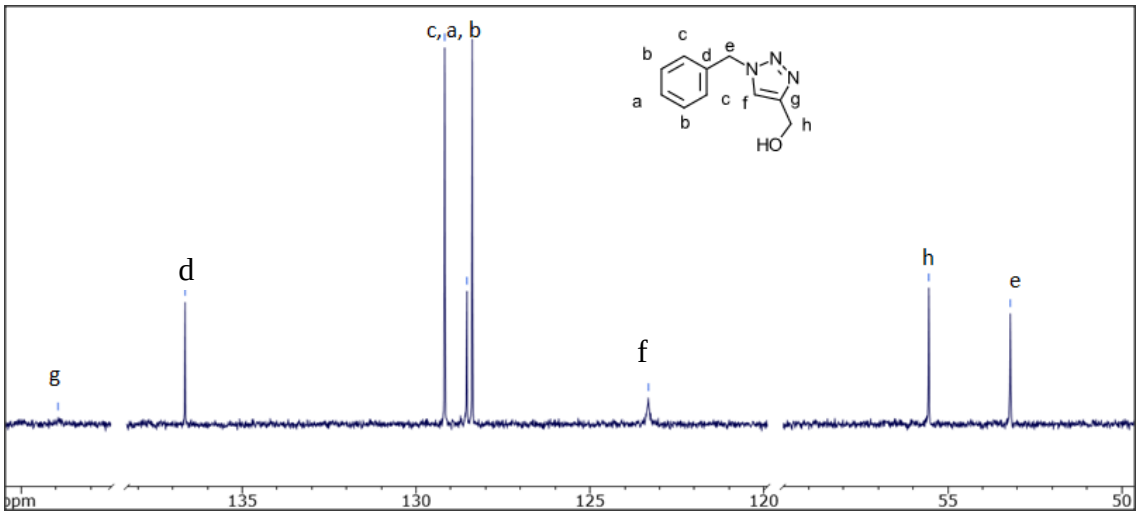

Figure 6- ^{13}C NMR ($CDCl_3$) spectrum of 1-benzyl-4-(hydroxymethyl)-1*H*-1,2,3-triazole (**49**)

As mentioned before, this reaction using the inexpensive surrogate benzylic bromide (**46**) was first attempted using $^{t}BuOH/H_2O$ as solvent and as before initial attempts at the click reaction of propargyl alcohol (**50**) with 2-fluoroethyl tosylate (**45**) and sodium azide in the presence of copper sulfate/sodium ascorbate in $^{t}BuOH/H_2O$ were not encouraging. Upon utilization of the $EtOH/H_2O$ and triethylamine system,[131] [1-(2-fluoroethyl)-1*H*-1,2,3-triazol-4-yl]methanol (**51**) was obtained in good yields [via the intermediacy of fluoroethyl azide (**37**)].This keystone building block, while potentially amenable to Mitsunobu type couplings to substrates, could also be converted to a variety of building blocks upon subsequent reactions.

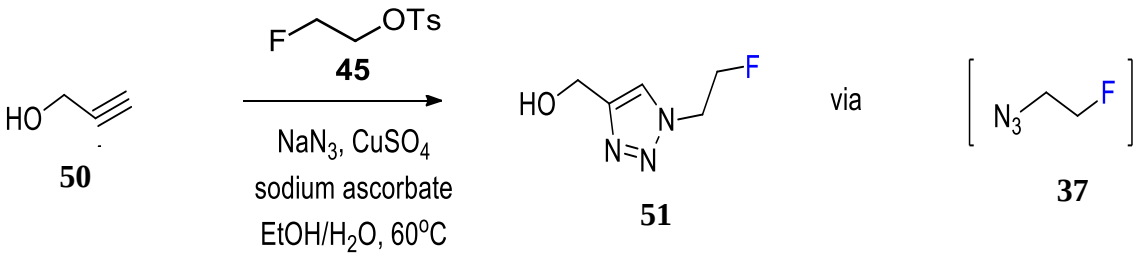

The ^{1}H NMR of compound **51** ($CDCl_3$) shows six sets of peaks due to the splitting caused by the ½ nuclear spin of fluorine.[136,137] ^{1}H has a ½ nuclear spin also which is why the fluorine can cause splitting in the ^{1}H NMR. The singlet peak labeled **c**, at 7.68 ppm, is assigned to the proton on the triazole ring. The multiplet labeled **a**, at 4.87 ppm corresponds to one of the multiplets arising from the CH_2 adjacent to the fluorine. The other multiplet of this group overlaps one of the multiplets from the adjacent CH_2 group labeled **b** and centered at 4.71 ppm. The other multiplet **b** arises from the CH_2 of the ethyl moiety farthest from the fluorine and occurs at 4.62 ppm. The splitting of both sets of methylene hydrogens is attributed to coupling to the adjacent CH_2 group as well as the fluorine atom ipso or one carbon away. These peaks resemble a doublet of triplets, however the splitting is not first order so *J* values cannot be determined. The singlet at 4.79ppm, labeled **d**, represents the two hydrogens next to the hydroxyl group. Finally, the proton of the hydroxyl group is represented by the broad peak labeled **e** at 2.98ppm.

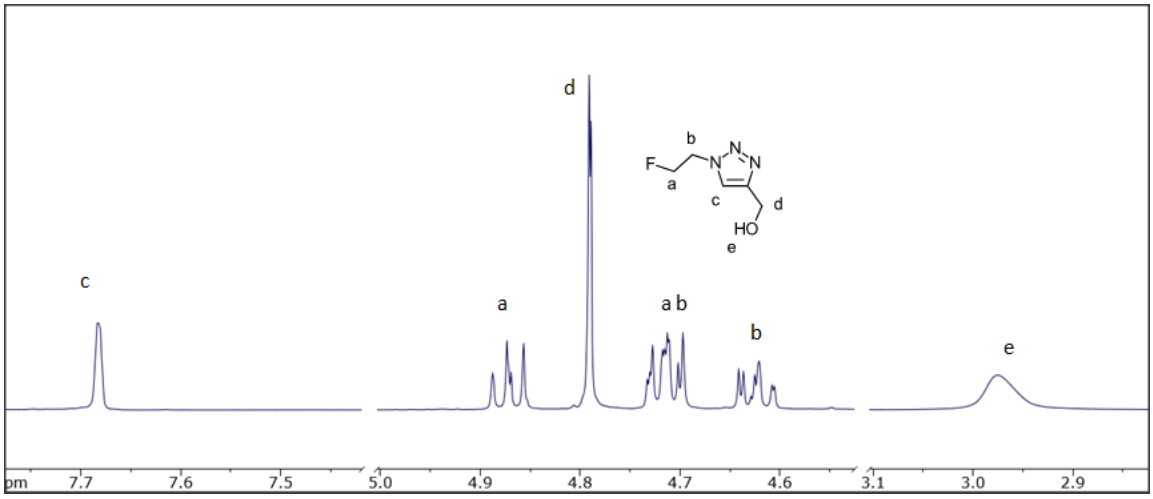

Figure 7- ^{1}H NMR ($CDCl_3$) spectrum of 1-(2-fluoroethyl)-1*H*-1,2,3-triazol-4-yl]methanol(**51**)

Again, upon switching solvent to DMSO-d_6, changes are observed in the spectrum. Unlike the case of compound **49**, where only minor changes upon switching solvents were observed, there are significant changes in the spectrum of compound **51** in DMSO-d_6. Most notable again is the change in the hydrogen labeled **e** (the hydroxyl hydrogen); once a singlet at 2.98 ppm in $CDCl_3$, it now appears as a triplet at 5.22 ppm ($J_{H\text{-}H}$=5.65 Hz). The chemical shift of the protons labeled **d** adjacent to the OH group was also affected: as the singlet at 4.79ppm is now a doublet at 4.52 ppm. The splitting ($J_{H\text{-}H}$=5.58 Hz) is caused by the coupling to the adjacent hydrogen labeled **e**.

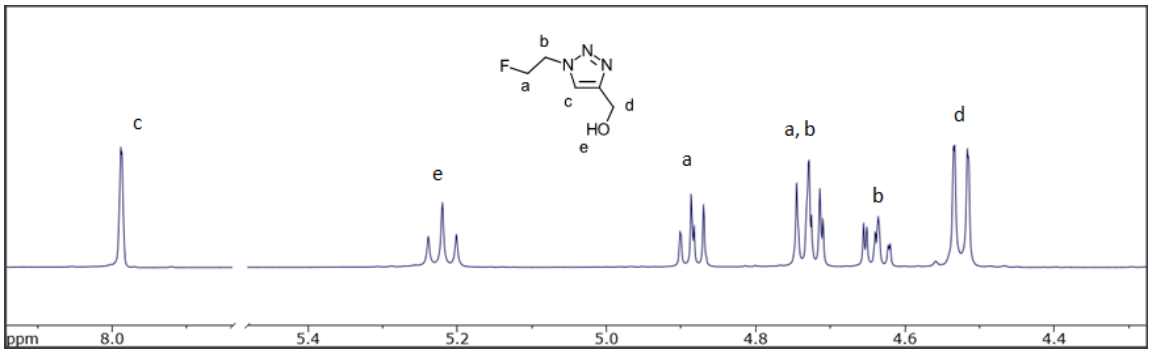

Figure 8- ^{1}H NMR (DMSO-d_6) spectrum of 1-(2-fluoroethyl)-1*H*-1,2,3-triazol-4-yl]methanol (**51**)

The ^{13}C NMR ($CDCl_3$) of compound **51** shows seven peaks when only five carbons are present in the molecule. This is due to the two CH_2's between the triazole ring and the fluorine being split each other as well as by the fluorine. The most downfield peak at 148.1 ppm, labeled **d,** represents the quaternary carbon in the triazole ring. The peak labeled **c,** at 122.8 ppm, is assigned to the other carbon in the triazole ring. These carbons were assigned based on where they appeared in compound **49**. The doublet at 81.5 ppm, labeled **a**, is the carbon adjacent to the fluorine ($J_{C\text{-}F}$=177.9 Hz). Greater splitting is observed with carbon **a** than at the carbon labeled **b**, at 50.5 ppm ($J_{C\text{-}F}$ =20.5 Hz) because of the proximity to the fluorine. The C adjacent to the OH group is labeled **e** and represented in the spectrum at 56.2 ppm.

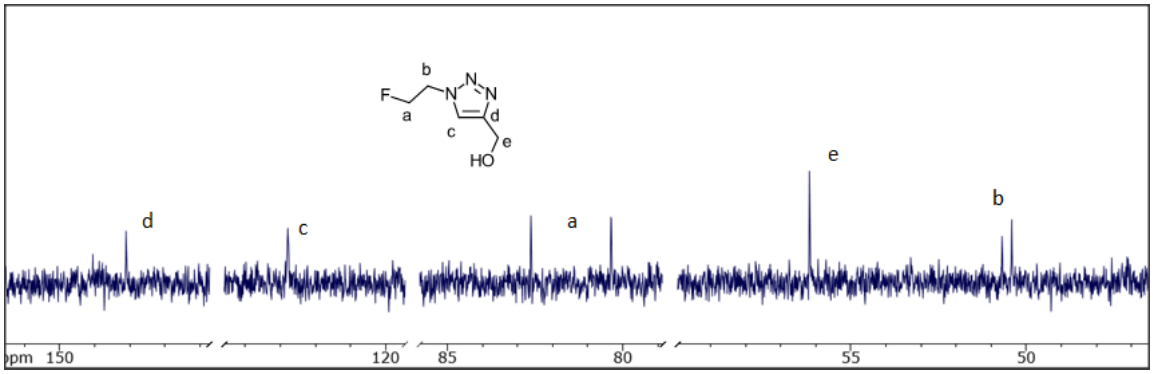

Figure 9- ^{13}C NMR ($CDCl_3$) spectrum of 1-(2-fluoroethyl)-1*H*-1,2,3-triazol-4-yl]methanol (**51**)

Having this primary building block in hand, it was envisaged that **51** might be convertible to alternative functionalities (*e.g.*, carboxylic acid, aldehyde, halide or

tosylate) by a series of simple reactions. First though, we again turned to the benzyl surrogate **49** to test out methods, making sure they would work with a similar more robust molecule before attempting the reactions on **51**.

Oxidation of **49** with MnO_2 led to smooth conversion to the corresponding aldehyde**52**while reaction with PBr_3 afforded the alkyl bromo derivative **53**. Since it was believed that the carboxylic acid **56** could be prepared from the analogous click reaction involving propiolic acid (**54**), an oxidative route to **56** was not explored.

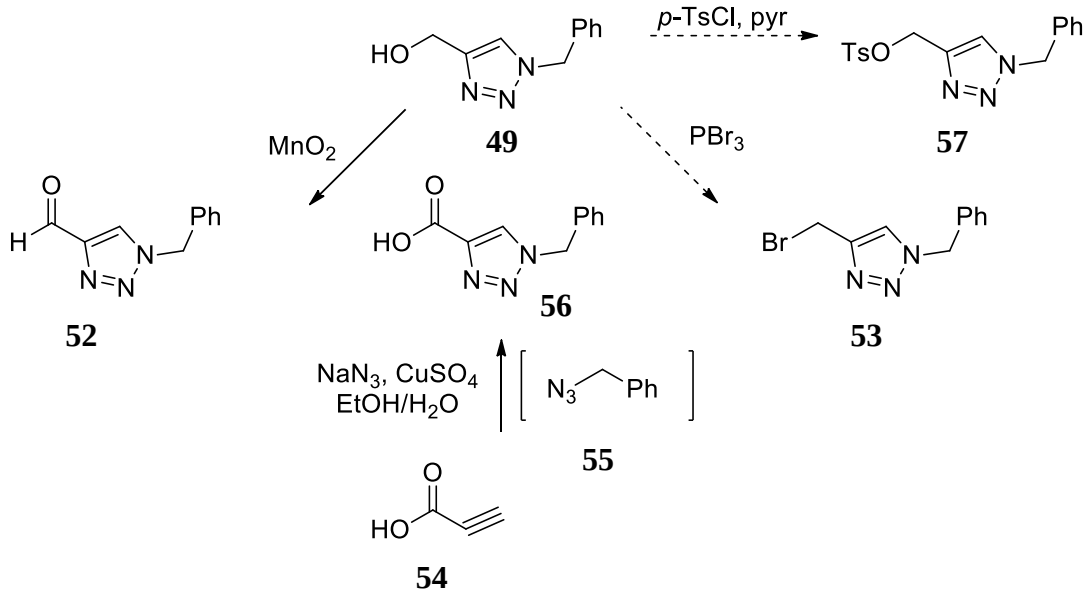

Scheme 1

Treatment of compound **49** with MnO_2 in dichloroethane (DCE) for 18h at 80°C yielded the aldehyde **52** in 73% yield. Anticipated uses of such triazole aldehydes include appending to substrates via aldol type reactions or via reductive amination processes. The ^{1}H NMR of compound **52** (DMSO-d_6) confirms that the alcohol derivative **49** was in fact oxidized to the aldehyde **52** since there is no longer a broad OH peak and there is only

one CH_2 signal represented. The benzene carbons are represented by the multiplet labeled **a** (7.39-7.35 ppm), and the CH_2 between the benzene ring and the triazole ring is still near where it was before moving from 5.59 ppm in compound **49** to 5.71 ppm (peak **b**) in compound **52**. The peak at 10.03 ppm, labeled **d**, represents the proton that is part of the aldehyde functional group. Finally, proton **c** representing the proton on the triazole ring appears at 9.00 ppm.

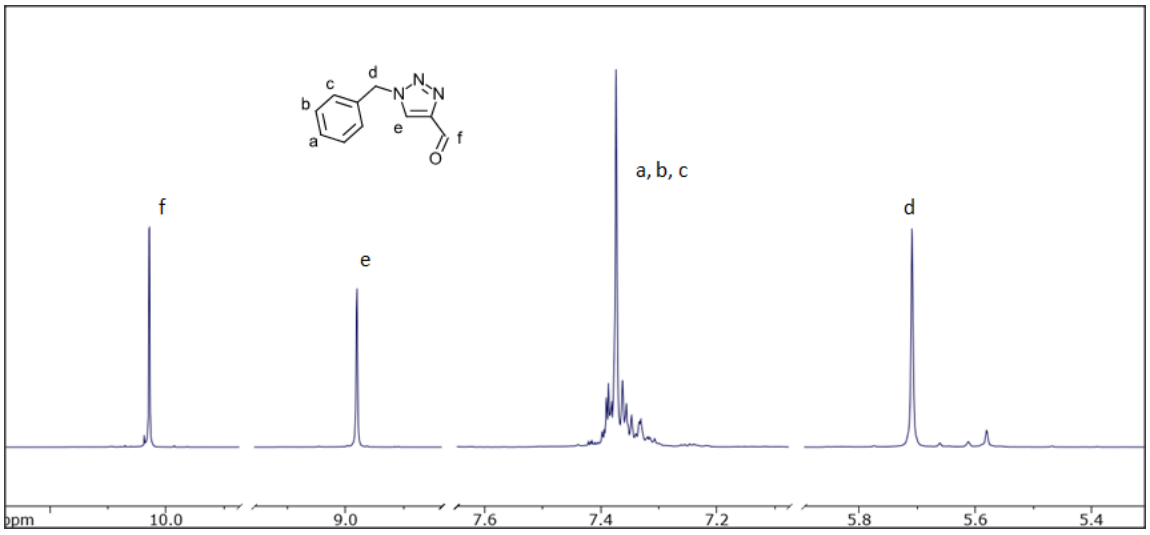

Figure 10- ^{1}H NMR spectrum of 1-benzyl-4-(carboxaldehyde)-1*H*-1,2,3-triazole (**52**)

The ^{13}C NMR spectrum also confirms the production of the compound **52**. Carbon **h** is furthest downfield appearing at 185.4 ppm which is typical of an aldehyde carbonyl group. The quaternary carbon in the triazole ring is represented at 147.5 ppm and labeled **g**. The peak labeled **f** corresponds to the CH in the triazole ring and is at 135.8 ppm. The carbon labeled **g** is shifted further downfield because of its proximity to the aldehyde. The four non-equivalent benzene carbons are represented as follows:129.3 ppm, peak **c**, 128.8 ppm, peak **d**, 128.7 ppm, peak **a**, and 128.6 ppm, peak **b**. Finally, the carbon between the two rings, **e**, appears at 53.7 ppm.

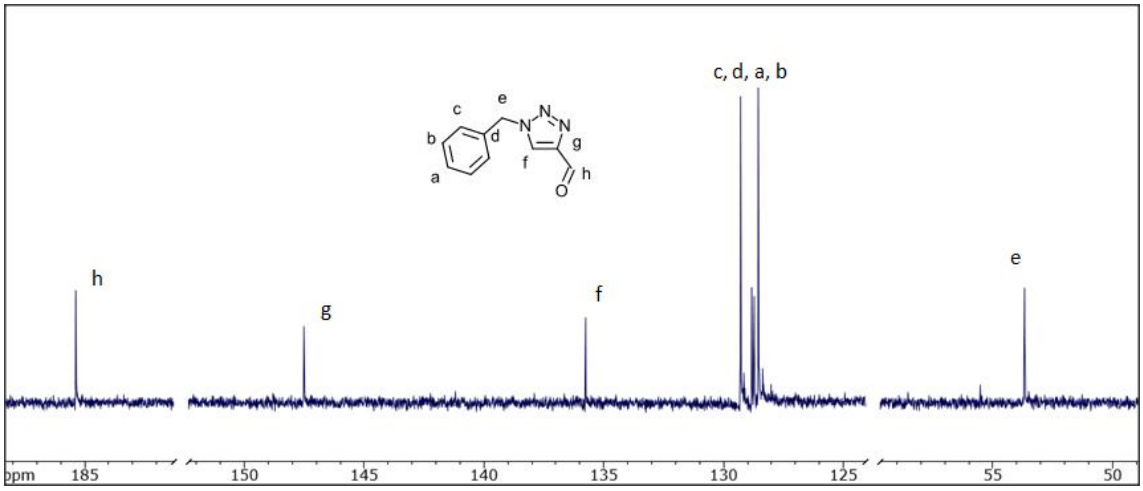

Figure 11- ^{13}C NMR spectrum of 1-benzyl-4-(carboxaldehyde)-1*H*-1,2,3-triazole (**52**)

The bromo derivative **53** was produced by adding **49** to PBr_3 in DCM. The ^{1}H NMR and ^{13}C NMR spectra confirm the production of compound **53**. The ^{1}H NMR spectrum shows the absence of the broad hydroxyl peak, which is the only major difference from the ^{1}H NMR spectrum ($CDCl_3$) of the starting material.

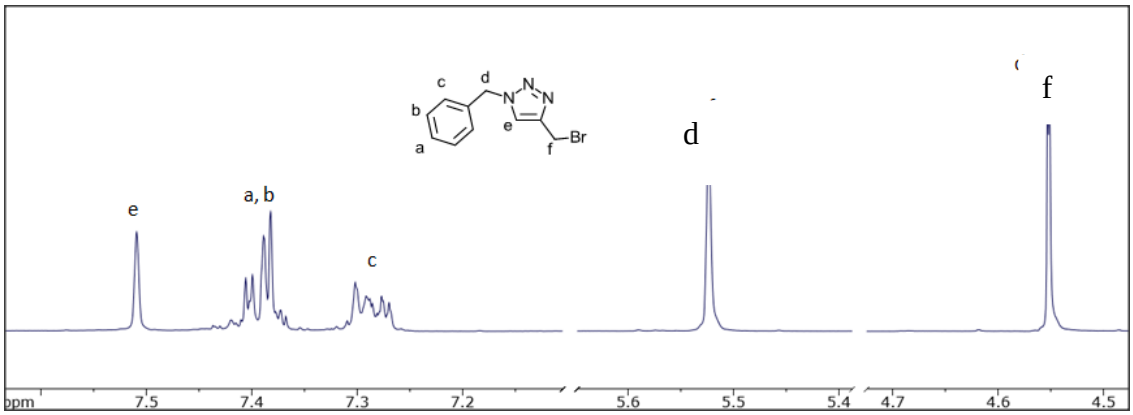

Figure 12- ^{1}H NMR spectrum of 1-benzyl-4-(bromomethyl)-1*H*-1,2,3-triazole (**53**)

In the ^{13}C NMR spectrum of compound **53** all the peaks remained unchanged from the starting material **49** except for the carbon **h**. In the starting material **49**, the

carbon was next to a hydroxyl group whereas now it is adjacent to bromine. Carbon **h** is now represented at 21.5 ppm when before it appeared at 56.1 ppm. However, in this spectrum peak **g** (145.0 ppm) representing the quaternary carbon in the triazole ring is present more clearly.

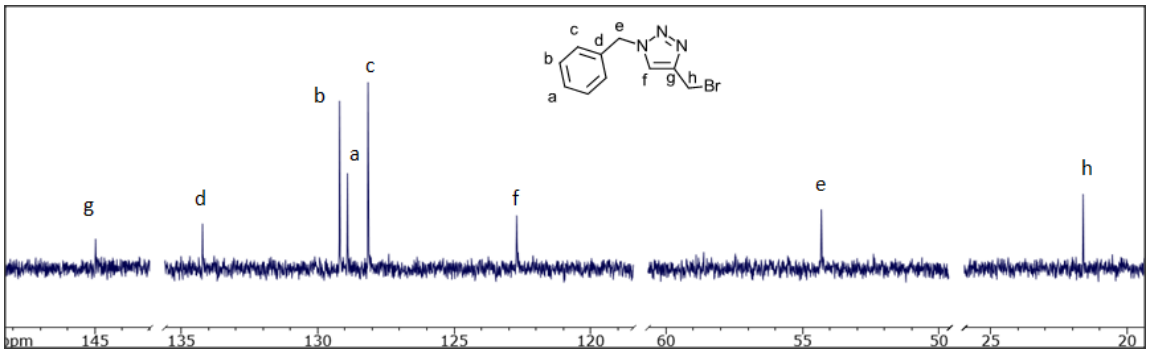

Figure 13- ^{13}C NMR spectrum of 1-benzyl-4-(bromomethyl)-1*H*-1,2,3-triazole (**53**)

It is interesting to note that while this bromomethyl compound was originally made as a surrogate to examine the critical reaction process and the functional group interconversion of an alcohol to a bromo derivative, this group could also be used to practice the *N*-alkylation of an isatin to yield a triazole linked potential imaging agent. It turns out that this triazole moiety had already been put at the *N*-position of isatin but not by the same method as employed herein. The other group first *N*-alkylated with propargyl bromide and then clicked on the benzyl azide **55** moiety.[138] Discussion of how and why **53** was introduced onto isatin will follow.

The method used to produce compound **49** was again used to produce the acid derivative **56**. The only difference was that propiolic acid **54** was added in place of propargyl alcohol. The workup was a little different too, in that with compound **56**, since HCl was used to acidify the aqueous layer to extract more product into the organic layer.

The ^{1}H NMR of compound **56** confirms that a compound containing a triazole ring was produced however not necessarily the carboxylic acid. The multiplet labeled **a**, **b**, **c** represents the protons on the benzene ring. The hydrogen, labeled **f**, associated with the carboxylic acid moiety is not represented in this ^{1}H NMR. If it were to be visible it would appear at about 11.4 ppm as a broad peak. A broad peak in this region was detectable but only upon peak enhancement. Based on this data it cannot be confirmed that the carboxylic acid was produced.

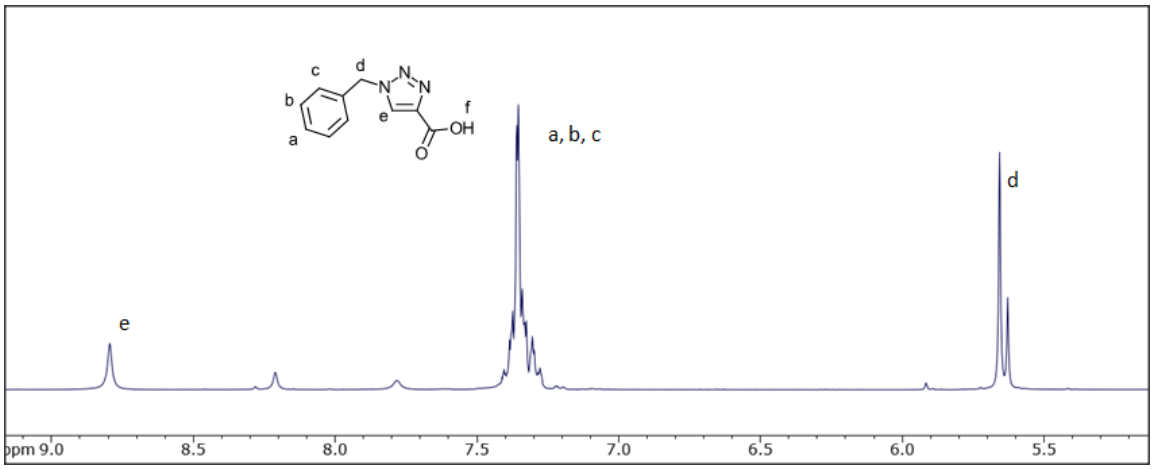

Figure 14- ^{1}H NMR spectrum of1-benzyl-1H-1,2,3-triazole-4-carboxylic acid (**56**)

The ^{13}C NMR of compound **56** also differs from compound **49** but it does not definitively confirm the presence of the carboxylic acid functionality. The patterns in which the peaks appear in this spectrum are different than those of the alcohol derivative **49** however they do not confirm the product was produced. The melting point of the product **56** was much higher than the alcohol **49** which indicated that the acid had been produced; however the melting point of the product was lower than the literature melting point.

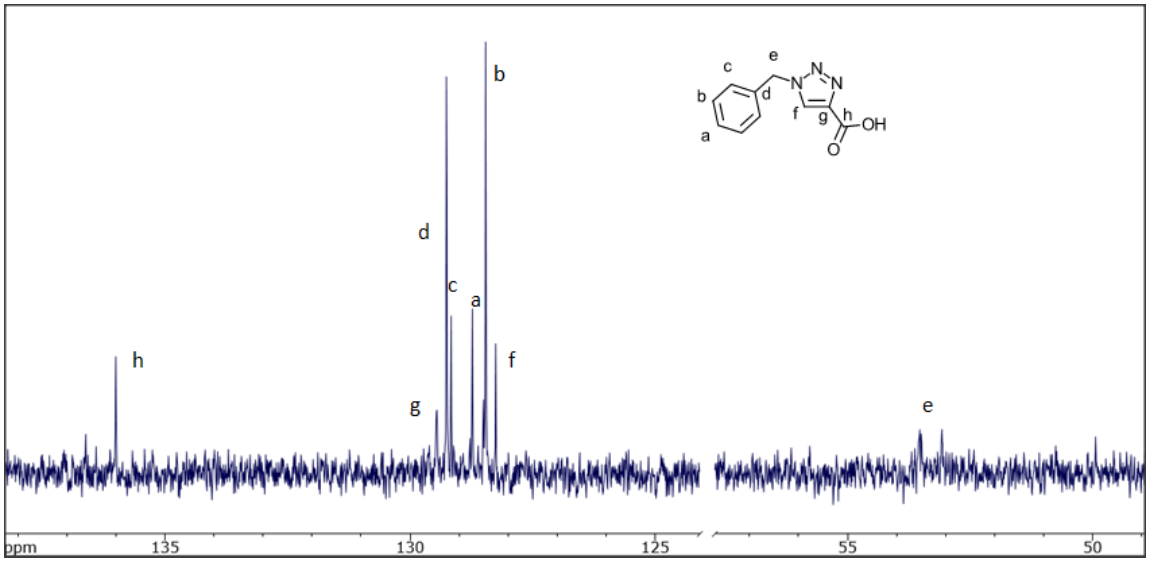

Figure 15- ^{13}C NMR spectrum of 1-benzyl-1H-1,2,3-triazole-4-carboxylic acid (**56**)

The carboxylic acid would be potentially useful to cap a peptide as shown in the example reaction on page 24. However, we did not use the compound in any subsequent reactions because peptides were not used in this thesis.

After it was determined that the MnO_2 and PBr_3 reaction worked well with the benzyl surrogate, to develop additional building blocks the reactions were attempted with the desired fluoroethyl derivative **51**. Although oxidation with MnO_2 led to smooth conversion to the corresponding aldehyde **58**, reaction with PBr_3 failed to efficiently afford the bromo derivative **59**. The carboxylic acid derivative **60** was prepared via addition of propargylic acid (**54**) to fluoroethyl azide (**37**) under the same conditions as used in the attempted preparation of **51**. Compound **60** had NMR data to suggest it had been created, however the sample was too impure to report and since this was not the building block we were going to use in the near future the reaction was abandoned and the product was not further purified.

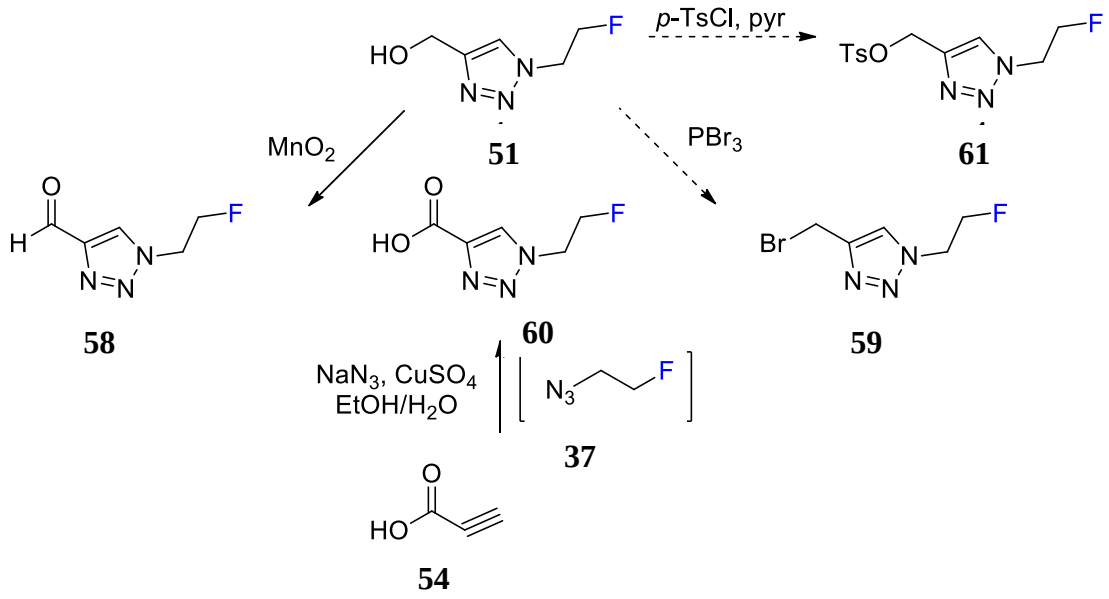

The ^{1}H NMR of the aldehyde derivative **58** provides confirmation of structure. The peak located at 10.11 ppm, labeled **d**, represents the H of the aldehyde moiety. A singlet labeled **c**, at 8.27 ppm, represents the one proton on the triazole ring. The two multiplets centered at 4.91 ppm and 4.81 ppm represent the two protons adjacent to the fluorine labeled **a**; whereas the multiplet at 4.75 ppm represents the two protons labeled **b**. The splitting here is, in the case of the protons labeled **a**, caused by the neighboring fluorine and CH_2. These peaks confirm the production of the aldehyde because of the similarities to the spectrum of the starting material **51** (Figure **7**) as well as the peak at 10.11 ppm which is indicative of an aldehyde function group and is not present in the starting material spectrum.

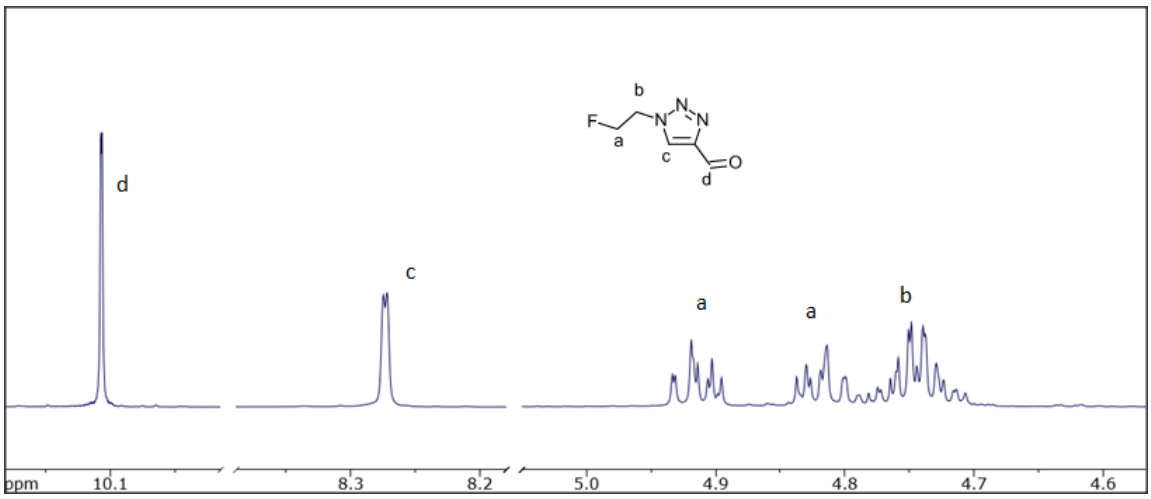

Figure 16- ^{1}H NMR spectrum of 1-(2-fluoroethyl)-1*H*-1,2,3-triazole-4-carbaldehyde (**58**)

Additionally, the ^{13}C NMR spectrum (Figure 17) confirms the starting material **51** was converted to the aldehyde **58**. The peak furthest downfield at 184.8 ppm, labeled **e**, is representative of an aldehyde carbonyl group. The peak at 147.9 ppm, labeled **d**, corresponds to the quaternary carbon also labeled **d**. Peak **c** at 126.5 ppm is due to the C-H in the triazole ring; this peak is shifted downfield compared to the starting material **51**, where it appears at 122.8 ppm. The peaks labeled **a** at 81.5 ppm (midpoint), corresponding to the C adjacent to the fluorine, appears at the same position as in the starting material. Finally, the peaks labeled **b** at 50.9 ppm (midpoint) represent the carbon on the ethyl moiety adjacent to the triazole ring.

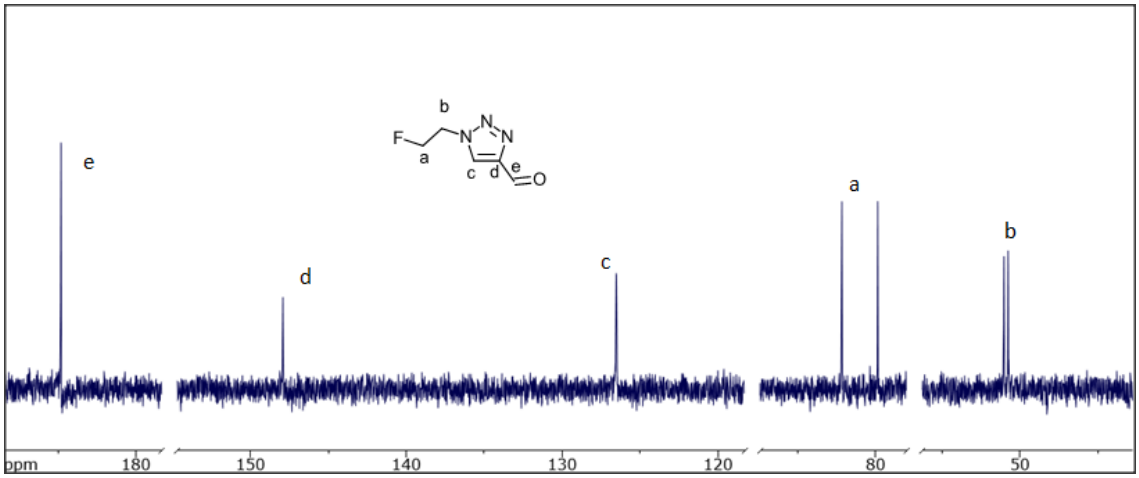

Figure 17- ^{13}C NMR spectrum of 1-(2-fluoroethyl)-1*H*-1,2,3-triazole-4-carbaldehyde (**58**)

An elemental analysis was completed on this molecule **58** and the results confirmed the C, H, and N percentages were within 0.4% of the calculated value for the expected structure. Since the alcohol starting material **51** exists as an oil and it was not possible to obtain an elemental analysis for it; the conclusion that **51** had been produced based on the results of the elemental analysis on the aldehyde derivative **58**.

After many unsuccessful attempts to produce and isolate the bromo derivative **59**, it was envisaged that tosylation of the alcohol derivative **51** could be an alternative route to producing a building block that would be introduced via *N*-alkylation. Again it was elected to test reactions on **49** before attempting them with **51**. Upon researching the topic it was found that the tosylation of benzyl alcohols has been accomplished many times over the years; employing various methods that seemed relatively simple.[139-143] However, after attempting to tosylate benzyl alcohol (as a model study) four times with no formation of product, it became apparent that tosylation of such species was difficult. A general method was followed from an article published in 2010 titled "A detailed

investigation of the aza-Prins reaction". In this paper, Dobbs et al. added the alcohol **62** to be tosylated to DCM, cooled the solution to 0°C and then added 4-dimethylaminopyridine (DMAP), tosylchloride (**44**) and triethylamine in portions. The reaction was held at 0°C until complete as determined via thin layer chromatography (TLC).[142] In the present work, the first attempt consisted of adding all the reactants to a vial at once and letting it stir at room temp for 4h. The reaction was chilled because of a procedure from a patent that stated the reactions were successful at 25°C.[143] After two failed attempts, the reaction conditions were modified slightly. Thus, the reaction mixture was chilled, the TEA was added dropwise over 5 min and then the benzyl alcohol was added dropwise. Once all the reactants were added the temperature was allowed to reach rt and stirred for an additional 48 h. Based on TLC examination, the product was never formed as the R_f of the "product" matched the R_f of the starting material even after reacting for 48 h. For the final attempt the reaction was kept colder for an extended period of time which resulted in failure also. Finally, an article was discovered that supported these negative findings, it was titled "Treatment of Alcohols with Tosyl Chloride Does Not always Lead to the Formation of Tosylates."[144]

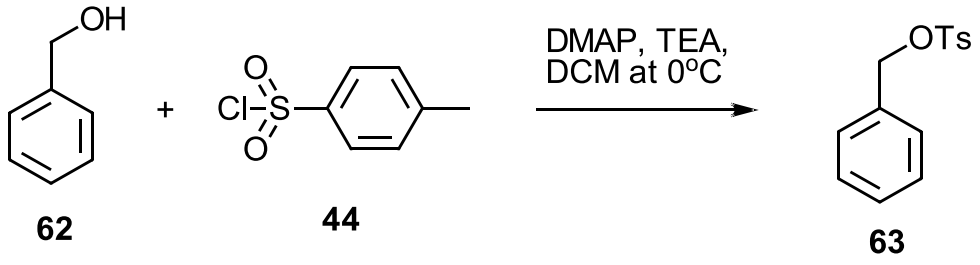

62 **44** **63**

In order to utilize the aldehyde **58**, isatin (**23**) and 5-chloro isatin (**64**) were reduced to the corresponding oxindoles **24** and **65**, respectively. This was accomplished using 80% hydrazine hydrate over 4 h while refluxing.

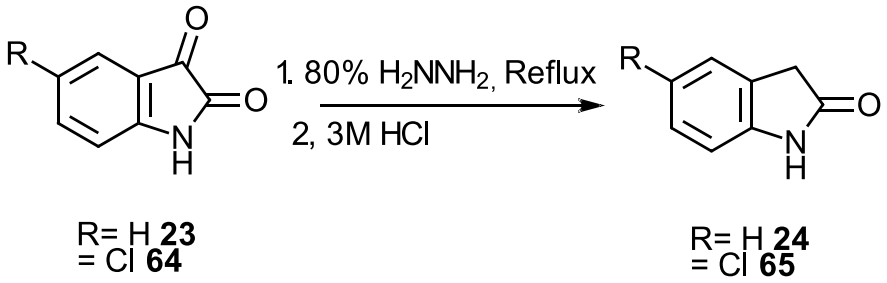

R= H **23**
= Cl **64**

R= H **24**
= Cl **65**

As outlined in the introduction, oxindole and isatin scaffolds were chosen because of their "privileged"nature.[96] Oxindoles have a broad range of biological activities, including protein kinase inhibitors,[98] and possible caspase inhibitor,[145] cdk5 inhibitor,[146] and casein kinase inhibitor. Isatins have been shown to inhibit caspase-3/7.[108]

To demonstrate the usefulness of the building blocks produced as a means of appending a fluoroethyl group to a scaffold of interest, the aldol reaction of 5-chloro-2-indolinone (**65**) and aldehyde **58** was explored; the reaction was effective to yield **67**. Likewise,the aldol reaction between 2-indolinone (**24**) and aldehyde **53** was also effective to yield **66**. It can readily be seen that *N*-alkylation of this substrate would yield a new library of compounds of PET-ready targeting agents.

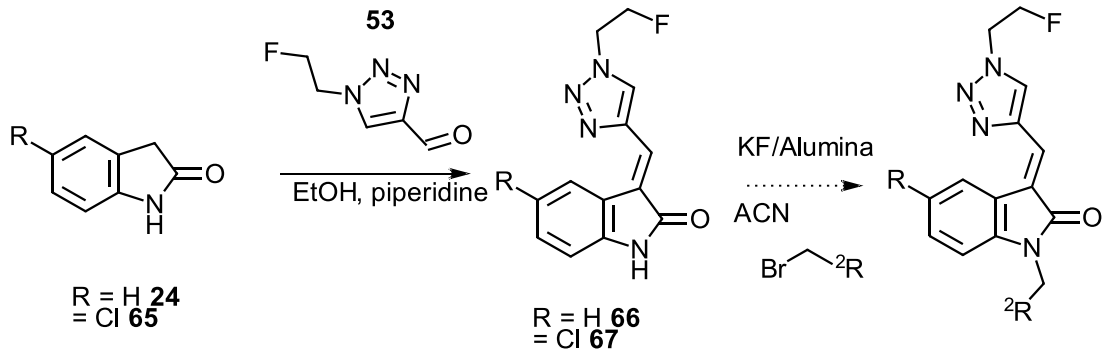

The ^{1}H NMR and ^{13}C NMR spectra of **66** and **67** confirm the structures of the products synthesized. Elemental analyses were completed for both molecules **66** and **67** and the results confirmed the C, H, and N percentages were within 0.4% of the calculated values for each of the molecules.

Compound **67** exists as a mixture of *E* and *Z* isomers which was determined by the ^{1}H NMR spectrum. Traditionally, *E* and *Z* isomers of benzylidene oxindoles are determined based on the chemical shifts of the aromatic protons on the benzylidene ring (H-2' and H-6') as well as the shift of the vinylic proton.[147] Compound **67** is similar to but not actually a benzylidene oxindole, but due to the lack of a model compound of this type, we have likened the proton of the triazole ring to the H-2' proton present in a benzylidene oxindole. Additionally, the vinylic proton can be used as a reference as to ascertain which isomer is present as well. The *E*-isomer has a vinylic proton that is more deshielded due to the influence of the C-2 carbonyl causing a downfield shift. The H-2 and H-6 protons (ortho-benzylidene protons) are affected by the C-2 carbonyl also. Deshielded protons will be shifted further downfield compared to their shielded counterparts. In the case of compound **67** there is only one quasi "ortho" proton to observe. *Ortho* protons of the *E* isomer of benzylidene oxindoles are expected to appear

between 7.45-7.84 ppm, whereas *ortho* protons in the *Z* isomer will appear between 7.85-8.53 ppm. The vinylic proton exhibits chemical shifts as a consequence of shielding also, however in the *E* isomer the vinyic proton is deshielded appearing around 7.84 ppm and in the *Z* isomer is shielded appearing at about 7.55 ppm.[147,148]

In the ^{1}H NMR of **67** the peak furthest downfield at 10.8 ppm, labeled **h**, represents the proton on the nitrogen. It is shown as two singlets because of the presence of both the *E/Z* isomers. The peaks labeled **c**, also two singlets, at 9.45 ppm and 8.78 ppm, are assigned to the "ortho" proton on the triazole ring. The peak at 9.45 ppm indicates there is 30% Z isomer and the peak at 8.78 ppm designates 70% E isomer. The two doublets labeled **d**, represent the vinylic proton. The doublet at 9.16 ppm represents the *E* isomer 70% and the other doublet 7.99 ppm is assigned to the of the *Z* isomer 30%. The singlets at 8.06 ppm and 7.62 ppm, labeled **e**, are representing the *Z* and *E* isomers of the proton next to the chlorine respectively. Proton **f** is represented as a doublet of doublets of doublets at 7.29 ppm and proton **g** at as an odd looking triplet at 6.88 ppm. The multiplet at **b** represents the protons adjacent to the triazole ring whereas the singlet at 4.82 ppm represents the protons adjacent to the fluorine.

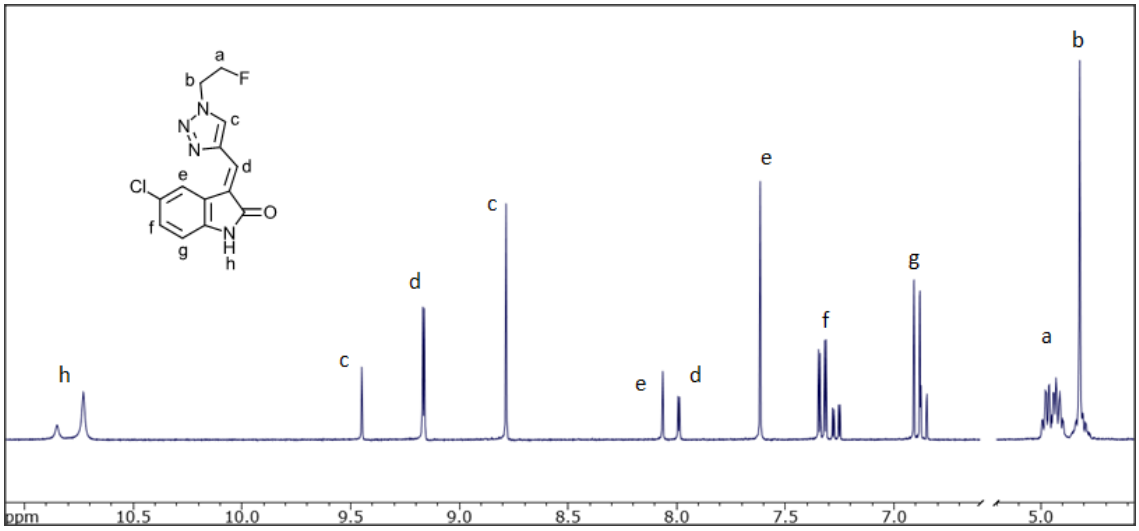

Figure 18- ^{1}H NMR spectrum of 3-{[1-(2-fluoroethyl)-1*H*-1,2,3-triazol-4-yl]methylidene}-5-chloro-1*H*-indol-2-one (**67**)

The ^{1}H NMR of compound **66** indicates that only one isomer is present, unlike compound **67** which was 70:30 *E/Z*. The singlet at 10.73 ppm represents the proton on the nitrogen. The singlet at 9.44 ppm, labeled **c**, is indicative of the hydrogen of the triazole ring. The final singlet, **d**, appearing at 7.90 ppm, is associated with the vinylic proton. Based on comparison with the vinylic and C-2 proton in the ^{1}H NMR of compound **67** it can be determined that this compound (**66**) exists as the *Z* isomer (100%). Proton **e**, is represented by the doublet ($J_{H\text{-}H}$=7.51 Hz) at 7.80 ppm; the splitting is caused by the adjacent proton **f**. Proton **f**, a triplet at 7.23 ppm (J=7.61 Hz) and is split by two neighboring hydrogens (**e** and **g**) both ortho. Proton **g** is also a triplet split by two neighboring hydrogens; the peak appears at 6.99 (J=7.52 Hz). The doublet at 6.87 ppm represents proton **h**, which is split by the ortho hydrogen **g** (J=7.72Hz). The multiplets, **a** and **b**, at 4.94 ppm and 4.81 ppm represent the CH_2 adjacent to the triazole ring and the CH_2 adjacent to the fluorine respectively.

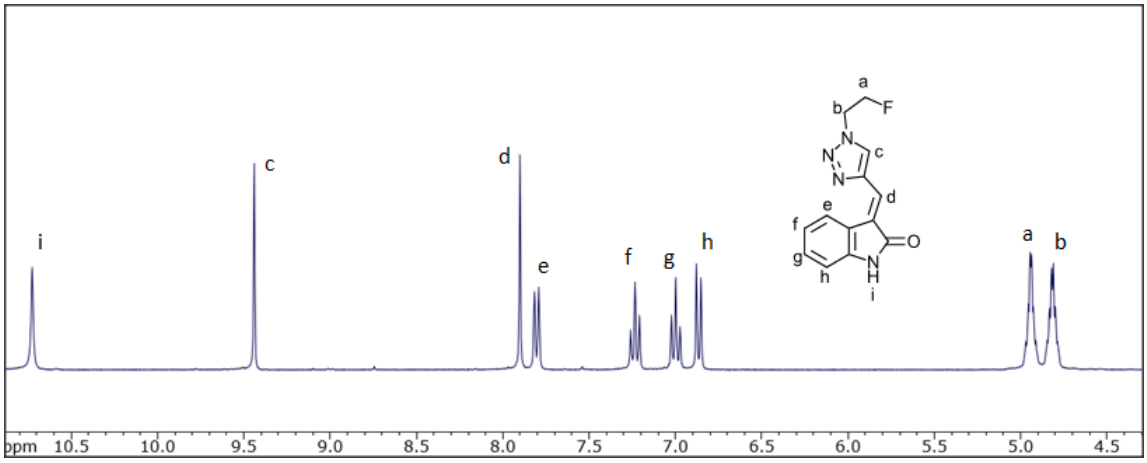

Figure 19- ^{1}H NMR spectrum of 3-{[1-(2-fluoroethyl)-1*H*-1,2,3-triazol-4-yl]methylidene}-1*H*-indol-2-one (**66**)

The ^{13}C NMR of **67** is shown next, where in peaks were estimated using nmrdb.org predicting program. The peak labeled **h** is furthest downfield as it should be since the carbon it represents is attached to the ketone moiety. The peak labeled **l** and the peak labeled **m** correlate to the ethyl moiety and the peaks appear as they did in the building block **58**. This ^{13}C NMR spectrum is not as clear as the ^{13}C NMR of compound **66.**

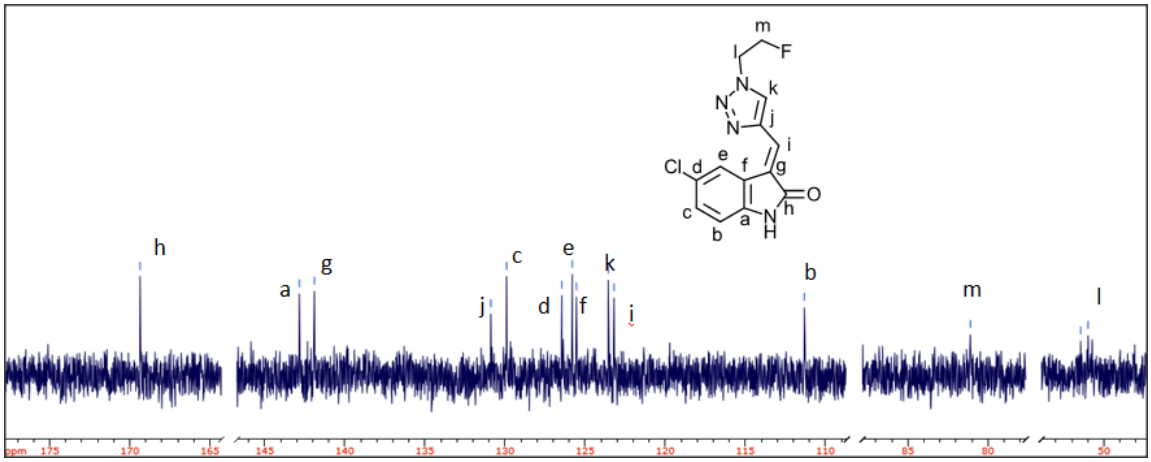

Figure 20- ^{13}C NMR spectrum of 3-{[1-(2-fluoroethyl)-1*H*-1,2,3-triazol-4-yl]methylidene}-5-chloro-1*H*-indol-2-one (**67**)

The ^{13}C NMR of compound **66** resembles the ^{13}C NMR of compound **67** with the carbon attached to the double bond oxygen furthest downfield and the ethyl carbons furthest upfield. The ethyl moiety is represented more clearly in this spectrum.

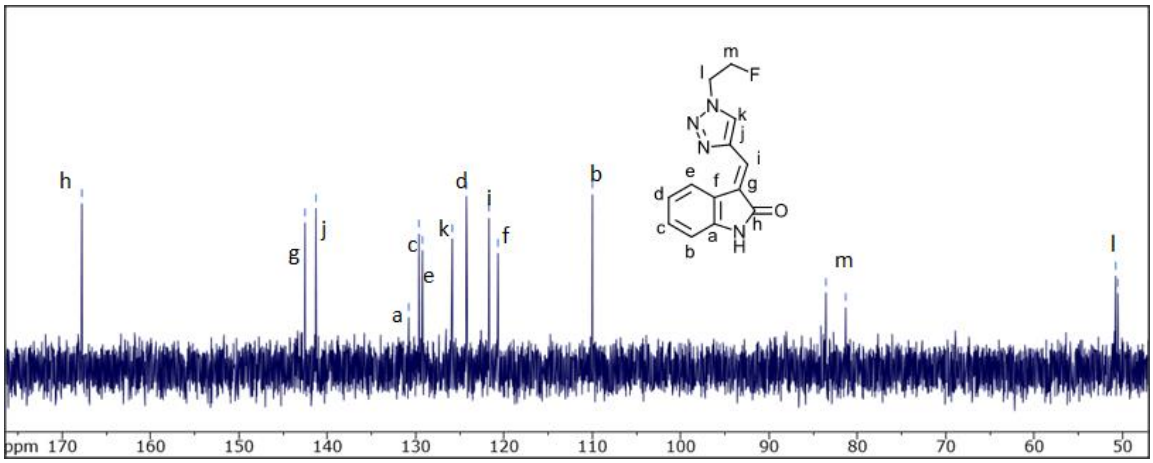

Figure 21- ^{13}C NMR spectrum of 3-{[1-(2-fluoroethyl)-1*H*-1,2,3-triazol-4-yl]methylidene}-1*H*-indol-2-one (**66**)

As suggested previously, *N*-alkylation of compounds **66** and **67** would yield a new library of compounds of PET ready targeting agents. The *N*-2,6-difluorobenzyl fragment had previously been shown by the Ketcha group to enhance the cell-death inhibitory properties of benzylidene oxindoles (presumably by inhibiting caspase-3). This caspase inhibitory fragment was therefore appended onto the C-3 triazolyl oxindole by *N*-alkylation of **66** with 2,6-difluorobenzyl bromine (**68**) resulting in **69**.

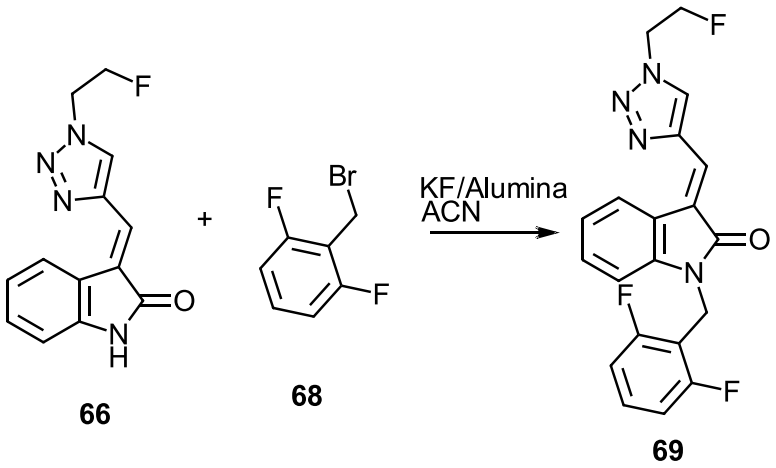

66 **68** **69**

The ^{1}H NMR of compound **69** confirms its stucture. Comparision to the ^{1}H NMR of the starting material **66** shows that the peak at 10.73 ppm assigned to the proton at the *N*-1 position is not present in the product. The singlet furthest downfield at 9.58 ppm, labeled **c**, corresponds to the proton on the triazole ring, which appears at 9.44 ppm in the spectrum of the starting material **66**. The second singlet at 7.85 ppm, labeled **d**, appeared at 7.90 ppm in the starting material and represents the vinylic proton. The protons of **h, f, g,** and **e**; indicating the aromatic protons of the oxindole backbone, all of which were represented in the spectrum of **66** also. The additional protons labeled **k** and **j** at 6.91 ppm as a multiplet represent the three protons on the aromatic ring that was added. Additionally, the peak labeled **i** represents the CH_2 between the nitrogen and the difluorobenzyl group. Finally, the ethyl moiety attached to the triazole ring is represented as three multiplets between 4.72 ppm and 4.97 ppm.

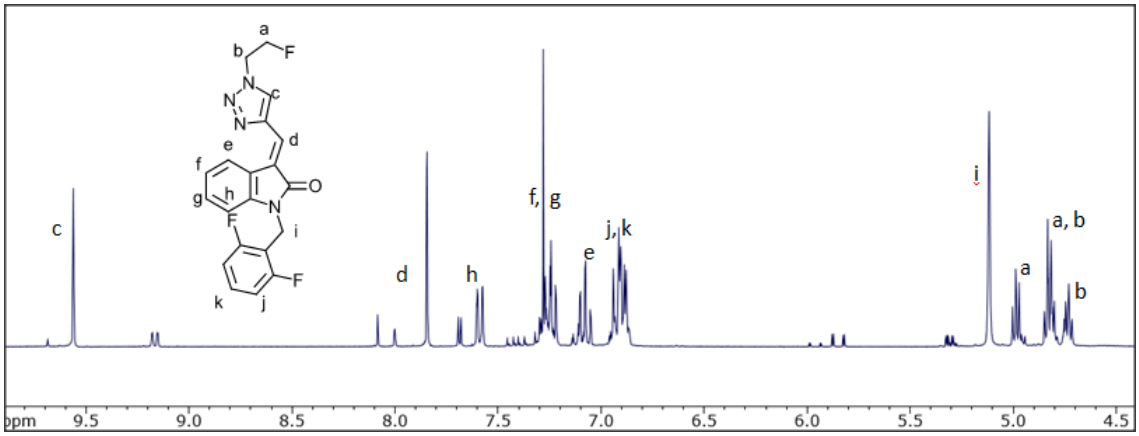

Figure 22- ^{1}H NMR spectrum of3-{[1-(2-fluoroethyl)-1*H*-1,2,3-triazol-4-yl]methylidene}-1-[(2,6-difluorophenyl)methyl]-1*H*-indol-2-one (**69**)

The ^{13}C NMR of compound **69** can be compared to the ^{13}C NMR of compound **66** to determine if the *N*-alkylation has occurred. The peak at 36.8 ppm labeled **n** confirms the presence of the benzylic carbon**.** Additionally it is important to note the appearance of 4 additional peaks in the aromatic region due to the 4 unique carbons on the difluorobenzyl moiety. Software was used to help assign carbons in the aromatic region due to the sheer number of carbons (nmrdb.org).

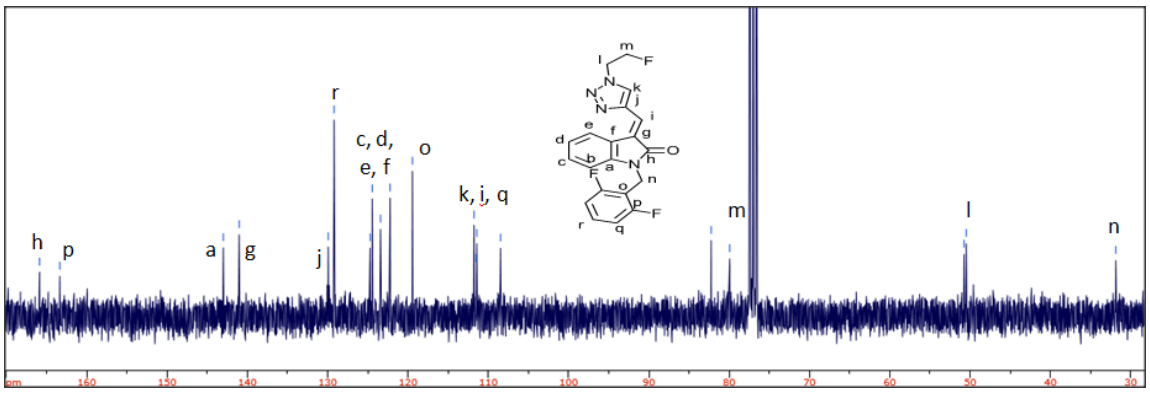

Figure 23-^{13}C NMR spectrum of 3-{[1-(2-fluoroethyl)-1*H*-1,2,3-triazol-4-yl]methylidene}-1-[(2,6-difluorophenyl)methyl]-1*H*-indol-2-one (**69**)

Although a library of *N*-triazole linked benzylidene oxindoles reporter groups were initially envisaged as arising via the *N*-alkylation of a sublibrary of N-H benzylidene oxindoles, it was also deemed valuable to initially *N*-alkylate an isatin with an appropriate triazole based alkylating agent and then conduct a reductive deoxygenation/aldol sequence. To that end, the bromo derivative **53** was used to directly alkylate isatin (**23**) using KF/alumina (6 equiv) in acetonitrile to afford an *N*-linked triazole isatin **70**. The use of KF/alumina as a solid-supported base was first introduced in 1979 by Ando et al.[149] and the Ketcha group has been using it to *N*-alkylate isatins since 2011.[150,151] The main advantage of employing KF/Alumina as a base for abstraction of the isatin N-H involves its being easily removed from the reaction mixture by simple filtration. In this case, possibly due to this basic catalyst, the reaction product was contaminated with impurities.

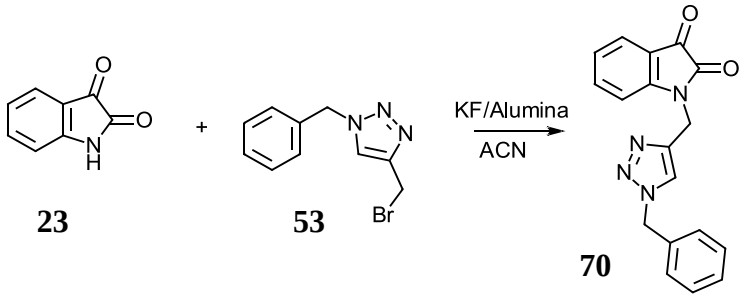

23 **53** **70**

First and foremost, molecule **70** was synthesized to demonstrate how the bromo building block could be used to create a "tertiary building block" of sorts (in anticipation of reduction and diversification by aldolization). Secondly, this molecule is an isatin derivative, which is significant because in 2008 Aboagye designed a caspase-3/7 inhibitor, and possible imaging agent, that had the isatin core as a critical part of its structure.[126] Also incorporated as part of its structure was the triazole ring. Additionally,

Jiang and Hansen[99] confirmed that the triazole ring at the *N*-position enhanced caspase-3 inhibition relative to an *N*-benzyl substituent, thus demonstrating the value of *N*-linked triazole isatins. One of their most potent caspase inhibitors contained a benzyl group attached to the triazole ring in a disubstituted pattern.[100]

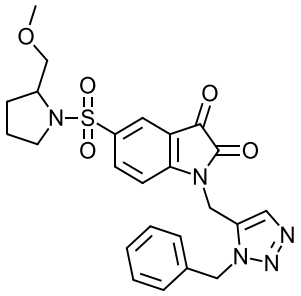

71

Ultimately, the goal was to show that being able to produce this *N*-alkylated isatin building block **70**, which may not be useful in the development of an imaging agent, may be very useful in creating a caspase-3 inhibitor.

The ^{1}H NMR and ^{13}C NMR spectra of compound **70** confirm its structure. Additionally, in this case there exists a literature melting point and NMR for comparison. In the following ^{1}H NMR spectrum (Fig. 24) each proton is represented. The multiplet that is furthest downfield at 7.58-7.56 ppm represents three protons: because of the shift of this set of peaks, it can be determined they represented three of the four protons on the isatin portion of the molecule, labeled **g**, **i**, and **j**. The next multiplet at 7.31-7.24 ppm is integrated as 6H; it is believed that the protons labeled **b** (x2),**c** (x2), **a**, and **e** are represented by this group of peaks because the latter are all aromatic protons and thus are appearing in the appropriate range. The final aromatic proton **h**, appears as a triplet of

doublets at 7.11 ppm. The splitting is caused by the protons that are ortho to **c** ($J_{H\text{-}H}$=7.54 Hz) and the proton that is meta to this proton ($J_{H\text{-}H}$=0.73 Hz). At 5.49 ppm two protons, labeled **f**, (located between the triazole ring and the nitrogen on the isatin), are represented by a singlet. The final peak at 4.99 ppm, labeled **d**, is also a singlet and is associated with the two protons that exist between the triazole ring and the benzene ring.

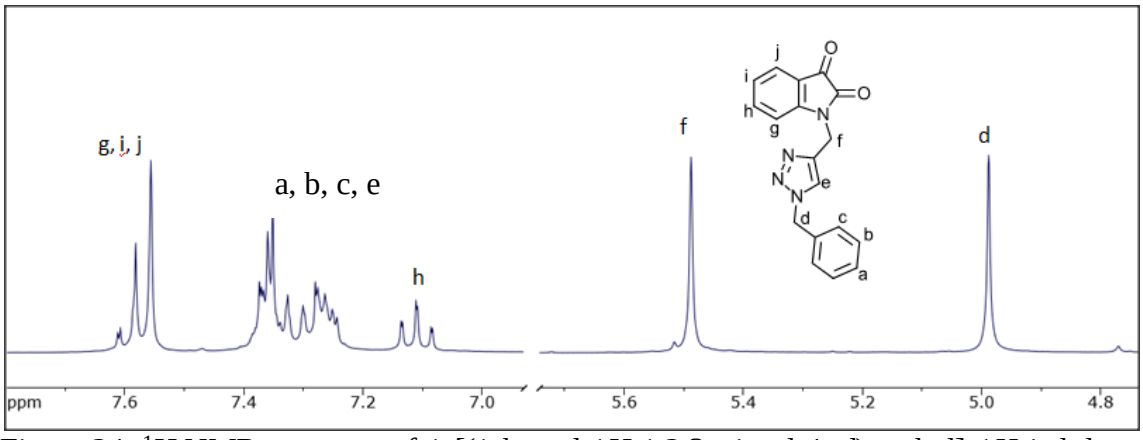

Figure 24- ^{1}H NMR spectrum of 1-[(1-benzyl-1*H*-1,2,3-triazol-4-yl)methyl]-1*H*-indole-2,3-dione (**70**)

The ^{13}C NMR of this structure **70** also confirms the *N*-alkylation of the isatin. The peak furthest downfield at 183.0 ppm, labeled **f**, is indicative of the ketone carbonyl carbon, while the peak labeled **g**, 157.9 ppm represents the carbon of the amide function. Peak **h**, at 150.2 ppm is attributed to the quaternary carbon next to the nitrogen in the isatin moiety. The peak at 142.1 ppm, labeled **j** represents the quaternary carbon on the triazole ring. Between peak **j** and peak **a**, 142.1-111.5 ppm the positions of most of these peaks were estimated using the free internet program offered at nmrdb.org. The peak labeled **i**, at 54.4 ppm, is the C between the triazole ring and the isatin moiety. Finally, the peak at 35.4 ppm is the C between the benzene ring and the triazole ring. These two

peaks appear in the bromo derivative **53** too, which makes it easier to determine which peaks represent the appropriate carbon atoms.

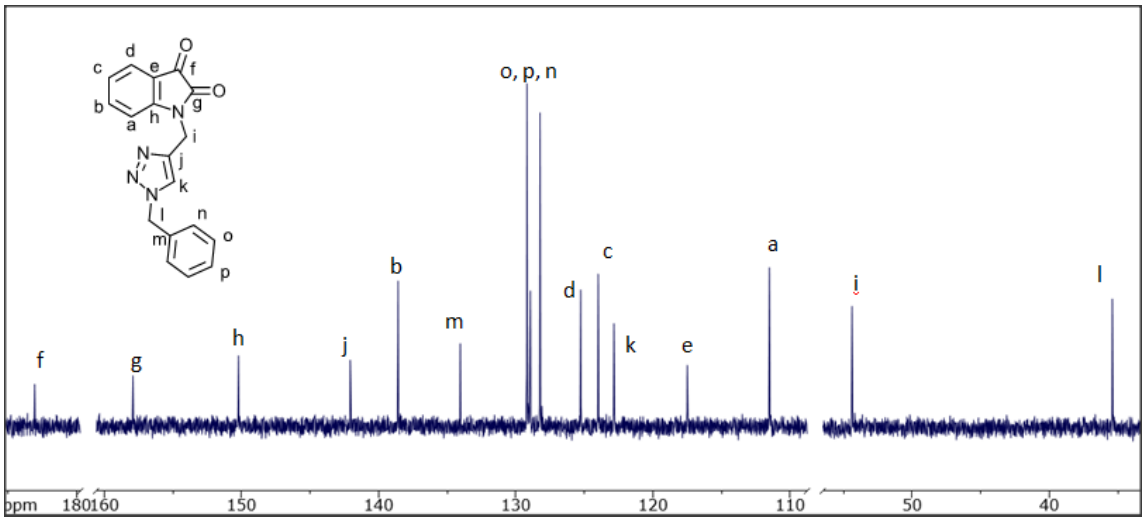

Figure 25- ^{13}C NMR spectrum of1-[(1-benzyl-1*H*-1,2,3-triazol-4-yl)methyl]-1*H*-indole-2,3-dione (**70**)

Having demonstrated the concept of utilizing a surrogate PET building block (i.e., triazole alkylating agent) to produce a new type of building block, it was necessary to demonstrate the reductive deoxygenation of such N-triazole linked isatins using hydrazine. In the event, the reduction of **70** to **72** worked very well which suggests that it will be possible to further derivatize such *N*-alkylated building blocks at the 3-position via an aldol condensation, especially in the context of caspase-3 inhibitors.

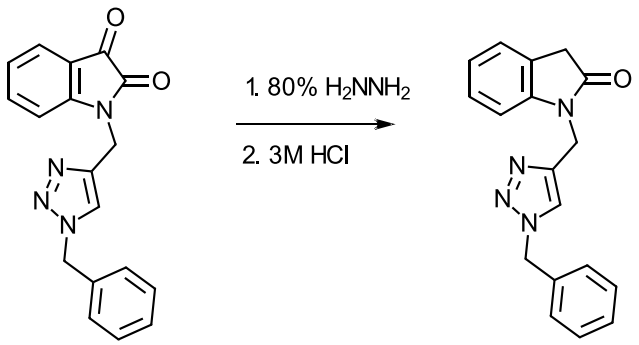

70 **72**

The ^{1}H NMR of compound **72** (Fig 26) confirms its structure. When compared to the ^{1}H NMR of compound **70**, the starting material, two extra peaks are observed in the proton NMR due to the reduction of the ketone at the C-3 position. The protons labeled **k** are represented as two doublets at 10.53 ppm (J=14.04 Hz) and 9.77 ppm (J=13.47 Hz), each doublet representing one hydrogen. As to why these hydrogens are at such a downfield ppm is baffling. The software used and even experimental spectra of oxindole represent these hydrogens as a singlet around 3.5 ppm. Even with this evidence that contradicts the possibility of these hydrogens being represented in this way it is believed this is the structure of the product produced. All the other peaks present in the starting material ^{1}H NMR spectrum match up with the peaks shown here. Also, GC/MS analysis confirms the expected molecular mass.

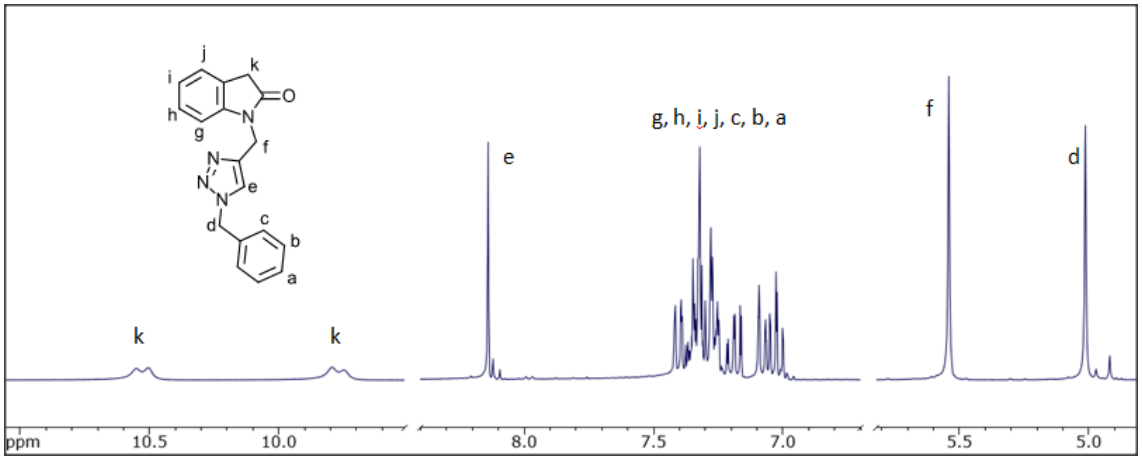

Figure 26- ^{1}H NMR spectrum of 1-[(1-benzyl-1*H*-1,2,3-triazol-4-yl)methyl]-2-indolinone (**72**)

The ^{13}C NMR of this structure **72** fits what might be expected or predicted more closely. In comparison to the starting material **70** two peaks moved, both upfield. Most notably the peak that had been at 183.0 ppm (labeled **f**) is shifted to 109.8 ppm, labeled **g**: a good indicator that the product had in fact been reduced. Other peaks were assigned to carbons based on NMR predicting software.

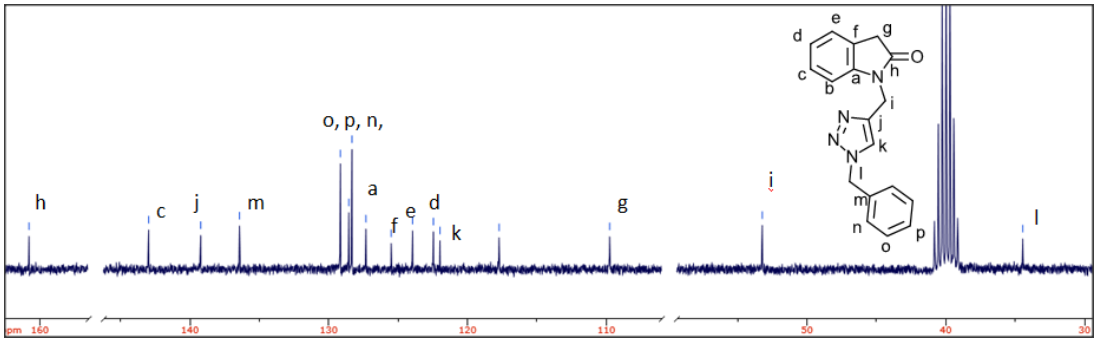

Figure 27- ^{13}C NMR Spectrum of 1-[(1-Benzyl-1*H*-1,2,3-triazol-4-yl)methyl]-2-indolinone (**72**)

Given that so much difficulty had been faced earlier when attempting to prepare the bromo derivative **59**, it was decided to first *N*-alkylate the benzylidene oxindole **73** with3-bromo-1-propyne (**75**) and then "click" with fluoroethylazide (**37**). This general approach had been accomplished by other groups and, in fact, all the groups that append isatin or oxindole with a triazole first *N*-alkylate with an alkyne. First, as a model study (not shown), isatin (**23**) was *N*-alkylated with 3-bromo-1-propyne (**75**) and the resulting product was then "clicked" with FEA. Evidence that this reaction was successful was based on the appearance of the characteristic fluoroethyl triazole peaks in the ^{1}H NMR appearing as multiplets between 4.5 and 5.0 ppm, as well as the correct mass peak in the LC/MS spectra, however there was also evidence of slight impurities. This compound was not isolated, but it provided evidence that the reaction concept would work.

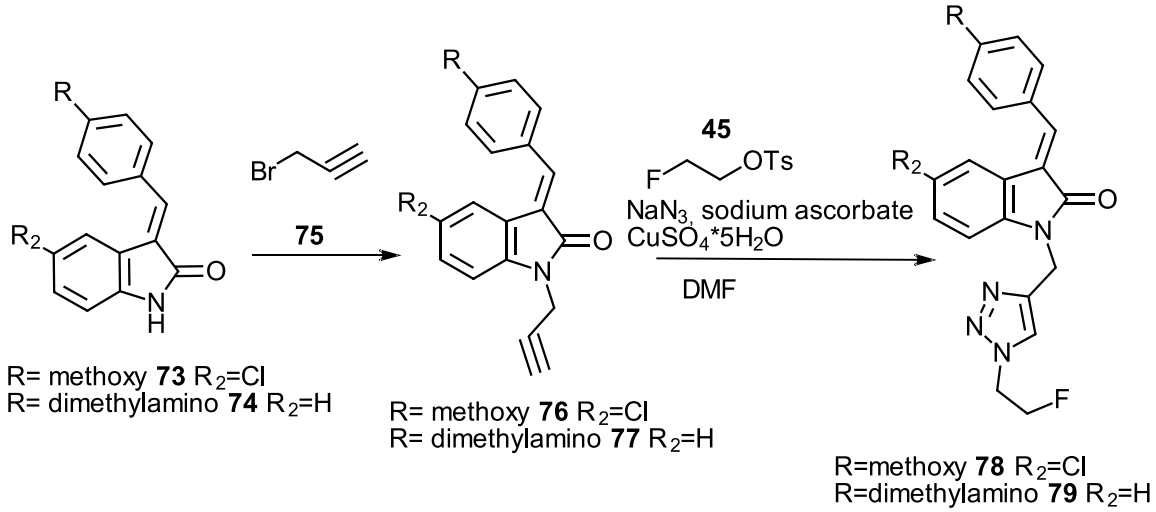

The *N*-propargyl benzylidene oxindole **76** was added to DMF and stirred at 50°C for 30min before the copper (II) sulfate pentahydrate and sodium ascorbate were added to

the mixture and the resulting mixture was stirred for an additional 2 min. Finally, sodium azideand2-fluoroethyltosylate (**45**) were added and allowed to react with the *N*-terminal alkyne at 80°C for 24 h, yielding **78**.

The ^{1}H NMR spectrum of compound **78** displayed a number of peaks and may show some impurities. Alternatively, the extra peaks may be due to more than one isomer or possibly splitting caused by the fluorine. The presence of some product can be confirmed because of the peaks between 5.5 ppm and 4.0 ppm which relate to the formation of the triazole ring linker. Clarity and separation of the peaks could be better but one can see the three sets of triplets and one singlet representative of the fluoroethyl triazole ring that have been observed in many previous ^{1}H NMR spectra of the fluoroethyl triazole building blocks.

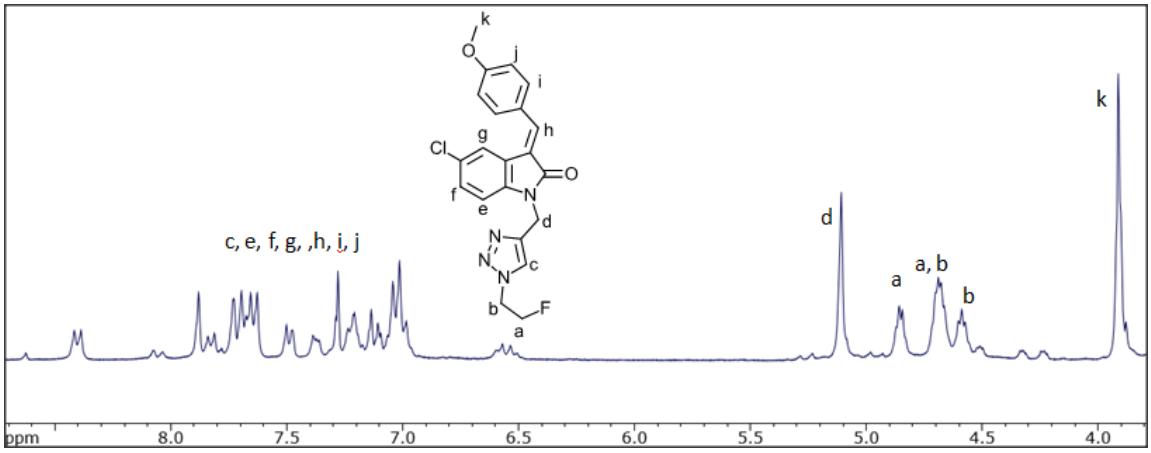

Figure 28- ^{1}H NMR spectrum of 3-[(*p*-methoxyphenyl)methylidene]-5-chloro-1-{[1-(2-fluoroethyl)-1*H*-1,2,3-triazol-4-yl]methyl}-1*H*-indol-2-one (**78**)

For the next product, **79**, the starting material **74** was synthesized and appended with the propargyl group **75** by Amanda Lock Boyer and used in present work to perform

the click reaction as described above. This molecule was chosen since Kuret's group at Ohio State University determined that 3-(4-dimethylaminobenzylidene) oxindole (**74**) was a good candidate molecule for binding to the tau protein.[97] As expressed, one of the goals of the present research was to develop a PET imaging agent selective for tau. Results showed that **77** was an effective binder to tau protein, $A\beta_{1-42}$, and α-synuclein filaments. Binding to more than one protein in the brain is not ideal in the sense that tau selectivity, alone, is desired. Of the molecules that Kuret identified as selective for tau, none were able to cross the BBB.[97] Since Ketcha's research group at WSU had been working with benzylidene oxindoles in the past for other pharmaceutical purposes, it seemed natural for this group to further examine and derivatize **74** in attempt to make the molecule more selective for tau over $A\beta_{1-42}$. Kuret discovered that an iodo group at the C-5 position on the benzenoid ring did not affect binding to tau so Knisley, with the Ketcha group, produced compounds containing a chloro group at the C-5 position as well as a fluoro group. Both derivatives showed enhanced binding to tau. It was determined that the chloro group on the benzenoid ring enhanced tau binding the most.[152] As a result, Cox, also with the Ketcha group, put the chloro group at different positions on the benzenoid ring; discovering the chloro at the C-5 position was best for tau binding. Cox also studied the effects of extended conjugation at the C-3 site. Finally, Cox showed that *N*-alkylation of **74** with a methyl group did not affect binding affinity. This discovery opened up the option to put a reporter group at the *N*-position so this molecule could be used as a PET imaging agent for Alzheimer's Disease.[153] Lock, also in Ketcha's group, attached a fluoroethyl group at the *N*-position as a reporter group.[154] This molecule will likely have the proper lipophilicity in order to cross the BBB. This finding led to

exploring how to introduce a reporter group at the *N*-position while modifying the lipophilicity. Using click chemistry to introduce a triazole ring to this position would effectively alter lipophilicity and provide another way to introduce the reporter group.[123] The triazole ring would also add a third ring moiety. This has the potential to be beneficial to increasing this molecule's specific binding to tau since the molecules that are known to bind to tau selectively have at least three aromatic ring regions connected by two rotatable bonds.[97]

The ^{1}H NMR spectrum of compound **79** shows another derivative of benzylidene oxindole being first *N*-alkylated with propargyl bromide **75** and then clicked with fluoroethyl azide **37**. The doublet at 8.41 ppm (J=7.37 Hz) represents the carbon labeled **e**. The splitting is due to the neighboring hydrogen at the ortho position. The singlet and doublet that integrate to 1H at 7.88 ppm, labeled **i**, describe the *E/Z* isomer possibility of the vinylic hydrogen. The peak at 7.67 ppm represents the protons labeled **j** and seemingly appears to be a doublet of doublets which also suggests a mixture of *E/Z* isomers. The peak at 7.50 ppm that looks as if it is a triplet, labeled **g**, is associated with the proton with the same label and the splitting is due to the two ortho hydrogens **f** and **h**. The multiplet of peaks between 7.25 ppm and 6.92 ppm is in the aromatic region and represents 3H; which are labeled **f**, **h**, and **c**. The final peak in the aromatic region is a multiplet at 6.75 ppm which represents the hydrogens labeled **k**. The peaks between 5.14 and 4.50 ppm are indicative of the formation of the triazole ring and elimination of the alkyne. Finally, the peak at 3.09 ppm, labeled **l**, is representative of the six equivalent hydrogens on the dimethylamino group.

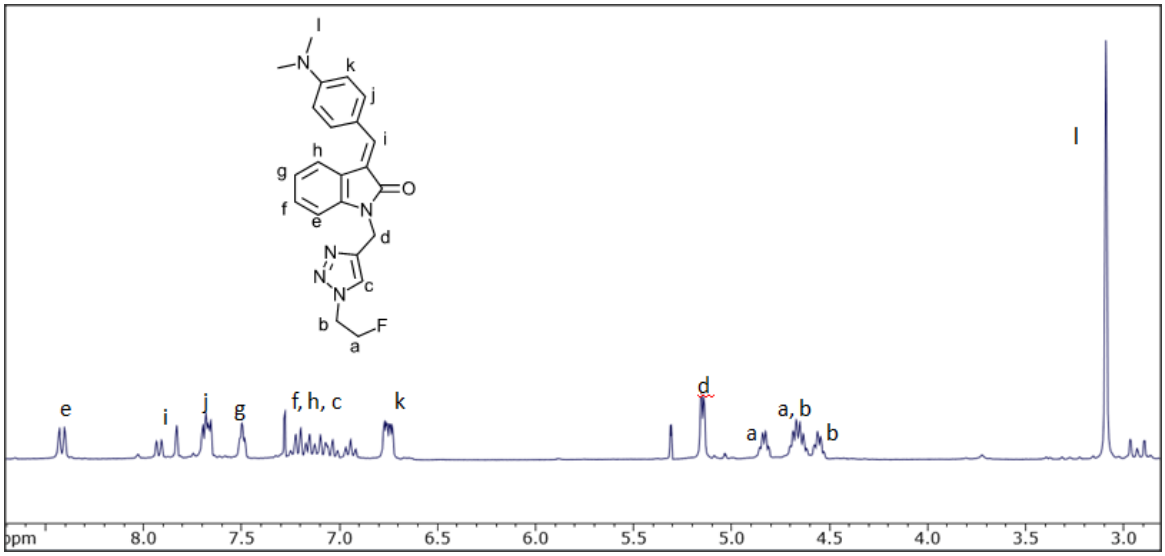

Figure 29- ^{1}H NMR spectrum of 3-{[*p*-(dimethylamino)phenyl]methylidene}-1-{[1-(2-fluoroethyl)-1*H*-1,2,3-triazol-4-yl]methyl}-1*H*-indol-2-one (**79**)

In hindsight the compounds **78** and **79** should have been prepared in EtOH/H_2O as a solvent instead of DMF since EtOH/H_2O is much easier to remove from a product. The solvent used in the click reactions to produce the primary building blocks **49** and **51** was EtOH/H_2O so it would have made sense to perform the click reaction of **37** to **78** and **79** in the same solvent. Additionally, it would not have mattered if the starting materials for **78** and **79** were totally soluble in EtOH/H_2O based on evidence that a click reaction will take place even in the event that all of the starting materials are not soluble.[163,164] As the saying goes, hindsight is 20:20.

The following salts were produced mainly as possible AChE inhibitors. AChE has been implicated into the complex web that is the development of AD. As mentioned in the Introduction section four of the five drugs that are available to help with symptoms of AD are AChE inhibitors. Donepezil hydrochloride (**79a**) shown below is an FDA

approved AChE inhibitor which is able to cross the BBB. Recently, indolinone-based inhibitors of acetylcholinesterase were developed based on the structural resemblance to Donepezil hydrochloride. Many of the compounds synthesized were superior to Donepezil hydrochloride, especially the 2-chlorobenzyl derivative **79b**.[155] Given this level of AChE inhibitory activity exhibited by these benzylidene oxindoles, it was decided to create a triazolyl analog, first to examine the efficacy of this fragment towards AChE but also to possibly create an imaging agent for AChE in the case of a fluoroethyl derivative. To initiate a program towards these goals, the surrogate building block **49** was used to create a quaternary nitrogen of a 3-pyridyl substituted oxindole (e.g., **80**).

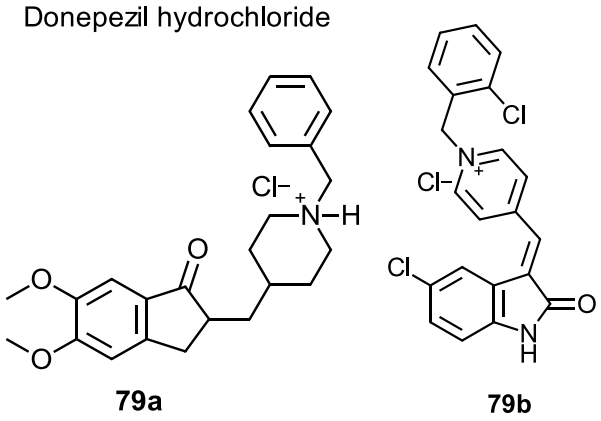

To that end, building block **49** was simply added to a solution of **80** in acetonitrile and allowed to react for 24 h at 60°C resulting in compound **81**.

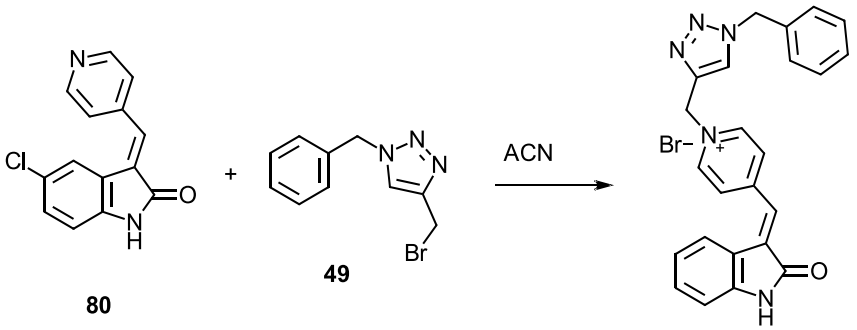

80 49 81

The ^{1}H NMR spectra (DMSO-d_6) of compound **81** confirms its structure. The peak at 11.0 ppm, labeled **m**, is indicative of the proton attached at the *N*-1 position as seen in other spectra of compounds with the proton. The doublet at 9.18 ppm labeled **f** ($J_{H\text{-}H}$=6.96 Hz) represents the protons on the benzyl ring close to the quaternary carbon. The splitting is caused by the protons that are *ortho*, labeled **e** which are represented at 8.68 ppm as a doublet ($^3J_{H\text{-}H}$=6.82 Hz) also. The vinylic proton is represented at 8.43 ppm as a singlet. Peak **h**, at 8.09 ppm is attributed to proton on the triazole ring. The doublet at 7.92 ppm, labeled **c**, is due to the proton at the C-4 position of the oxindole backbone, splitting is caused by the meta proton at the C-6 position. At 7.42-7.33 ppm there is a multiplet that represents the protons labeled **a**, **j**, **k**, and **l**. The doublet at 6.88 ppm ($J_{H\text{-}H}$=8.38 Hz) represents the proton at the C-6 position. Finally the singlet labeled **g** at 5.97 ppm and the singlet at 5.65 ppm labeled **i** represent the hydrogens of the two CH_2 groups. These peaks are represented in the bromo building block **53** also.

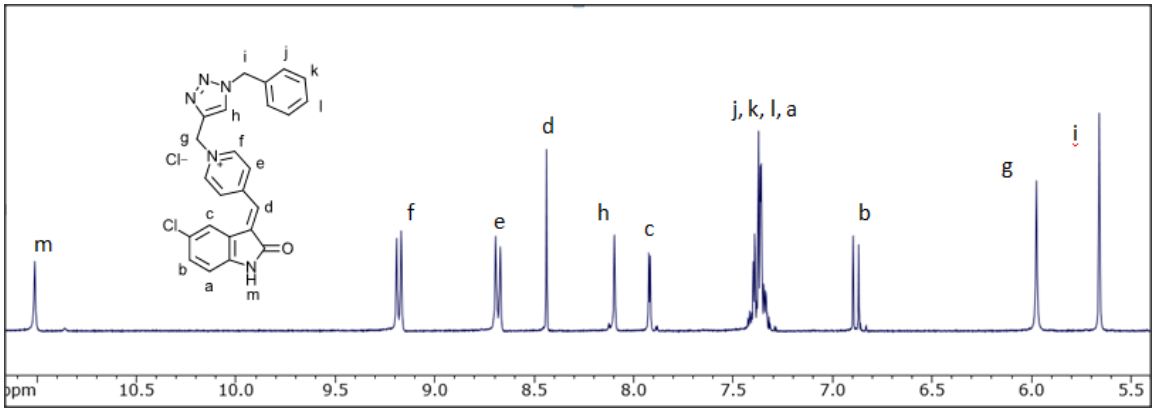

Figure 30- ^{1}H NMR spectrum of 3-({1-[(1-benzyl-1*H*-1,2,3-triazol-4-yl)methyl]-4-pyridyl}methylidene)-5-chloro-1*H*-indol-2-one (**81**)

The ^{13}C NMR of displays peaks labeled **m** and **p** which are indicative of the carbons associated with the CH_2 groups of the molecule. The peaks between 149.9 ppm and 112.1 ppm are in the aromatic region and represent the 17 unique aromatic carbons. The peak at 166.5 ppm, labeled **h**, is indicative of the amide carbonyl carbon.

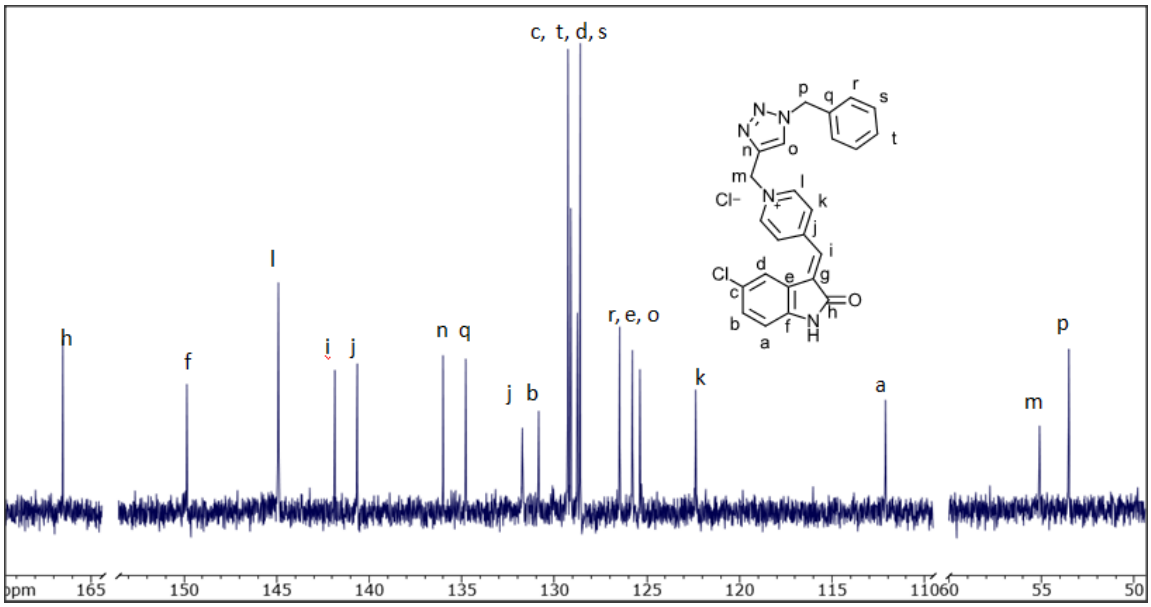

Figure 31- ^{13}C NMR spectrum of 3-({1-[(1-benzyl-1*H*-1,2,3-triazol-4-yl)methyl]-4-pyridyl}methylidene)-5-chloro-1*H*-indol-2-one (**81**)

For eventual comparison purposes, the 5-chloro version of the previously determined optimal derivative bearing a 2-chlorobenzyl capping group was also synthesized. Thus, compound **83** was likewise made by reaction of 80 with 2-chlorobenzyl chloride (82). Compound **83** incorporates the 2-chlorobenzyl fragment which is effective for Ache inhibition, however it is also possible that such quaternization might not adversely affect caspase-3 inhibition and such molecules make serve as a dual function drug.[155]

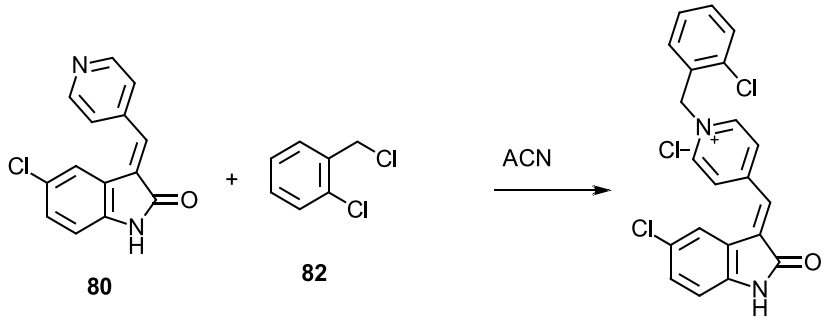

The ^{1}H NMR spectrum of compound **83** indicated that in fact the product was formed however impurities may be present. The peak at 11.20 ppm, labeled **l**, represents the hydrogen on the nitrogen. The doublet of doublets at 9.24 ppm ($J_{H\text{-}H}$=6.80 Hz) represents the two equivalent hydrogens on the pyridine ring closest to the nitrogen. Splitting is due to the hydrogens at the ortho position and the fact that *E* and *Z* isomers are present. The doublets at 8.76 ppm and 8.44 ppm, both labeled **e**, are associated with the other two hydrogens on the pyridine ring furthest from the *N*. These peaks could be represented as a doublet of doublets at 8.60 ppm, and again splitting is due to the ortho

hydrogens ($J_{H\text{-}H}$=6.69 Hz) and the presence of the *E* and *Z* isomers. The split singlet at 8.18 and 7.73 ppm, labeled **d** is due to the *E* and *Z* isomers also. Each peak represents 0.5H and together represent the vinylic proton **d**. The multiplet at 7.65-7.21 ppm represents 6H. Those six hydrogens are all associated with an aromatic ring, they are labeled **a**, **b**, **h**, **k**, **i**, and **j**. Next, another multiplet labeled **c**, represents the hydrogen next to the chlorine on the lower 6 member ring. The tiny peak in the middle is not counted as a peak (an impurity), the peaks are considered a doublet of doublets, with splitting indicative of interaction with hydrogens **e** and **d**. The final peak at 6.07 ppm, labeled **g**, is considered a multiplet because of the uneven splitting (J=13.5 Hz). This splitting does not match with any other splitting patterned in the molecule. Since the CH_2 group is the last moiety to be assigned, this peak is assumed to correspond with those protons.

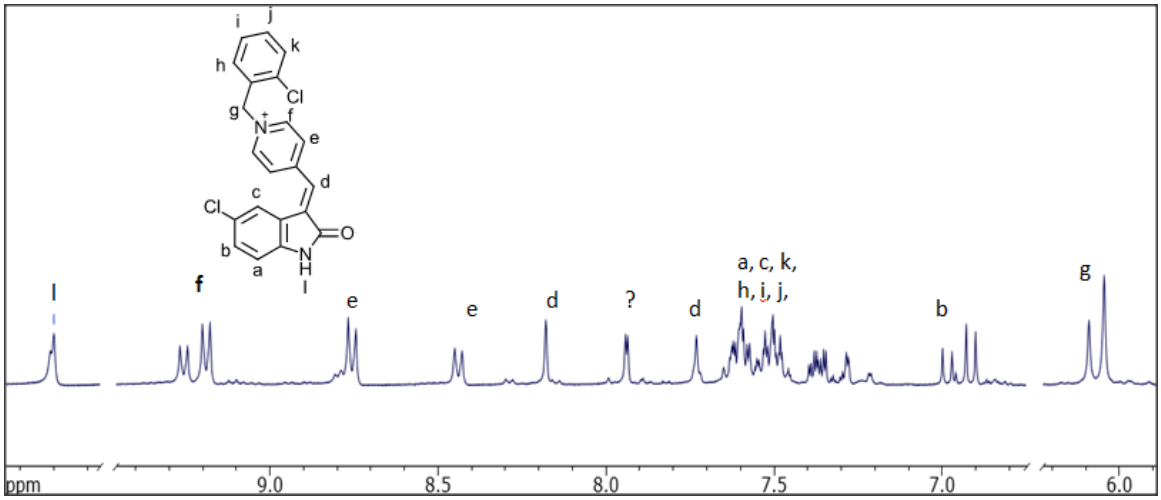

Figure 32- ^{1}H NMR spectrum of 3-({1-[(*o*-chlorophenyl)methyl]-4-pyridyl}methylidene)-1*H*-indol-2-one (**83**)

The ^{13}C NMR spectrum of compound **83** has the appropriate number of peaks at the appropriate chemical shifts to lead to the conclusion that the product was in fact formed. The carbon labeled **g** appears furthest downfield at as it should since it is part of an amide moiety.

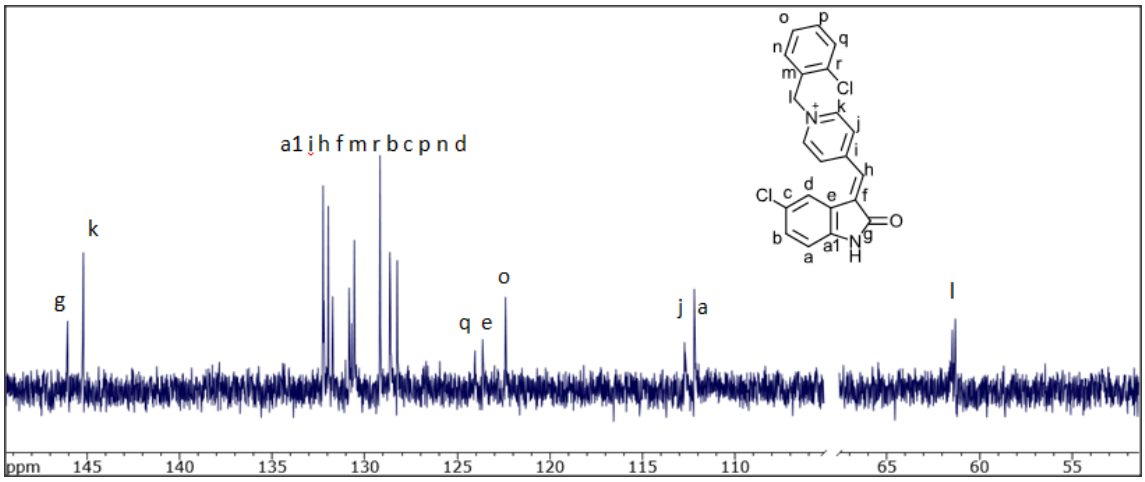

Figure 33- ^{13}C NMR spectrum of 3-({1-[(*o*-chlorophenyl)methyl]-4-pyridyl}methylidene)-1*H*-indol-2-one (**83**)

Following the theme of dual function drugs, it was decided to create molecules containing a fragment demonstrated to lower Aβ such as a 2,4,6- or 3,4,5-trimethoxy fragment with a fragment possibly capable of acting towards GSAP. To the end, the known molecule **85** was prepared via an aldol condensation between oxindole **24** and the trimethoxybenzyaldehyde **84**. It was envisioned that once appended at the *N*-position, this species would be a potential multitarget drug as well. This is not a novel compound, but as detailed in the multitarget drug section of the introduction, it is useful for cdk-5 inhibition and it was envisioned that appending a 2,6-difluorobenzyl "fragment" at the *N*-position would create a cdk-5 inhibitor as well as a caspase inhibitor.

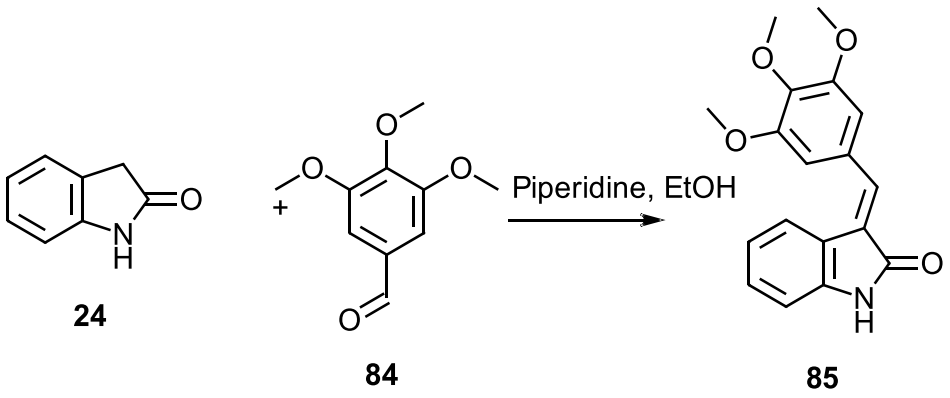

24 **84** **85**

The ^{1}H NMR of compound **85** shows the expected and appropriate peaks. At 10.6 ppm a singlet labeled **l**, represents the proton bonded to the nitrogen. Another singlet at 8.02 ppm, labeled **f**, represents the two hydrogens, also labeled **f**, on the trimethoxy benzene. The vinylic hydrogen is represented next as a singlet at 7.76 ppm. The doublet furthest downfield, labeled **a**, represents the proton closest to the nitrogen on the oxindole. Splitting of this peak ($J_{H\text{-}H}$=7.37 Hz) is due the hydrogen present at the ortho position. The triplets of doublets, at 7.20 ppm ($J_{H\text{-}H}$=7.62, 0.95 Hz) and 6.99 ppm ($J_{H\text{-}H}$=7.57, 0.86 Hz) represent the protons labeled **b** and **c** respectively. The triplet splitting is caused by ortho protons whereas the doublet splitting is caused by each having a proton that is meta. The final doublet at 6.85 ppm, labeled **d**, represents the final proton on the oxindole. Splitting, once again, is due to the ortho interaction ($J_{H\text{-}H}$=7.60 Hz) with the neighboring hydrogen. The singlet at 3.85 ppm, labeled **g**, represents six hydrogens and is associated with the six equivalent hydrogens of the trimethoxy moiety. The final singlet at 3.75 ppm, integrated to three protons, represents the other three hydrogens of the remaining methoxy group, labeled as **h**.

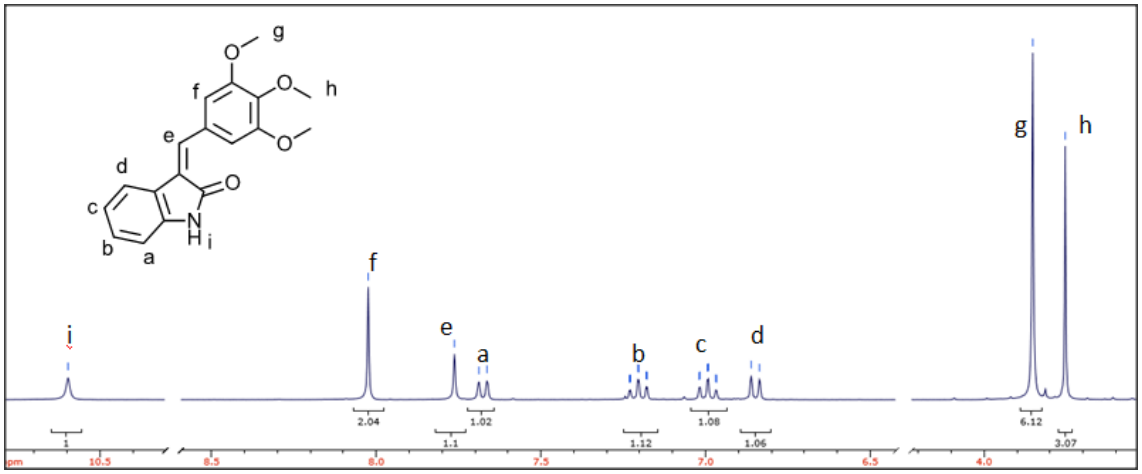

Figure 34- ^{1}H NMR spectrum of 3-[(3,4,5-trimethoxyphenyl)methylidene]-1*H*-indol-2-one (**85**)

The ^{13}C NMR of compound **85** shows 15 peaks as expected. The peak at 167.7 ppm is definitely the carbon labeled **n**. The peaks from 152.7 ppm and 109.8 ppm were assigned based on an internet program that predicts the location of each carbon based on the structure. Additionally a DEPT90 of this product was used to determine which peaks were C-H peaks. The peaks at 137.8, 129.1, 121.5, 119.8, 110.6, 109.8 ppm were C-H peaks and assigned accordingly. The peak labeled **m** at 60.6 ppm, and the peak labeled **k** at 56.3 ppm represent the three primary carbons each attached to oxygen.

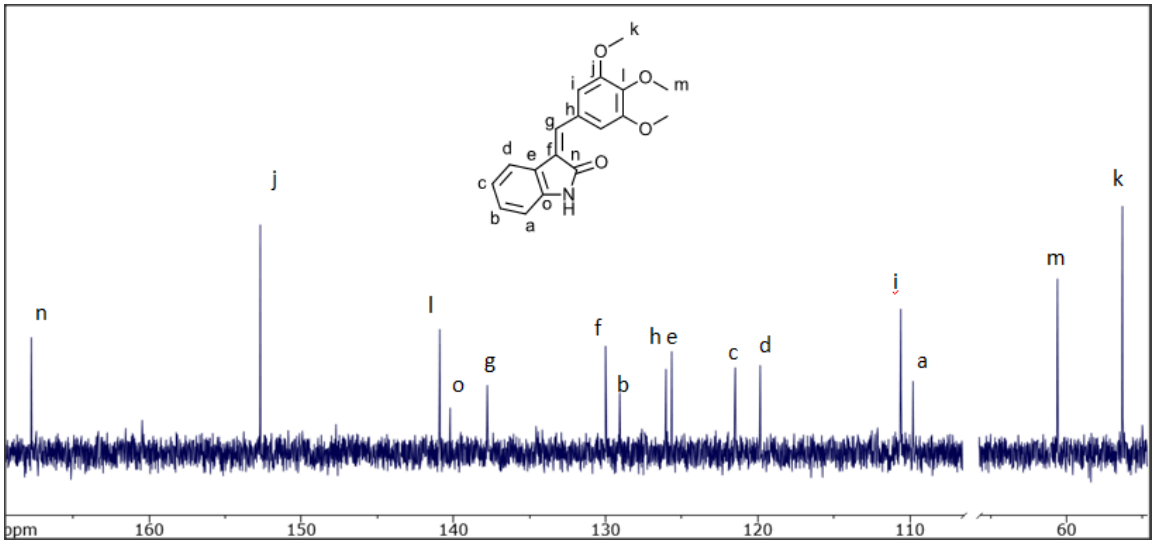

Figure 35- ^{13}C NMR spectrum of 3-[(3,4,5-trimethoxyphenyl)methylidene]-1*H*-indol-2-one (**85**)

The final molecule synthesized was also envisioned as a possible multitarget drug. The isatin starting material **86** was reduced to **87** with hydrazine in order to allow for an aldol reaction with the trimethoxybenzaldehyde **84** resulting in composite compound **88**. The trimethoxy group has been linked to lowering the Aβ burden in the AD brain as demonstrated by Greengard in 2007 with compound **21**which incorporates the same 2,4,6-trimethoxy benzylidene group as used in this molecule. The difluoro moiety was also used because of results that support its value in creating an effective caspase inhibitor as demonstrated by Abogye and team in 2008 with compound **42.**

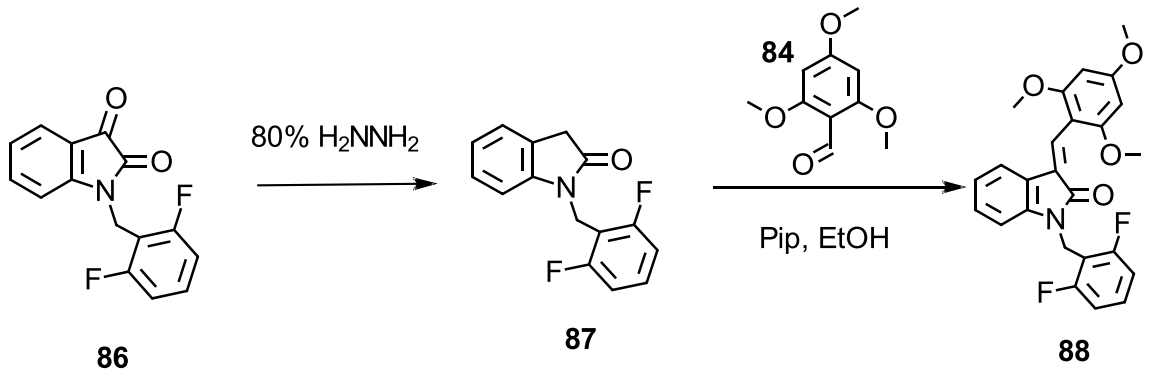

86 **87** **88**

The ^{1}H NMR of compound **88** provides structural evidence that the product was in fact produced. The singlet **e**, at 7.52 ppm represents the vinylic photon. The multiplet at 7.47-7.37 ppm, represents the proton labeled **k**. The triplet of doublets at 7.20 ppm, labeled **a**, represents the proton at the C-7 position. It is split by the neighboring proton, **b**, but also is effected by the fluorine atoms that are in close proximity. The triplet at 7.11 ppm represents the protons at the C-5 and C-6 positions. The multiplet represented at 6.93-6.85 ppm labeled **j**, **d** is associated with protons on the difluoro benzyl moiety as well as the proton at the C-4 position. The singlet at 6.37 ppm represents the two equivalent protons each on the ring of the trimethyl benzyl group. The singlet at 5.03 ppm labeled **i** represents the alkyl protons and finally the peaks at 3.87 ppm **h** and 3.75 ppm **f**, together represent the 9 protons of the methoxy groups.

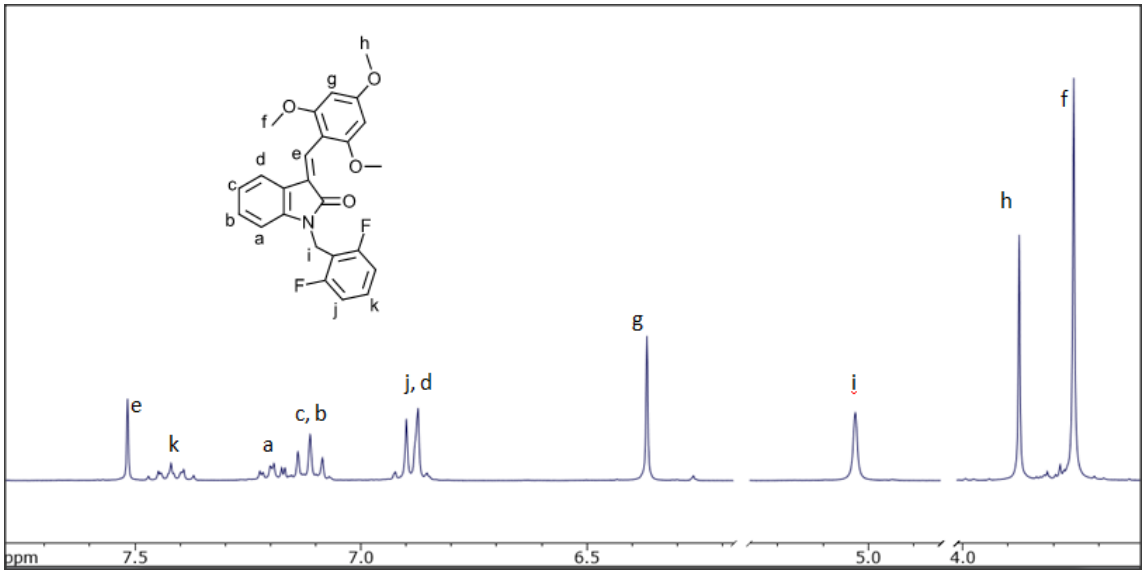

Figure 36- ^{1}H NMR spectrum of 3-[(2,4,6-trimethoxyphenyl)methylidene]-1-[(2,6-difluorophenyl)methyl]-1*H*-indol-2-one (**88**)

The original goals of this research were to provide a proof of concept synthetic basis for the so-called Proxy PET concept developed at WSU. To that end, families of triazolyl linking building blocks containing either a cold fluoroethyl reporter group as well as the more easily accessible benzyl substituted surrogate group were prepared and attached to potential targeting agents based on either the isatin or oxindole scaffolds. Although conversion of the progenitor alcohol building blocks to the corresponding tosylate building blocks could not be achieved, N-alkylation of the analogous bromo building block was demonstrated as well as aldolization of an aldehyde building block. Additionally, a new class of building blocks were demonstrated wherein a primary building block was attached to an isatin, whereupon reduction to the corresponding oxindole creates building block which might be diversified by subsequent aldolization with aryl aldehydes.

Experimental

General. Melting points were determined via the use of open capillaries with an Electro thermal melting point apparatus. The ^{1}H and ^{13}C NMR data were obtained on a Bruker Avance 300 MHz NMR in either $CDCl_3$ or DMSO-d_6 solution. Chemical shifts for proton NMR are reported in δ (ppm) downfield from tetramethylsilane and ^{13}C NMR shifts are calibrated on the DMSO-d_6 resonance at 39.50 ppm or the $CDCl_3$ resonance at 77.16 ppm. Coupling constants (*J*) are in Hz. The following abbreviations are used to describe peak patterns where appropriate: s, singlet; d, doublet; dd, double doublet; t, triplet; q, quartet; dt, doublet of triplet; m, multiplet. GC/MS measurements were performed using Hewlett-Packard 6890 Series GC with auto injection and mass fragments are reported a mass per charge, *m/z*. The GC was coupled with a mass spectrometer with Hewlett-Packard 5973 mass selective detector/quadrupole system. Flash column (Silica Gel, Premium R_f, 200-400 mesh, Sorbent Technologies) and thin layer chromatography reactions were performed on silica gel with indicated solvent systems.

2-Fluoroethyl tosylate (45)

To a 50 mL vial charged with dichloromethane (25 mL) and a magnetic stir bar was added *p*-toluenesulfonyl chloride (11.7 mmol, 2.234 g), triethylamine (5.4 mL, 39.025 mmol), and 4-dimethylaminopyridine (0.0639 g, 0.523 mmol) while chilling in an ice bath for 5 min. 2-Fluoroethanol was then added drop wise over 15 min. After stirring at rt for 20 h the reaction was vacuum filtered and rinsed with hexanes. The solid was discarded and the filtrate was evaporated under reduced pressure. The resulting oil was purified by silica gel column (5:1 petroleum ether: ethyl ether). Pure product

(GCMS/TLC) was collected as a yellow oil (134 mg, 5.13%); R_f=0.72 (EtOAc): ^{1}H NMR (300 MHz, $CDCl_3$) δ 7.84-7.80 (m, 2H), 7.39-7.36 (m, 2H), 4.68-4.65 (m, 1H), 4.52-4.49 (m, 1H), 4.34-4.31 (m, 1H), 2.47 (s, 3H); ^{13}C NMR (75MHz, $CDCl_3$) δ 145.1, 129.9, 127.9, 80.55 (d, J=173.5, 1C), 68.43 (d, J=21.23, 1C), 21.64ppm; GCMS (*m/z*) 218 (M^+1) 91 (100%).

1-Benzyl-4-(hydroxymethyl)-1*H*-1,2,3-triazole (49)

To a 10 mL vial charged with EtOH/H_2O (1:1v/v, 6 mL) and a magnetic stir bar was added benzyl bromide (360 µL, 3.03mmol), sodium azide (220 mg, 3.38 mmol), triethylamine (40 µL, 0.28 mmol), $CuSO_4$*$5H_2O$ (78.0 mg, 10mol%), sodium ascorbate (112.7 mg, 20mol%) and propargyl alcohol (200 µL, 3.44 mmol). The reaction vessel was capped and heated at 70 ºC for 3.5 h. H_2O (10 mL) was added to the mixture. The product was extracted from the water layer with EtOAc (3 x 20 mL). The organic layer was dried using Na_2SO_4, filtered and evaporated under reduced pressure to afford a pure (LC/MS, TLC) off-white solid (527 mg, 92.3%) after allowed to sit overnight: mp 71-74 ºC (lit.[131]mp 76-77 ºC; R_f = 0.26 (EtOAc): ^{1}H NMR (300 MHz DMSO) δ 8.04 (s, 1H), 7.37 - 7.32 (m, 5H), 5.59 (s, 2H), 5.24 (s, 1H), 4.55 (s, 2H); ^{13}C NMR (75 MHz, DMSO) δ148.9, 136.6, 129.2, 128.5, 128.4, 123.3, 55.5, 53.2ppm; LCMS190 (M+1)

[1-(2-Fluoroethyl)-1*H*-1,2,3-triazol-4-yl]methanol (51)

To a 10 mL vial charged with EtOH/H_2O (1:1v/v 6 mL) and a magnetic stir bar was added 2-fluoroethyl tosylate (500 µL, 2.95 mmol), sodium azide (0.3285 g, 5.05 mmol), and triethylamine (20 µL, 5 mol%). The reaction vessel was capped and heated at 60°C for 18 h. Then the remaining reactants of propargyl alcohol (200 µL, 3.43 mmol), copper

sulfate pentahydrate (79.7 mg, 10 mol%), and sodium ascorbate (0.1145 g, 20 mol%) were added and the mixture was heated at 60°C for an additional 24 h. After cooling to rt, H_2O (8 mL) was added to the reaction vial and the reaction was vacuum filtered. The water layer was extracted with EtOAc (3x 15 mL) and the combined organic layers were evaporated under reduced pressure to afford pure (GCMS/TLC) product as a tan oil. The aqueous layer was then saturated with Na_2SO_4 and extracted with EtOAc to provide additional product as a tan oil (0.1585 g, 60.48%): R_f = 0.75 (MeOH) ^{1}H NMR (300 MHz $CDCl_3$) δ 7.68 (s, 1H), 4.87 (t, *J*=4.84, *J*= 75.72, 1H), 4.79 (s, 2H), 4.71 (t, *J*=4.4, 2H), 4.62 (t, *J*=4.84, *J*=75.72, 1H), 2.98 (s, 2H); ^{13}C NMR (75MHz, $CDCl_3$) δ 148.1, 122.8, 81.5 (d, *J*=177.9, 1C), 56.2, 50.5 (d, *J*= 20.5, 1C); GCMS (*m/z*) 145 (M^+), 54 (100%).

1-Benzyl-4-(carboxaldehyde)-1*H*-1,2,3-triazole (52)

To a 20 mL vial charged with DCE (7 mL) and a magnetic stir bar was added 1-benzyl-4-(hydroxymethyl)-1*H*-1,2,3-triazole (**49**) (190 mg, 1 mmol) and MnO_2 (267 mg, 3 mmol). The reaction mixture was stirred at 80 ºC for 4 h and vacuum filtered through a pad of zeolite. The pad was washed with DCE (3x 10 mL) and the filtrate evaporated under vacuum using rotary evaporation to afford a pure (GC-MS / TLC) off-white solid (136.1 mg, 72.8%): mp 79-82 ºC (lit.[13]mp89-90 ºC; R_f = 0.70 (EtOAc): ^{1}H NMR (300 MHz, DMSO) δ; 10.03 (s, 1H), 8.98 (s, 1H), 7.39-7.35 (m, 5H), 5.71 (s, 2H); ^{13}C NMR (75 MHz $CDCl_3$) δ 185.4, 147.5, 135.8, 129.3, 128.8, 128.7, 128.6, 53.7ppm; GC-MS (m/z) 187 (M+) 91 (100).

1-Benzyl-4-(bromomethyl)-1*H*-1,2,3-triazole (53)

To a 10 mL round-bottom flask charged with DCM (10 mL) and a magnetic stir bar was added 1-benzyl-4-(hydroxymethyl)-1*H*-1,2,3-triazole (**49**) (1.006 g, 5.3 mmol) and PBr_3 (1.5 mL, 16 mmol). The reaction mixture was stirred at rt for 4 h, quenched with H_2O (2 mL) and extracted with DCM (3 x15 mL). The combined organic layers were dried using anhydrous Na_2SO_4, filtered and evaporated under reduced pressure to afford a pure (LC-MS/TLC) white solid (1.0216 g, 75.9%): mp 124-126 ºC; R_f = 0.74 (EtOAc): ^{1}H NMR (300 MHz $CDCl_3$);δ 7.51 (s, 1H), 7.42-7.37 (m, 3H), 7.31-7.27 (m, 2H), 5.52 (s, 2H), 4.55 (s, 2H) ^{13}C NMR (75 MHz $CDCl_3$) δ; 144.9, 134.2,129.2, 128.2, 122.7, 54.3, 21.6ppm;LC MS (*m/z*) 254 (M^+1).

1-Benzyl-1*H*-1,2,3-triazole-4-carboxylic acid (56)

To a vial charged with EtOH/H_2O (1:1v/v, 10 mL) and a magnetic stir bar was added benzyl bromide (340 µL, 2.82 mmol)and sodium azide (190 mg, 2.90 mmol). The reaction mixture was allowed to stir at 60 ºC for 14 h, after which time the remaining reagents $CuSO_4$*$5H_2O$ (40.9 mg, 0.15 mmol), sodium ascorbate (59.9 mg, 0.29 mmol) and propiolic acid (200 µL 3 mmol) were added. The reaction mixture was allowed to stir at 60 ºC for 24h, after which time H_2O (1 mL) was added to the mixture and allowed to cool in an ice bath. Aqueous NaOH (10%, 3mL) was added to the mixture and then vacuum filtered. Concentrated HCl was then added to the filtrate until the mixture reached pH 2. Product was extracted from the filtrate with EtOAc (3 x15 mL) and the combined organic layers were dried with anhydrous Na_2SO_4, filtered and evaporated under reduced pressure to afford a pure (TLC) white solid. (471.8 mg, 80.4%): mp 159-162 ºC (lit.[11]mp177-179 ºC); R_f = 0.60 (EtOAc): ^{1}H NMR (300 MHz $CDCl_3$); δ 8.57 (s,

1H), 7.40-7.28 (m, 6H), 5.65 (s, 2H): ^{13}C NMR (75 MHz $CDCl_3$); δ 136.0, 129.4, 129.3, 129.2, 128.7, 128.5, 128.3, 53.5 (d, *J*=34.6Hz, 1C)ppm.

1-(2-Fluoroethyl)-1*H*-1,2,3-triazole-4-carbaldehyde (58)

To a 10mL vial charged with dichloroethane (7 mL) and a magnetic stir bar was added [1-(2-fluoro-ethyl)-1*H*-[1,2,3]triazol-4-yl]-methanol (**51**), (0.1410 g, 0.9719 mmol)and activated MnO_2 (0.237 g, 2.73 mmol). The reaction vessel was capped and heated at 80°C for 18 h. The reaction mixture was vacuum filtered over zeolite and washed with DCE (3 x 10 mL). The solvent was evaporated under reduced pressure to afford the pure off-white solid (0.1177 g, 84.66%): mp 70-72°C; R_f = 0.64 (MeOH); ^{1}H-NMR (300MHz, $CDCl_3$) δ: 10.11 (s, 1H), 8.27 (s, 1H), 4.91 (m, 1H), 4.77 (m, 3H); ^{13}C NMR (75MHz, $CDCl_3$) δ: 184.8, 147.9, 126.5, 81.0 (d, *J*=173.2, 1C), 50.9 (d, *J*=20.4, 1C); GCMS (*m/z*): 143 (M^+), 60 (100%); Anal. Calcd for $C_5H_6FN_3O_2$: C, 41.96; H, 4.23; N, 29.36 Found: C, 41.72; H, 4.14; N, 29.00

3-{[1-(2-Fluoroethyl)-1*H*-1,2,3-triazol-4-yl]methylidene}-5-chloro-1*H*-indol-2-one (67)

To a 10mL vial charged with EtOH (4 mL) and a magnetic stir bar was added 5-chloro-2-oxindole (171.8 mg, 1.0 mmol), piperidine (0.147 equiv, 16 µL), and 1-(2-fluoroethyl)-1*H*-1,2,3-triazole-4-carbaldehyde (**58**) (121.4 mg, 0.8 mmol). The mixture was allowed to stir for 3 h at 80°C at which time the temperature was decreased to 60°C for an additional 2 h. The mixture was then allowed to cool to rt and placed in the freezer overnight. The mixture was vacuum filtered and rinsed with EtOH (10 mL) affording afford a pure (LC/MS, TLC) solid (207.6 mg, 83.8%): R_f =0.43 (EtOAc); mp 264-266

ºC; ^{1}H NMR (300 MHz, DMSO-d_6) δ 10.8 (d, *J*=36.15, 1H), 9.45, 8.78 (s, 0.25H, 0.75H) , 9.16, 7.99 (d, *J*=2.25, 0.75H, 0.25H), 8.06, 7.62 (s, 0.25H, 0.75H), 7.30 (ddd, *J*=19.22, 8.29, 2.17, 1H), 6.88 (ddd, *J*=9.64, 8.30, 0.37, 1H), 4.99-4.9 (m, 2H), 4.82 (s, 1H); ^{13}C NMR (75MHz, $CDCl_3$) δ: 169.4, 142.8, 141.9, 130.9, 129.9, 126.5, 125.8, 125.6, 123.6, 123.2, 111.3, 81.1, 51.3 (d, *J*=19.26, 1H) ppm; MS (m/z) 293 (M^++1). Anal. Calcd for $C_{13}H_{10}ClFN_4O$: C, 53.34; H, 3.44; N, 19.14; Found: C, 53.38; H, 3.29; N, 18.92.

3-{[1-(2-Fluoroethyl)-1*H*-1,2,3-triazol-4-yl]methylidene}-1*H*-indol-2-one (66)

To a 10mL vial charged with EtOH (4 mL) and a magnetic stir bar was added oxindole (0.152g 1.0mmol), piperidine (0.147 equiv, 20 µL), and 1-(2-Fluoroethyl)-1*H*-1,2,3-triazole-4-carbaldehyde (**58**) (0.1657 g, 1.2 mmol). The mixture was allowed to stir for 5h at 70ºC. The mixture was then allowed to cool to rt and placed in the freezer overnight. The mixture was vacuum filtered and rinsed with cold EtOH (10 mL) affording afford a pure (LC/MS, TLC) solid (0.2601 g, 88.3%): R_f = 0.59 (EtOAc); mp 236-241ºC; ^{1}H NMR (300 MHz DMSO-d_6) δ 10.73 (s, 1H), 9.44 (s, 1H),7.90 (s, 1H), 7.80 (d, *J*=7.51, 1H), 7.23 (t, *J*=7.61, 1H), 6.99 (t, *J*=7.52, 1H), 6.87 (d, *J*=7.72, 1H), 4.94 (dq, *J*=6.64, 3.40, 2H), 4.81 (dq, *J*=6.67, 3.44, 2H); ^{13}C NMR (75MHz, DMSO- d_6) δ 167.8, 142.5, 141.3, 129.6, 129.2, 125.9, 124.3, 121.7, 120.7, 110.0, 82.4 (*J*=171.3), 50.67 (*J*=24.75) ppm; LC/MS (m/z) 259 (M^++1) Anal. Calcd for $C_{13}H_{10}FN_4O$: C, 60.46; H, 4.29; N, 21.69; Found: C, 60.49; H, 4.29; N, 21.70.

3-{[1-(2-Fluoroethyl)-1*H*-1,2,3-triazol-4-yl]methylidene}-1-[(2,6-difluorophenyl)methyl]-1*H*-indol-2-one (69)

To a rbf charged with acetonitrile (10 mL) and a magnetic stir bar was added KF/Alumina (745.1 mg, 5.36 mmol), and 3-{[1-(2-Fluoroethyl)-1*H*-1,2,3-triazol-4-yl]methylidene}-1*H*-indol-2-one (199.7mg, 0.9mmol). The mixture was stirred for 5 min at rt 2-(Bromomethyl)-1,3-difluorobenzene (293.7mg, 1.6mmol) was added and mixture was reflux for 18 h in which time all the acetonitrile evaporated but reaction was not lost. The sample was redissolved in acetonitrile and vacuum filtered and washed with hot acetone. The filtrate was evaporated under reduced pressure to afford a bright yellow solid that was purified via recrystallization (EtOH) to yield product as bright yellow crystals (72.6mg, 24.4%): R_f = 0.68 (EtOAC); mp 196-200ºC; ^{1}H NMR (300 MHz $CDCl_3$) δ 9.58 (s, 1H), 7.92 (dd, *J*=46.91, 0.62, 1H), 7.63 (m, 1H), 7.25 (m, 2H), 7.09 (m, 1H), 6.91 (m, 3H), 5.12 (s, 2H), 4.97 (dt, *J*= 8.74, 4.48, 1H), 4.81 (quintet,*J*=4.73, 2H), 4.74 (q, *J*=4.03, 1H); ^{13}C NMR (75MHz, $CDCl_3$) δ165.9, 163.3, 143.0, 141.0, 129.9, 129.2, 124.4, 123.4, 122.2, 119.4, 111.8, 111.4, 108.5, 82.3, 79.9, 50.5, 31.8ppm; LCMS (*m/z*) 385.1 (M^+1).

1-[(1-Benzyl-1*H*-1,2,3-triazol-4-yl)methyl]-1*H*-indole-2,3-dione (70)

To a solution of isatin (0.1869 g, 1.3 mmol), in acetonitrile (11 mL) was added 6 equiv of KF/alumina (1.09 g, 6.7 mmol) and the resulting mixture was stirred at rt for 5 min after which time 1-benzyl-4-(bromomethyl)-1*H*-1,2,3-triazole (**53**) was then added to the stirred solution and the mixture was refluxed for 24 h. The mixture was then allowed to cool to rt and the suspended KF/alumina was removed by vacuum filtration. The filtrate was evaporated under reduced pressure to afford a sticky orange solid. Recrystallization from EtOH afforded the pure (LC/MS / TLC) product as yellow crystals (0.1472g, 42.08%): mp 133-136ºC (lit.[138] 139-141ºC); R_f = 0.57 (EtOAc); ^{1}H NMR (300 MHz,

DMSO-d_6): 7.58-7.56 (m, 3H), 7.31-7.24 (m, 6H), 7.11 (td, J =7.54, J =0.73 1H), 5.49 (s, 2H) 4.99 (s, 2H); ^{13}C NMR (75MHz, $CDCl_3$) δ: 183.0, 157.9, 150.2, 142.1, 138.6, 134.0, 129.2, 128.9, 128.2, 125.3, 124.0, 122.8, 117.5, 111.5, 54.4, 35.4 ppm; MS (*m/z*) 318 (M^+ +1).

1-[(1-Benzyl-1*H*-1,2,3-triazol-4-yl)methyl]-2-indolinone (72)

To a rbf charged with hydrazine hydrate 80% (8 mL) and a magnetic stir bar was added 1-[(1-benzyl-1*H*-1,2,3-triazol-4-yl)methyl]-1*H*-indole-2,3-dione (**70**) (0.79 mmol, 0.2515 g). The reaction mixture was reflux for 4 h. The reaction mixture was added to beaker in an ice bath. Aqueous HCl (3M) was added until a pH of 4 was attained and the mixture was allowed to stand overnight. The mixture was vacuum filtered to afford the pure (LC/MS, TLC) product as golden crystals (188.8 mg, 78.6%): R_f = 0.61 (EtOAc): mp190-194°C; ^{1}H NMR (300 MHz DMSO-d_6) δ 10.53 (d, J=14.04, 1H), 9.77 (d, J=13.47, 1H), 8.14 (s, 1H), 7.40 (ddd, J= 7.45, 1.24, 0.61, 1H), 7.38-7.34 (m, 1H), 7.33-7.30 (m, 2H), 7.26 (dd, J=7.60, 1.91, 2H), 7.19 (ddd, J=7.88, 7.46, 1.29, 1H), 5.54 (s, 2H), 4.99 (s, 2H); ^{13}C NMR (75MHz, DMSO- d_6) δ160.8, 142.9, 139.2, 136.4, 129.2, 128.6, 128.3, 127.3, 125.5, 123.9, 122.5, 121.9, 117.7, 109.8, 53.2, 34.5 ppm; LC/MS (*m/z*) 305 (M^+ +1)

3-[(*p*-Methoxyphenyl)methylidene]-5-chloro-1-{[1-(2-fluoroethyl)-1*H*-1,2,3-triazol-4-yl]methyl}-1*H*-indol-2-one (78)

To a 10mL vial charged with *N*,*N*-dimethylformamide (5 mL) and a magnetic stir bar was added 2-fluoroethyltosylate (1 equiv, 0.0648 g,0.224 mmol), and sodium azide (1.1 equiv, 0.0180 g, 0.25 mmol). The mixture was heated for 30min at 50 °C. After 30min,

copper (II) sulfate pentahydrate (9.4 mg, 10 mol%) and sodium ascorbate (12.4 mg, 20 mol%) were added to the mixture turning the solution reddish/brown. The mixture was stirred for 1-2 min in which time the solution changed back to a clear color. 3-[(*p*-Methoxyphenyl)methylidene]-5-chloro-1-(2-propynyl)-1*H*-indol-2-one (**76**) (1 equiv., 0.0708 g, 0.219 mmol) was added to the mixture and the whole was heated at 80 ºC for 24 h. The reaction was cooled in an ice bath and transferred to a beaker with 30 mL cold water after which 10% NH_4OH (5 mL) was added to the reaction with stirring. The reaction mixture was then vacuum filtered and then extracted with DCM (40 mL). The organic layer was evaporated under reduced pressure to afford the desired product as a pure (LC/MS, TLC) greenish solid (0.0424 g, 46.9%): mp 159-162ºC; R_f =0.53; ^{1}H NMR (300 MHz DMSO-d_6) δ 8.63-6.97 (m, 9H), 5.11 (s, 2H), 4.53 (dt, J=107.63, 40.98, 4H), 3.85 (d, 3H); ^{13}C NMR (75 MHz, DMSO-d_6)δ 167.3, 161.6, 151.5, 142.6, 141.8, 139.5, 135.4, 132.2, 130.7, 128.0, 126.6, 123.9, 122.7, 114.9, 114.4, 113.8, 111.4, 55.9, 35.3ppm; LC/MS (*m/z*) 413 (M^+1).

3-{[*p*-(Dimethylamino)phenyl]methylidene}-1-{[1-(2-fluoroethyl)-1*H*-1,2,3-triazol-4-yl]methyl}-1*H*-indol-2-one (79)

To a 10mL vial charged with dimethylformamide (5 mL) and a magnetic stir bar was added 2-fluoroethyltosylate (1 equiv, 0.0502 g,0.224 mmol), and sodium azide (1.1 equiv, 0.0228 g, 0.25 mmol). The mixture was heated for 30min at 50 ºC. After 30 min, copper (II) sulfate pentahydrate (8.7 mg, 10 mol%) and sodium ascorbate (12.8 mg, 20 mol%) were added to the mixture turning the solution reddish/brown. The mixture was stirred for 1-2 min. in which time the solution changed back to a clear color. 3-{[*p*-(Dimethylamino)phenyl]methylidene}-1-(2-propynyl)-1*H*-indol-2-one (**77**) (1 equiv.,

0.1046g, 0.219mmol) was added to the mixture and heated at 80 ºC for 24 h. The reaction was cooled in an ice bath and transferred to a beaker with 30 mL cold water after which 10% NH_4OH (5 mL) was added to the reaction with stirring. The reaction mixture was then extracted with DCM (3x 15 mL). The combined organic layers were evaporated under reduced pressure to afford product as a red oil (LC/MS, TLC). Recrystallization (DCM/Hexanes) was attempted and was not successful. The DCM/Hexanes were evaporated under reduced pressure to obtain the oil once again which was added to two other samples (LJM-2-83 and LJM-2-85) and was purified *via* silica gel chromatography (EtOAc/Hexanes 40:60 and flushed with MeOH), to afford pure product (LC/MS, TLC) as orange/red crystals (0.1668g, 47.6%): R_f = 0.48 (EtOAc); mp 110-115 ºC; ^{1}H NMR (300 MHz DMSO-d_6) δ 8.41 (d, *J*=7.37, 1H), 7.93-7.83 (m, 1H), 7.68 (dd, J=7.26, 4.50, 2H), 7.51-7.48(m, 1H), 7.25-6.92(m, 3H), 6.75 (td, *J*=4.48, 2.63, 2H), 5.14 (d, *J*= 3.65, 2H), 4.83 (q, *J*=4.36, 1H), 4.66 (dq, *J*=10.36, 5.03, 2H), 4.55 (q, *J*=4.86, 1H), 3.09 (s, 6H)ppm; LC/MS (m/z) 319 (M^++1).

3-({1-[(1-Benzyl-1*H*-1,2,3-triazol-4-yl)methyl]-4-pyridyl}methylidene)-5-chloro-1*H*-indol-2-one (81)

To a rbf charged with acetonitrile (5 mL) and a magnetic stir bar was added 1-benzyl-4-(bromomethyl)-1*H*-1,2,3-triazole (**53**) (135.6mg, 0.54mmol), and 3-[(4-pyridyl)methylidene]-5-chloro-1*H*-indol-2-one (**80**) (101.5mg, 0.43mmol). The reaction was refluxed for 1 h then transferred to a vial (10 mL) where it was heated for 23 h at 60°C. The solution was allowed to cool to rt then vacuum filtered and washed with hexane (10 mL) to afford a purple solid which was recrystallized with EtOH/H_2O (1:1

v/v) . A pure (LC/MS) dark purple solid (0.0810 g, 43.9%) was collected by vacuum filtration and washed with cold EtOH: mp 248-250°C; ^{1}H NMR (300 MHz DMSO-d_6) δ 11.0 (s, 1H), 9.18 (d, J=6.96, 2H), 8.68 (d, J=6.82, 2H), 8.43 (s, 1H), 8.09 (s, 1H), 7.92 (s, 1H), 7.42-7.33 (m, 6H), 6.88 (d, J=8.38, 1H), 5.97 (s, 2H), 5.65 (s, 2H)ppm. LC/MS (*m/z*) 430 (M^+ +1); ^{13}C NMR (75MHz, DMSO- d_6) δ 166.5, 149.9, 144.9, 141.9, 140.6, 136.0, 134.8, 131.7, 130.8, 129.3, 129.1, 128.8, 128.6, 126.5, 125.8, 125.4, 122.4, 112.1, 55.1, 53.5 ppm; Anal. Calcd for $C_{24}H_{19}ClFN_5O$+: C, 54.72; H, 4.02; N, 12.83; Found: C, 54.81; H, 3.76; N, 12.83.

3-({1-[(*o*-Chlorophenyl)methyl]-4-pyridyl}methylidene)-1*H*-indol-2-one (83)

To a 20mL vial charged with acetonitrile (8 mL) and a magnetic stir bar was added 3-[(4-pyridyl)methylidene]-5-chloro-1*H*-indol-2-one (**80**) (209.4 mg, 0.9 mmol), and 2-chlorobenzyl chloride (160 µL, 1.5 mmol). The mixture was stirred at 60°C for 23 h after which time the reaction was cooled to rt, vacuum filtered, and washed with hexanes (10 mL). The resulting solid was purified via recrystallization (EtOH:H_2O, 1:1) to afford the pure product (LC/MS, TLC) as black crystals (211.2 mg, 56.9%):R_f = 0.00 (EtOAC); mp 155-160 ºC;^{1}H NMR (300 MHz DMSO-d_6) δ 11.20 (s, 1H), 9.22 (dd, *J*=20.15, 6.80, 2H), 8.76 (d, *J*=6.86, 1H), 8.44 (d, *J*=6.51, 1H), 8.18, 7.73 (s, 0.5H, 0.5H), 7.65-7.21 (m, 6H), 6.95 (m, 1H), 6.07 (d, *J*=13.46, 2H);^{13}C NMR (75MHz, DMSO-d_6) δ146.1, 145.2, 132.2, 131.9, 131.7, 130.8, 130.7, 130.5, 129.2, 128.6, 128.2, 124.0, 123.6, 122.4, 112.7, 112.2, 61.3ppm LCMS (*m/z*) 383/385 (M^+1).

3-[(3,4,5-Trimethoxyphenyl)methylidene]-1*H*-indol-2-one (85)

To a 10 mL vial charged with EtOH (5 mL) and a magnetic stir bar was added isatin (158.1 mg, 1.1 mmol), 3,4,5-trimethoxybenzaldehyde (259.8 mg, 1.3 mmol) and piperidine (0.147 equiv, 20 µL). The reaction was stirred at 70°C for 6 h, allowed to cool to rt and then placed in the freezer overnight to crystallize. The product was collected via vacuum filtration. Pure product (LC/MS, TLC) was obtained as a yellow powder (211.2 mg, 56.9%): R_f =0.56 (EtOAC); mp 194-196 ºC;^{1}H NMR (300 MHz DMSO-d_6) δ 10.6 (s, 1H), 8.02 (s, 2H), 7.76 (s, 1H). 7.67 (d, *J*= 7.37, 1H), 7.20 (td, *J*=7.62, 0.95, 1H), 6.99 (td, *J*=7.57, 0.86, 1H), 6.85 (d, *J*=7.60, 1H), 3.85 (s, 6H), 3.75 (s, 3H);^{13}C NMR (75MHz, $CDCl_3$) δ 167.7, 152.7, 140.9, 140.2, 137.8, 130.0, 129.1, 125.6, 121.5, 119.8, 110.6, 109.8, 60.6, 56.3ppm; LCMS (*m/z*) 312 (M^+1).

3-[(2,4,6-Trimethoxyphenyl)methylidene]-1-[(2,6-difluorophenyl)methyl]-1*H*-indol-2-one (88)

To a 15 mL vial charged with EtOH (5 mL) and a magnetic stir bar was added 1-[(2,6-difluorophenyl)methyl]-2-indolinone (**87**) (250.2 mg, 1 mmol), 2,4,6-trimethoxybenzaldehyde (259.8 mg, 1.3 mmol) and piperidine (0.147 equiv, 20 µL). The reaction was stirred at 70°C for 48 h at which time it was cooled to rt and put in the freezer for 48 h to crystallize. Product was collected via vacuum filtration. Recrystallization with EtOH was performed on the solid to obtain the pure product (GCMS/TLC) as yellow crystals (145 mg, 34.4%). R_f=0.50 (60:40 EtOAc: Hexanes) ^{1}H NMR (300 MHz DMSO-d_6) δ 7.52 (s, 1H), 7.47-7.37 (m, 1H), 7.20 (td, J=7.26, 2.24, 1H), 7.11 (t, J=8.15, 2H), 6.93-6.85 (m, 3H), 6.37 (s, 2H), 5.03 (s, 2H), 3.87 (s, 3H), 3.75 (s, 6H); ^{13}C NMR (75MHz, DMSO-d_6) δ 167.5, 163.45-163.04 (m, 1H), 159.8-159.6 (m, 1H), 142.3, 130.9 (t, J=10.61, 1H), 129.1, 128.6, 126.3, 124.1, 122.2, 121.9, 112.4 (d,

J=7.53, 1H), 112.1 (d, J=7.57, 1H), 108.2, 105.0, 91.3, 32.2, 19.0; GCMS (*m/z*) 437.1 (M^+1) 406 (100%).

References

1. Alzheimer, A. Uber eineeigenartie Erkankung der Hirnrinde. *Allg. Z. Psychiatr.***1907**, *64*, 146.

2. Hippius, H.; Neundörfer, G. The discovery of Alzheimer's disease. *Dialogues in Clin. Neurosci.* **2003**, *5*, 101-108.

3. 2014 Alzheimer's Disease Facts and Figures. *Alzheimer's and Dementia*. **2014**, *10*, 47-92

4. Hyman, B.T.; Phelps, C.H.; Beach, T.G.;Bigio, E.H.; Cairns, N.J.; Carrillo, M.C.;Dickson, D.W.; Duyckaerts, C.; Frosh, M.P.; Masliah, E.; Mirra, S.S.; Nelson, P.T.; Schneider, J.A.; Thal, D.R.; Thies, B.; Trojanowski, J.Q.; Vinters, H.V.; Montine, T.J. National Institute on Aging–Alzheimer's Association guidelines on neuropathologic assessment of Alzheimer's disease. *AlzheimersDemen.* **2012**, *8*, 1–13.

5. Goedert, M.; Spillantini, M.G.; A Century of Alzheimer's Disease. *Science.* **2006**, *314*, 777-781.

6. Life expectancy in 2006 in the United States. http://data.worldbank.org/indicator/SP.DYN.LE00.IN/countries/US--XS?display=graph

7. Life expectancy in 1906 in the United States. https://www.census.gov/statab/hist/HS-16.pdf

8. Hirtz, D.; Thurman, D.J.; Gwinn-Hardy, K.; Mohamed, M.; Chaudhuri, A.R.; Zalutsky, R. How common are the "common" neurologic disorders? *Neurology* **2007**, *68*, 326-337.

9. Schneider, J.A.; Arvanitakis, Z.; Bang, W.; Bennett, D.A. Mixed brain pathologies account for most dementia cases in community-dwelling older persons. *Neurology* **2007**, *69*, 2197-2204.

10. Jellinger, K.A.; Attems, J. Neuropathological evaluation of mixed dementia. *J. Neurol. Sci.* **2007**, *257*, 80-87.

11. National Plan to Address Alzheimer's Disease: **2014** Update.http://aspe.hhs.gov/daltcp/napa/NatlPlan2015.pdf

12. Ronch, J.L. Mourning and Grief in late life Alzheimer's dementia: Revisiting the vanishing self. *Am. J.Alzheimers Dis.* **1996**, *11(4)*, 25-28.

13. Hardy, J.A.; Higgins, G.A. Alzheimer's disease: The amyloid cascade hypothesis. *Science* **1992**, *256*, 184-185.

14. Querfurth, H.W.; LaFerla, F.M. Alzheimer's disease. *N. Engl. J. Med.* **2010**, *362*, 329-344.

15. Haass, C.; Selkoe, D.J. Soluble protein oligomers in neurodegeneration: lessons from the Alzheimer's amyloid β-peptide. *Nat. Rev. Mol. Cell Biol.* **2007**, *8*, 101-112.

16. Lichtenthaler, S.F.; Wang, R.; Grimm, H.; Uljon, S.N.; Masters, C.L.; Beyreuther, K. Mechanism of the cleavage specificity of Alzheimer's disease γ-secretase identified by phenylalanine-scanning mutagenesis of the transmembrane domain of the amyloid precursor protein.*Proc. Natl. Acad. Sci. USA* **1999,** *96*, 3053-3058

17. Arriagada, P.V.; Growdon, J.H.; Hedley-Whyte, E.T.; Hyman, B.T. Neurofibrillary tangles but not senile plaques parallel duration and severity of Alzheimer's disease. *Neurology* **1992**, *42*, 631-639.

18. Sadeghi-Nejad, N. The lessons of failure: What we can learn from bapineuzuinab's blowup. *Forbes* (Pharma & Healthcare) August 7, 2012.

19. Therapeutics. Flurizan. http://www.alzforum.org/therapeutics/flurizantm

20. Therapeutics. Semagacestat. http://www.alzforum.org/therapeutics/semagacestat

21. Weggen, S.; Erikson, J.L.; Sagi, S.A., Pietrzil, C.U.; Ozols, V.; Fauq, A.; Golde, T.E., Koo, E.H. Evidence that nonsteroidal anti-inflammatory drugs decrease amyloid beta 42 production by direct modulation of gamma-secretase activity. *J. Biol. Chem*. **2003**, *278*, 31831-31837.

22. Winblad, B.; Giacobini, E.; Frolich, L.; Friedhoff, L.T., Bruinsma, G.; Becker, R.E.; Greig, N.H. Pherserine efficacy in Alzheimer's disease. *J. Alzheimer's Dis*. **2010**, *22*, 1201-1208.

23. Therapeutics. Bapineuzumab. http://www.alzforum.org/therapeutics/bapineuzumab

24. Therapeutics. Solanezumab. http://www.alzforum.org/therapeutics/solanezumab

25. Cramer, P.E. *et al.* ApoE-directed therapeutics rapidly clear beta-amyloid and reverse deficits in AD mouse models. *Science* **2012**, *335*, 1503–1506.

26. Schenk, D. *et al.* Immunization with amyloid-beta attenuates Alzheimer-disease-like pathology in the PDAPP mouse. *Nature* **1999**, *400*, 173–177.

27. Dodart, J.C. *et al.* Immunization reverses memory deficits without reducing brain Aβ burden in Alzheimer's disease model. *Nat. Neurosci.* **2002**, *5*, 452–457.

28. Holmes, C. *et al.* Long-term effects of Aβ42 immunisation in Alzheimer's disease: follow-up of a randomised, placebo-controlled phase I trial. *Lancet* **2008**, *372*, 216–223.

29. Salloway, S. *et al.* Two phase 3 trials of bapineuzumab in mild-to-moderate Alzheimer's disease. *N. Engl. J. Med.* **2014**, *370*, 322–333.

30. Doody, R.S. *et al.* Phase 3 trials of solanezumab for mild-to-moderate Alzheimer's disease. *N. Engl. J. Med.* **2014**, *370*, 311–321.

31. Vellas, B. *et al.* Designing drug trials for Alzheimer's disease: what we have learned from the release of the phase III antibody trials: a report from the EU/US/CTAD Task Force. *Alzheimers Dement.* **2013**, *9*, 438–444.

32. Lue, L.F.; Kuo, Y.M.; Roher, A.E.; Brachova, L.; Shen, Y.; Sue, L.; Beach, T.; Kurth, J.H.; Rydel, R.E.; Rogers, J. Soluble amyloid β peptide concentration as a predictor of synaptic change in Alzheimer's disease. *Am. J.Pathol.* **1999**, *155*, 853-862.

33. Braak, H.; Braak, E. Neuropathological stageing of Alzheimer-related changes. *Acta.Neuropathol.* **1991**, *82*, 239-259.

34. Hardy J. Alzheimer's disease: The present situation and our tasks. *Neurobiol Aging*. **1994**, *15*, S111-S112.

35. Lindsley, C.W. Alzheimer's Disease: Development of Disease-Modifying Treatments Is the Challenge for Our Generation.*ACS Chem. Neurosci.* **2012**, *3*, 804-805.

36. Forman, M.S.; Trojanowski, J.Q.; Lee, V.M-Y. Neurodegenerative diseases: a decade of discoveries paves the way for therapeutic breakthroughs. *Nature Medicine*. **2004**, *10*, 1055-1063.

37. Trojanowski, J.Q.; Lee, V.M-Y. The Alzheimer's brain. *American Journal of Pathology*. **2005**, *167*, 1183-1188.

38. Skovronsky, D.M.; Lee, V. M-Y.; Trojanowski, J.Q. Neurodegenerative diseases: New concepts of pathogenesis and their therapeutic implications. *Annu Rev PatholMech Dis*. **2006**, *1*, 151-170.

39. Mohandas, E.; Rajmohan, V.; Raghunath, B. Neurobiology of Alzheimer's disease. *Indian J. Psychiatry* **2009**, *51*, 55-61.

40. Maccioni, R.B.; Farias, G.; Morales, I.; Navarrete, L. The revitalized tau hypothesis on Alzheimer's disease*Arch MedRes*. **2010**, *41*, 226-231.

41. Lee, V. M-Y.; Trojanowski, J.Q. The disordered neuronal cytoskeleton in Alzheimer's disease. *CurrOpinNeurobiol*. **1992**, *2*, 653-656.

42. Kosik, K.S.; Joachim, C.L.; Selkoe, D.J. Microtubule-associated protein tau (tau) is a major antigenic component of paired helical filaments in Alzheimer disease. *Proc. Natl. Acad. Sci. USA*. **1986**, *83*, 4044-4048.

43. Braak, H.; Braak, E. Neuropathological staging of Alzheimer-related changes. *ActaNeuropathol*. **1991**, *82*, 239-259.

44. Duyckaerts, C.; Hauw, J.J. Prevalence, incidence and duration of Braak's stages in the general population: can we know? *Neurobiol Aging*. **1997**, *18*, 389-392.

45. Morsch, R.; Simon, W.; Coleman, P.D. Neurons may live for decades with neurofibrillary tangles. *J NeuropatholExp Neurol*. **1999**, *58*, 188-197.

46. Bierer, L.M.; Hof, P.R.; Purohit, D.P.; Carlin, L.; Schmeidler, J.; Davis, K.L.; Perl, D.P. Neocortical neurofibrillary tangles correlate with dementia severity in Alzheimer's disease. *Arch Neurol*. **1995**, *52*, 81-88.

47. Arriagada, P.V.; Growdon, J.H.; Hedley-Whyte, E.T.; Hyman, B.T. Neurofibrillary tangles but not senile plaques parallel duration and severity of Alzheimer's disease. *Neurology* **1992**, *42*, 631-639.

48. Maccioni, R.B.; Lavados, M.; Guillón, M.; Mujica, C.; Bosch, R.; Farías, G.; Fuentes, P. Anomalously phosphorylated tau and Abeta fragments in the CSF correlates with cognative impairment in MCI subjects. *Neurobiol Aging*. **2006**, *27*, 237-244.

49. Masliah, E.; Mallory, M.; Hansen, L.; DeTeresa, R.; Terry, R.D. Quantitative synaptic alterations in the human neocortex during normal aging. *Neurology* **1993**, *43*, 192-197.

50. Kaduszkiewicz, H.; Zimmermann, T.; Beck-Bornholdt, H-P.; van den Bussche, H. Cholinesterase inhibitors for patients with Alzheimer's disease: systematic review of randomised clinical trials. *The BMJ*. **2005**, *331*, 321-327.

51. https://www.nia.nih.gov/alzheimers/publication/alzheimers-disease-medications-fact-sheet

52. https://www.alz.org/national/documents/topicsheet_treatments.pdf

53. Danysz, W.; Parsons, C.G. The NMDA receptor antagonist memantine as a symptomatological and neuroprotective treatment for Alzheimer's disease: preclinical evidence. *Int J Geriatr Psychiatry*. **2003**, *18*, S23-32.

54. Chen, F.; Hasegawa, H.; Schmitt-Ulms, G.; Kawarai, T.; Bohm, C.; Katayama, T.; Gu, Y.; Sanjo, N.; Glista, M.; Rogaeva, E.; Wakutani, Y.; Pardossi-Piquard, R.; Ruan, X.; Tandon, A.; Checler, F.; Marambaud, P.; Hansen, K.; Westaway, D.; St George-Hyslop, P.; Fraser, P. TMP21 is a presenilin complex component that modulates gamma-secretase but not epsilon-secretase activity.*Nature*. **2006**, *440*, 1208-1212.

55. Fraering, P.C.; Ye, W.; LaVoie, M.J.; Ostaszewski, B.L.; Selkoe, D.J.; Wolfe, M.S. Gamma-secretase substrate selectivity can be modulated directly via interaction with a nucleotide-binding site. *J Biol Chem*. **2005**, *51*, 41987-41996.

56. Netzer, W.J.; Dou, F.; Cai, D.; Veach, D.; Jean, S.; Li, Y.; Bornmann, W.G.; Clackson, B.; Xu, H.; Greengard, P. Gleevec inhibits β-amyloid production but not notch cleavage. *Proc. Natl. Acad. Sci. USA* **2003**, *100*, 12444-12449.

57. Eriksen, J.L.; Sagi, S.A.; Smith, T.E.; Weggen, S.; Das, P.; McLendon, D.C.; Ozols, V.V.; Jessing, K.W.; Zavitz, K.H.; Koo, E.H.; Golde, T.E. NSAIDs and enantiomers of flurbiprofen target ɣ-secretase and lower Aβ42 in vivo. *J Clin Invest* **2003**, *112*, 440-449.

58. Lleó, A.; Berezovska, O.; Herl, L.; Raju, S.; Deng, A.; Bacskai, B.J.; Frosch, M.P.; Irizarry, M.; Hyman, B.T. Nonsteroidal anti-inflammatory drugs lower $A\beta_{42}$ and change presenilin 1 conformation. *Nat Med*. **2004**, *10*, 1065-1066.

59. Ohno, M.; Chang, L.; Tseng, W.; Oakley, H.; Citron, M.; Klein, W.L.; Vassar, R.; Disterhoft, J.F. Temporal memory deficits in Alzheimer's mouse models: rescue by genetic deletion of BACE1. *Eur J Neurosci*. **2006**, *23*, 251-260.

60. Esler, W.P.; Wolfe, M.S. A portrait of Alzheimer secretases--new features and familiar faces. *Science* **2001**, *293*, 1449-1454.

61. Roberson, E.D.; Mucke, L. 100 years and counting: Prospects for defeating Alzheimer's disease. *Science* **2006**, *314*, 781–784. doi:10.1126/science.1132813.

62. Gervais, F.; Paquette, J.; Morissette, C.; Krzywkowski, M.Y.; Azzi, M.; Lacombe, D.; Kong, X.; Aman, A.; Laurin, J.; Szarek, W.A.; Tremblay, P. Targeting soluble Aβ peptide with Tramiprosate for the treatment of brain amyloidosis. *Neurobiol Aging* **2007**, *28*, 537-547.

63. Therapeutics. Alzhemed. http://www.alzforum.org/therapeutics/alzhemedtm

64. Rolland, Y.; Van Kan, G.A.; Vellas, B. Physical activity and Alzheimer's disease: From prevention to therapeutic perspectives. *J Am Med Dir Assoc*. **2008**, *9*, 390-405.

65. Ringman, J.M.; Frautschy, S.A.; Cole, G.M.; Masterman, D.L.; Cummings, J.L. A Potential Role of the Curry Spice Curcumin in Alzheimer's Disease. *Curr. Alzheimer Res*. **2005**, *2*, 131-136.

66. Paddock, C. Scientists discover big clue to how caffeine wards off Alzheimer's. Medical News Today. **2014**. http://www.medicalnewstoday.com/articles/275181.php

67. Arendash, G.W. Caffeine Reverses Cognitive Impairment and Decreases Brain Amyloid-β Levels in Aged Alzheimer's Disease Mice. *J Alzheimers Dis*. **2009**, *17*, 661-680.

68. Kung, H.F. "The β-Amyloid Hypothesis in Alzheimer's Disease: Seeing Is Believing." *ACS Med. Chem. Lett*. **2012**, *3*, 265-267.

69. Jeffery, S. FDA approves thrid amyloid PET tracer for Alzheimer's. *Medscape*. Mar 21, **2014**. http://www.medscape.com/viewarticle/822370

70. Mathis, C.A.; Wang, Y.; Klunk, W.E. Imaging β-amyloid plaques and neurofibrillary tangles in the aging Human Brain. *Curr Pharm Design* **2004**, *10*, 1469-1492.

71. Zimmer, E.R.; Leuzy, A.; Gauthier, S.; Rosa-Neto, P. Developments in tau PET imaging. *Can J Neurol Sci*. **2014**, *41*, 547-553.

72. Shoghi-Jadid, K.; Small, G.W.; Agdeppa, E.D.; Kepe, V.; Ercoli, L.M.; Siddarth, P.; Read, S.; Satyamurthy, N.; Petric, A.; Huang, S-C.; Barrio, J. Localization of neurofibrillary tangles and beta-amyloid plaques in the brains of living patients with Alzheimer disease. *Am J GeriatrPsychiatr*. **2002**, *10*, 24-35.

73. Villemagne, V.L.; Furumoto, S.; Fodero-Tavoletti, M.T.; Mulligan, R.S.; Hodges, J.; Harada, R.; Yates, P.; Piguet, O.; Pejoska, S.; Doré, V.; Yanai, K.; Masters, C.L.; Kudo, Y.; Rowe, C.C.; Okamura, N. In vivo evaluation of a novel tau imaging tracer for Alzheimer's disease. *Eur J Nucl Med Mol Imaging*. **2014**, *41*, 816-826.

74. Maruyama, M.; Shimada, H.; Suhara, T.; Shinotoh, H.; Ji, B.; Maeda, J.; et al. Imaging of tau pathology in a tauopathy mouse model and in Alzheimer patients compared to normal controls. *Neuron* **2013**, *79*, 1094-1108.

75. Chien, D.T.; Bahri, S.; Szardenings, A.K.; Walsh, J.C.; Mu, F.; Su, M.Y.; Shankle, W.R.; Elizarov, A.; Kolb, H.C. Early clinical PET imaging results with the novel PHF-tau radioligand [F-18]-T807. *J Alzheimers Dis*. **2013**, *34*, 457-468.

76. Okamura, N.; Furumoto, S.; Fodero-Tavoletti, M.T.; Mulligan, R.S.; Harada, R.; Yates, P.; et al. Non-invasive assessment of Alzheimer's disease neurofibrillary pathology using ^{18}F-THK5105 PET. *Brain* **2014**, *137*, 1762-1771.

77. Iqbal, K.; Grundke-Iqbal, I. Alzheimer disease is multifactorial and heterogeneous. *Neurobiol Aging* **2000**, *21*, 901-902.

78. Zhang, H-Y. One-compound-multiple-targets strategy to combat Alzheimer's disease. *FEBS Letters* **2005**, *579*, 5260-5264.

79. Cavalli, A.; Bolognesi, M.L.; Minarini, A.; Rosini, M.; Tumiatti, V.; Recanatini, M.; Melchiorre, C. Multi-target-directed ligands to combat neurodegenerative diseases. *J. Med. Chem*. **2008**, *51*, 347-372.

80. León, R.; Garcia, A.G.; Marco-Contelles, J. Recent advances in the multitarget-directed ligands approach for the treatment of Alzheimer's disease. *Med Res Rev*. **2013**, *33*, 139-189.

81. Sabbagh, M.N. Drug development for Alzheimer's disease: Where are we now and where are we headed? *Am. J. Geriatr. Pharmacother*. **2009**, *7*, 167-185.

82. Cavalli, A.; Bolognesi, M.L.; Capsoni, S.; Andrisano, V.; Bartolini, M.; Margotti, E.; Cattaneo, A.; Recanatini, M.; Melchiorre, C. A small molecule targeting the multifactorial nature of Alzheimer's Disease. *Angew. Chem. Int. Ed*. **2007**, *46*, 3689-3692.

83. Bolognesi, M.L.; Cavalli, A.; Melchiorre, C. Memoquin: A multi-target-directed ligand as an innovative therapautic opportunity for Alzheimer's disease. *Neurotherapeutics*. **2009**, *6*, 152-162.

84. Mariano, M. Schmitt, C.; Miralinaghi, P.; Catto, M.; Hartmann, R. W.; Carotti, A.; Engel, M. First selective dual inhibitors of tau phosphorylation and beta-amyloid aggregation, two major pathogenic mechanisms in Alzheimer's disease. *ACS. Chem. Neurosci*. **2014**, *5*, 1198-1202.

85. Anighoro, A.; Bajorath, J.; Rastelli, G. Polypharmacology: Challenges and oportunities in drug discovery. *J. Med. Chem*. **2014**, *57*, 7874-7887.

86. Flajolet, M.; He, G.; Heiman, M.; Lin, A.; Nairn, A.C.; Greengard, P. Regulation of Alzheimer's disease amyloid-β formation by casein kinase 1. *Proc Natl AcadSci USA*. **2007**, *104*, 4159-4164.

87. Höttecke, N.; Liebeck, M.; Baumann, K.; Schubenel, R.; Winkler, E.; Steiner, H.; Schmidt, B. Inhibition of ɣ-secretase by the CK1 inhibitor IC261 does not depend on CK1δ. *Bioorg Med Chem Lett*. **2010**, *20*, 2958-2963.

88. He, G.; Luo, W.; Li, P.; Remmers, C.; Netzer, W.; Hendrick, J.; Bettayeb, K.; Flajolet, M.; Gorelick, F.; Wennogle, L.P.; Greengard, P. Gamma-secretase activating protein, a therapautic target for Alzheimer's disease. *Nature* **2010**, *467*, 95-98.

89. Stadelmann, C.; Deckwerth, T.L.; Srinivasan, A.; Bancher, C.; Bruck, W.; Jellinger, K.; Lassmann, H. Activation of caspase-3 in single neurons and autophagic granules of granulovacuolar degeneration in Alzheimer's Disease: Evidence for apoptotic cell death. *Am J Pathol*. **1999**, *155*, 1459-1466.

90. Chu, J.; Li, J. G.; Joshi, Y. B.; Giannopoulos, P. F.; Hoffman, N. E.;Madesh, M.; Pratico, D. Gamma secretase-activating protein Is a substrate for caspase-3: implications for Alzheimer's disease. *Biol Psychiatry*. **2015**, *77*, 720-728.

91. Joshi, G.; Wang, Y. Golgi defects enhance APP amyloidogenic procession in Alzheimer's Disease. *Bioessays* **2015**, *37*, 240-247.

92. Johnson, K.; Liu, L.; Majdzadeh, N.; Chavez, C.; Chin, P.C.; Morrison, B.; Wang, L.; Park, J.; Chugh, P.; Chen, H.M.; D'Mello, S.R. Inhibition of neuronal apoptosis by the cyclin-dependent kinase inhibitor GW8510: Identification of 3' substituted indolones as a scaffold for the development of neuroprotective drugs. *J. Neurochem*. **2005**, *93*, 538-548.

93. Ishiguro K.; Takamatsu M.; Tomizawa K.; Tomizawa K.; Omori, A.; Takahashi M.; Arioka M.; Uchida T.; Imahori, K. Tau protein kinase I converts normal tau protein into A68 like component of paired helical filaments, *J. Biol. Chem*. **1992**, *267*, 10897–10901.

94. Baloyannis, S.J. Golgi apparatus and protein trafficking in Alzheimer's disease. *J Alzheimer Dis*. **2014**, *42*, 153-162.

95. De Sa Alves, F.R.; Barreiro, E.J.; FragaManssour, C.A. "From nature to drug discovery: the indole scaffold as a 'privileged structure'." *Mini-Rev. Med. Chem.* **2009**, *9*, 782-793

96. Evans, B.E.; Rittle, K.E.; Bock, M.G.; DiPardo, R.M.; Freidinger, R.M.; Whitter, W. L.; Lundell, G.F.; Veber, D.F.; Anderson, P.S.; Chang, R.S.L.; Lotti, V.J.; Cerino, D.J.; Chen, T.B.; Kling, P.J.; Kunkel, K.A.; Springer, J.P.; Hirshfield, J. Methods for drug discovery: development of potent, selective, orally effective cholecystokinin antagonists*J. Med. Chem*. **1988**, *31*, 2235-2246

97. Honson, N.S.; Johnson, R.L.; Huang, W.; Inglese, J.; Austin, C.P.; Kuret, J. Differentiating Alzheimer disease-associated aggregates with small molecules. *Neurobiol Dis.* **2007**, *28,* 251-260.

98. Cohen, P. "Protein Kinases the Major Drug Targets of the Twenty First Century?" *Nature Rev,. Drug Discov*. **2002**, *1*, 309-315; b) Prakash, C.R.; Theivendren, P.; Raja, S. "Indolin-2-ones in clinical trials as potential kinase inhibitors: a review." *Pharmacology & Pharmacy* **2012**, *3*, 62-71; c) Noble, M.E.M.; Endicott, J.A.; Johnson, L.N. "Protein kinase inhibitors: insights into drug design from structure" *Science* **2004**, *303*, 1800-1805.

99. Chu, W.; Zhang, J.; Zeng, C.; Rothfuss, J.; Tu, Z.; Chu, Y.; Reichert, D.; Welch, M.J.; Mach, R.H. N-benzylisatin sulfonamide analogues as potent caspase-3 inhibitors: Synthesis in vitro activity and molecular modeling studies. *J.Med. Chem*. **2005,** *48,* 7637-7647.

100. Jiang, Y.; Hansen, T.V. Isatin 1,2,3-triazoles as potent inhibitors against caspase-3. *Bioorg Med Chem Lett*. **2011**, *21,* 1626-1629.

101. Chu, W.; Rothfuss, J.; Zhou, D.; Mach, R.H. Synthesis and evaluation of isatin analogs as caspase-3 inhibitors: Introduction of a hydrophilic group increases potency in a whole cell assay. *Bioorg Med Chem Lett*. **2011**, *21*, 2192-2197.

102. Zhang, W.; Oya, S.; Kung, M.P.; Hou, C.; Maier, D.L.; Kung, H.F. F-18 Polyethyleneglycol stilbenes as PET imaging agents targeting Aβ aggregates in the brain. *Nuc Med and Bio*. **2005**, *32*, 799-809.

103. Glaser, M.; Arstad, E. "Click Labeling" with 2-[^{18}F]Fluoroethylazide for Positron Emission Tomography. *Bioconjugate Chem*. **2007**, *18*, 989-993.

104. Ono, M.; Watanabe, R.; Kawashima, H.; Cheng, Y.; Kimura, H.; Watanabe, H.; Haratake, M.; Saji, H.; Nakayama, M. Fluoro-pegylated Chalones as positron

emission tomography probes for in Vivo imaging of β-amyloid plaques in Alzheimer's disease. *J. Med. Chem*. **2009**, *52*, 6394-6401.

105. Stephenson, K.A.; Chandra, R.; Zhuang, Z.; Hou, C.; Oya, S.; Kung, M.; Kung, H.K. Fluoro-pegylated (FPEG) Imaging Agents Targeting Aβ Aggregates. *Bioconjugate Chem*. **2007**, *18*, 238-246.

106. Ametamey, S.M., Honer, M.; Schubiger, P.A. Molecular Imaging with PET. Chem Rev. **2008**, *108*, 1501-1516.

107. Marik, J.; Sutcliffe, J.L. Click for PET: rapid preparation of [^{18}F]fluoropeptides using Cu^{I} catalyzed 1,3-dipolar cycloaddition. *Tetrahedron Lett*. **2006**, *47*, 6681-6684.

108. Nguyen, Q.D.; Challapalli, A.; Smith, G.; Fortt, R.; Aboagye, E.O. Imaging apoptosis with positron emission tomography: 'Bench to bedside' development of the caspase-3/7 specific radiotracer [^{18}F]ICMT-11. European Journal of Cancer. **2012**, *48*, 432-440.

109. Jia, L.; Cheng, Z.; Shi, L.; Li, J.; Wang, C.; Jiang, D.; Zhou, W.; Meng, H.; Qi, Y.; Cheng, D.; Zhang, L. Fluorine-18 labeling by click chemistry: Multiple probes in one pot. *Appl. Radiat. Isotopes* **2013**, *79*, 64-70.

110. Glaser, M.; Robins, E.G. Click labeling in PET radiochemistry. *J Label CompdRadiopharm*. **2009**, *52*, 407-414.

111. Wang, M.; Yuan, Y.; Liang, G. "Click chemistry" for molecular imaging. *Current Molecular Imaging*. **2012**, *1*.

112. Phelps, M.E. Positron Emission Tomography Provides Molecular Imaging of Biological Processes. *Proc Nat Acad Sci*. **2000**, *97*, 9226-9233. D.O.I.: 10.1073/pnas.97.16.9226.

113. Gillings, N. Radiotracers for Positron Emission Tomography Imaging. *Magn.Reson. Mater. Phy*. **2013**, *26*, 149-158.

114. Ametamey, S.M.; Honer, M.; Schubiger, P.A. Molecular Imaging with PET. *Chem. Rev*. **2008**, *108*, 1501-1516.

115. Cherry, S. The 2006 Henry N. Wagner lecture: of mice and men (and positrons)-advances in PET imaging technology. *J. Nucl. Med*. **2006**, *47*, 1735-1745.

116. Muller, K.; Faeh, C.; Diederich, F. Fluorine in Pharmaceuticals: Looking Beyond Intuition. *Science* **2007**, *317*, 1881-1886.

117. Le Bars, D. Fluorine-18 and medical imaging: Radiopharmaceuticals for positron emission tomography. *J. Fluorine Chem*. **2006**, *127*, 1488-1493.

118. Meldal, M; Tornoe, C.W. "Cu-Catalyzed azide-alkyne cycloaddition" *Chem Rev*. **2008**, *108*, 2952-3015.

119. Rostovtsev, V.V.; Green, L.G.; Fokin, V.V.; Sharpless, K.B. A stepwise Huisgen cycloaddition process: copper(I)-catalyzed regioselective 'ligation' of azides and terminal alkynes. *Angew. Chem. Int. Ed*. **2002**, *41*, 2596-2599.

120. Tornoe, C.W.; Christensen, C.; Meldal, M. Peptidotriazoles on solid phase: [1,2,3]-triazoles by regiospecific copper(I)-catalysed 1,3-dipolar cycloadditions of terminal alkynes to azides. *J. Org. Chem*. **2002**, *67*, 3057-3064.

121. Moses, J.E.; Moorhouse, A.D. The growing applications of click chemistry. *Chem. Soc. Rev*. **2007**, *36*, 1249-1262.

122. Kolb, H.C.; Sharpless, K.B. The growing impact of click chemistry on drug discovery. *Drug Discov Today*. **2003**, *8*, 1128-1137.

123. Bock, V.D.; Hiemstra, H.; van Maarseveen, J.H. Cu^{I}-catalyzed alkyne-azide "click" cycloadditions from a mechanistic and synthetic perspective. *Eur. J. Org. Chem*. **2006**, *2006*, 51-68.

124. Bock, V.D.; Speijer, D.; Hiemstra, H.; Van Maarseveen, J.H. 1,2,3-triazoles as peptide bond isosteres: synthesis and biological evaluation of cyclotetrapeptide mimics. *Org.Biomol. Chem*. **2007**, *5*, 971-975.

125. Hausner, S.H.; Marik, J.; Gagnon, K.J.; Sutcliffe, J.L. In vivo positron emission tomography (PET) imaging with an $\alpha_v\beta_6$ specific peptide radiolabeled using ^{18}F-"click" chemistry: Evaluation and comparision with the corresponding 4-[^{18}F]Flurorbenzoyl- and 2-[^{18}F]Fluoropropional-peptides. *J Med Chem*. **2008**, *51*, 5901-5904.

126. Zhou, D.; Chu, W.; Peng, X.; McConathy, J.; Mach, R.H.; Katzenellenbogen, J.A. Facile purification and click labeling with 2-[^{18}F]fluoroethyl azide using solid phase extraction cartridges.*Tetrahedron Lett*. **2015**, *56*, 952-954.

127. Smith, G.; Glaser, M.; Nguyen, Q-D.; Shan, B.; Arstad, E.; Aboagye, E.O. Design, synthesis, and biological characterization of a caspase 3/7 selective isatin labeled with 2-[18F]fluoroethylazide. *J. Med. Chem*. **2008**, *51*, 8057-8067.

128. Shealy, Y. Fulmer, and Charles A. Krauth. (Alkylsulfonyl)methanesulfonates as Anticancer Agents. Southern Research Institute, assignee. Patent 4727174. 23 Feb. **1988**. Print.

129. Parenty, A.D.C; Smith, L.V.; Cronin, L. An unusual substitution reaction directed by an intramolecular re-arrangement. *Tetrahedron*. **2005**, *61*, 8410-8418

130. Bernard-Gauthier, V.; Aliaga, A.; Aliaga, A.; Boudjemeline, M.; Hopewell, R.; Kostikov, A.; Rosa-Neto, P.; Thiel, A.; Schirrmacher, R. Syntheses and evaluation of carbon-11- and fluorine-18-radiolabeled pan-tropomyosin receptor kinase (Trk) inhibitors: exploration of the 4-aza-2-oxindole scaffold as Trk PET imaging agents. *ChemNeurosci*. **2015**, *6*, 260-276.

131. Sarmiento-Sanchez, J.I.; Ochoa-Teran, A.; Rivero, I.A. Conventional and microwave assisted synthesis of 1,4-disubstituted 1,2,3-triazoles from Huisgen cycloaddition. *Arkivoc* **2011**, *4*, 177-188. b.) Mukherjee, N.; Ahammed, S.; Bhadra, S.;Ranu, B. Solvent-free one-pot synthesis of 1,2,3-triazole derivatives by the 'Click' reaction of alkyl halides or aryl boronic acids, sodium azide and terminalalkynes over a Cu/Al_2O_3 surface under ball-milling. *Green Chem*. **2013**, *15*, 389-397.

132. Reddy, K.R.; Rajgopal, K.; Kantam, M.L. Copper(II)-promoted regioselective synthesis of 1,4-disubstituted 1,2,3-triazoles in water. *Synlett*. **2006**, *6*, 957-959.

133. Sharghi, H.; Khalifeh, R.; Doroodmand, M.M. Copper nanoparticles on charcoal for multicomponent catalytic synthesis of 1,2,3-triazole derivatives from benzyl halides or alkyl halides, terminal alkynes and sodium azide in water as a "Green" solvent. *Adv. Synth.Catal.* **2009**, *351*, 207-218.

134. Kacprzak, K. Efficient one-pot synthesis of 1,2,3-Triazoles from benzyl and alkyl halides. *Synlett*. **2005**, *6*, 943-946.

135. Gallardo, H.; Conte, G.; Bryk, F.; Lourenco, M.C.S.; Costa, M.S.; Ferreira, V.F. Synthesis and evaluation of 1-alkyl-4-phenyl-[1,2,3]-triazole derivatives as antimycobacterial agent. *J. Braz. Chem. Soc.* **2007**, *18*, 1285-1291.

136. Lee, I.; Choe, Y.S.; Choi, J.Y.; Lee, K-H.; Kim, B-T. Synthesis and evaluation of ^{18}F-labeled styryltriazole and resveratrol derivatives for β-amyloid plaque imaging. *J. Med. Chem*. **2012**, *55*, 883-892.

137. Hugenburg, V.; Breyholz, H-J.; Riemann, B.; Hermann, S.; Schober, O.; Schafers, M.; Gangadharmath, U.; Mocharla, V.; Kolb, H.; Walsh, J.; Zhang, W.; Kopka, K.; Wagner, S. A new class of highly potent maetalloproteinase inhibitors based

on triazole-substituted hydroxamates: (Radio)synthesis and in Vitro and first in vivi evaluation. *J. Med. Chem*. **2012**, *55*, 4714-4727.

138. Bouhfid, R.; Joly, N.; Massoni, M.; Cecchelli, R.; Lequart, V.; Martin, P.; Essassi, E.M. An efficient synthesis of new spiro[indolo-3(1H),2'(3'H)-oxadiazolyl] and 1-(triazol-4-ylmethyl) isatin derivatives. *Heterocycles*. **2005**, *65*, 2949-2955.

139. Tipson, S. On esters of p-toluenesulfonic acid. *J. Org. Chem*. **1944**, *9*, 235-241.

140. Kazemi, F.; Massah, A.R.; Javaherian, M. Chemoselective and scalable preparation of alkyl tosylates under solvent-free conditions. *Tetrahedron* **2007**, *63*, 5083-5087.

141. Kabalka, G.W.; Varma, M.; Varma, R.S. Tosylation of alcohols. *J. Org. Chem*. **1986**, *51*, 2386-2388.

142. Dobbs, A.P.; Guesne, S.J.J.; Parker, R.J.; Skidmore, J.; Stephenson, R.A.; Hursthouse, M.B. A detailed investigation of the aza-Prins reaction. *Org.Biomol. Chem*. **2010**, *8*, 1064-1080.

143. Bottorff, E. Preparation of nitrobenzyl alcohol mesylates and tosylates. Lilly Co Eli, assignee. Patent 3745188. 10 Jul. 1973

144. Ding, R.; He, Y.; Wang, X.; Xu, J.; Chen, Y.; Feng, M.; Qi, C. Treatment of alcohols with tosylchoride does not always lead to the formation of tosylates. *Molecules*. **2011**, *16*, 5665-5673.

145. Abdallah, H.M. Small molecule caspase inhibitors using isatin and oxindole scaffolds and a combinatorial approach. WSU Master's Thesis **2010**.

146. Li, X.; Huang, P.; Cui, J.J.; Zhang, J.; Tang, C. Novel pyrrolyllactone and pyrrolyllactamindolinones as potent cyclin-dependent kinase 2 inhibitors. *Bioorg. Med. Chem. Lett*. **2003**, *13*, 1939-1942.

147. Zhang, W.; Go, M. L. Functionalized 3-benzylidene-indolin-2-ones: Inducers of NAD(P)H-quinone oxidoreductase 1 (NQO1) with antiproliferative activity. *Bioorg. Med. Chem*. **2009**, *17*, 2077-2090

148. Coda, A.C.; Invernizzi, A.G.; Righetti, P.P.; Tacconi, G.; Gatti, G. (Z)- and (E)-Arylidene-1,3-dihydroindol-2-ones: configuration, conformation, and infrared carbonyl stretching frequencies.*J ChemSocPerkin Trans. II* **1984**, *4*, 615-619.

149. Yamawaki, J.; Ando, T. Potassium fluoride on inorganic solid supports. A search for further efficient reagents promoting hydrogen-bond-assisted alkylations*Chem. Lett*. **1979**, *7*, 755-758

150. Clay C.M. Synthesis of isatin derivatives used for the inhibition of pro-apoptotic jurkat t cells. WSU Master's Thesis **2011**

151. Clay, C.M.; Abdallah, H.M.; Jordan, C.; Knisley, K.; Ketcha, D.M. N-Alkylation of isatins utilizing KF/Alumina. *Arkivoc* **2012**, *6*, 317-325.

152. Knisley, K.J. Libraries from libraries approach to the synthesis of arylidene oxindoles. WSU Master's Thesis. **2013**.

153. Cox, K.W. Synthesis and biological activity of indolinones. WSU Master's Thesis. **2014**.

154. Boyer, A.M.L. Unpublished WSU Master's Thesis. **2015.**

155. Akrami, H.; Mirjalili, B.F.; Khoobi, M.; Nadri, H.; Moradi, A.; Sakhteman, A.; Emami, S.; Foroumadi, A. Indolinone-based acetylcholinesterase inhibitors: Synthesis, bioligical activity and molecular modeling. *Eur. J. Med. Chem*. **2014**, *84*, 375-381.